NAVAL POSTGRADUATE SCHOOL
MONTEREY, CALIFORNIA

THESIS

ANODE FALL AS RELEVANT TO PLASMA THRUSTERS

by

Brigitte Horner

June, 1997

Thesis Advisor: Oscar Biblarz
Thesis Co-Advisor: Christopher L. Frenzen

Approved for public release; distribution is unlimited.

REPORT DOCUMENTATION PAGE

Form Approved OMB No. 0704-0188

1. AGENCY USE ONLY *(Leave blank)*	2. REPORT DATE	3. REPORT TYPE AND DATES COVERED
	June 1997	Engineer's and Master's Thesis

4. TITLE AND SUBTITLE **ANODE FALL AS RELEVANT TO PLASMA THRUSTERS**

5. FUNDING NUMBERS

6. AUTHOR(S) Horner, Brigitte

7. PERFORMING ORGANIZATION NAME(S) AND ADDRESS(ES)
Naval Postgraduate School
Monterey CA 93943-5000

8. PERFORMING ORGANIZATION REPORT NUMBER

9. SPONSORING/MONITORING AGENCY NAME(S) AND ADDRESS(ES)

10. SPONSORING/MONITORING AGENCY REPORT NUMBER

11. SUPPLEMENTARY NOTES The views expressed in this thesis are those of the author and do not reflect the official policy or position of the Department of Defense or the U.S. Government.

12a. DISTRIBUTION/AVAILABILITY STATEMENT
Approved for public release; distribution is unlimited.

12b. DISTRIBUTION CODE

13. ABSTRACT *(maximum 200 words)*

The behavior of the electric field together with the electron and ion densities in the vicinity of a non-emitting, plane anode is investigated. The selected approach involves non-linear analysis techniques on the continuum equations for steady-state, isothermal conditions where both ionization and two-body recombination are included. Ions, created through electron bombardment of neutral atoms, are repelled toward two stagnation regions: within or near the sheath boundary and near the plasma interface. These equilibria form as a result of the chemistry present: recombination establishes the latter while ionization stipulates the former. As presented, the sheath is fundamentally unstable - ions are driven toward the negative electrode. Using nitrogen data for a numeric example, the following observations are made: a sufficiently strong applied electric field pushes the ion density toward that of the electrons through a well - a constrictive phenomenon. Both a transition region, dominated by density gradients, and a diffusion-driven zone are found to move the system toward the plasma interface. The characteristics of this process are influenced by the applied electric field, but the instability of the chemistry-induced stagnation regions precludes numeric convergence. Insufficient dissipation may prevent the stability of the anode fall model as presented. Suggested improvements to the model descriptions include considering the effects of temperature gradients, magnetic fields, three-body recombination, diffusion written in terms of the electric field, multi-dimensionality and/or time-dependencies.

14. SUBJECT TERMS Magnetoplasma-dynamic (MPD), Electric Propulsion, Plasma Physics

15. NUMBER OF PAGES 150

16. PRICE CODE

17. SECURITY CLASSIFICATION OF REPORT	18. SECURITY CLASSIFICATION OF THIS PAGE	19. SECURITY CLASSIFICATION OF ABSTRACT	20. LIMITATION OF ABSTRACT
Unclassified	Unclassified	Unclassified	UL

NSN 7540-01-280-5500

Standard Form 298 (Rev. 2-89)

Approved for public release; distribution is unlimited.

ANODE FALL AS RELEVANT TO PLASMA THRUSTERS

Brigitte Horner
Lieutenant, United States Navy
B.S.A.E, U.S. Naval Academy, 1987

Submitted in partial fulfillment
of the requirements for the degree of

AERONAUTICAL & ASTRONAUTICAL ENGINEER
and
MASTER OF SCIENCE IN ASTRONAUTICAL ENGINEERING

from the

NAVAL POSTGRADUATE SCHOOL
June 1997

Author: Brigitte Horner
Brigitte Horner

Approved by: Oscar Biblarz
Oscar Biblarz, Thesis Advisor

Christopher L. Frenzen
Christopher L. Frenzen, Thesis Co-Advisor

D. J. Collins
D.J. Collins, Chair
Department of Aeronautical Engineering

ABSTRACT

The behavior of the electric field together with the electron and ion densities in the vicinity of a non-emitting, plane anode is investigated. The selected approach involves non-linear analysis techniques on the continuum equations for steady-state, isothermal conditions where both ionization and two-body recombination are included. Ions, created through electron bombardment of neutral atoms, are repelled toward two stagnation regions: within or near the sheath boundary and near the plasma interface. These equilibria form as a result of the chemistry present: recombination establishes the latter while ionization stipulates the former. As presented, the sheath is fundamentally unstable - ions are driven toward the negative electrode. Using nitrogen data for a numeric example, the following observations are made: a sufficiently strong applied electric field pushes the ion density toward that of the electrons through a well - a constrictive phenomenon. Both a transition region, dominated by density gradients, and a diffusion-driven zone are found to move the system toward the plasma interface. The characteristics of this process are influenced by the applied electric field, but the instability of the chemistry-induced stagnation regions precludes numeric convergence. Insufficient dissipation may prevent the stability of the anode fall model as presented. Suggested improvements to the model descriptions include considering the effects of temperature gradients, magnetic fields, three-body recombination, diffusion written in terms of the electric field, multi-dimensionality and/or time-dependencies.

TABLE OF CONTENTS

LIST OF FIGURES

LIST OF TABLES

ACKNOWLEDGMENTS

During the course of this thesis, invaluable assistance was provided by the expert research personnel at the Dudley Knox Library without whom much of the reference material used would have gone unfound. Additionally, the computer wizardry of the Computer Center staff provided much assistance to someone less "virtually" oriented.

But most of all, I would like to express my gratitude to Professor Biblarz and to Professor Frenzen who through inexhaustible patience allowed a thesis student to express creativity, who "paved the road". Further, I would like to express my appreciation to Professor Woehler, who through his genius was able not only to explain physics but also to convey his passion for the "why of nature" to his students. My deepest gratitude goes to my family and their encouragement that nothing is impossible.

Nomenclature	
D_a	Ambipolar diffusion coefficient
D_e	Electron diffusion coefficient
D_i	Ion diffusion coefficient
D_{o_i}	Undisturbed plasma diffusion coefficient of species: ion, electron
D_t	Transition diffusion coefficient
q	Electron charge
F_e	Electron frictional force
F_i	Ion frictional force
k	Boltzmann constant
ϵ_o	Permittivity of free space
m	Electron mass
M	Ion mass
$n_{o_{i,e}}$	Undisturbed plasma density of species: ion, electron
n_e	Electron density
n_i	Ion density
T_e	Electron temperature
T_i	Ion temperature
T_o	Undisturbed plasma temperature
v_e	Hydrodynamic electron velocity
v_i	Hydrodynamic ion velocity
y	Space coordinate for the plasma model
E	Electric field
E_o	Undisturbed plasma electric field
f_e	Electron collision (elastic) frequency
f_i	Ion collision (elastic) frequency
ν	Ionization coefficient function: Townsend's first coefficient
ν_o	Ionization coefficient numerical value^{-1}: Townsend's first coefficient
α_2	Electron-Ion (Two-body) recombination coefficient
μ_e	Electron Mobility
μ_i	Ion Mobility
j_e	Electron Current
j_i	Ion Current
$j_{o_{i,e}}$	Undisturbed plasma current due to species (ion, electron)
$L_{n_i}, L_{n_e}, L_{j_e}$,	Appropriate characteristic length scales
bar notation	Variables with bar notation: non-dimensional
Bold notation	Variables with bold notation: vectors
[ ] notation	Non-dimensional parameter groupings
λ_i	Jacobian Eigenvalues, I=1,2,3,...
λ_D	Debye Shielding, planar surface
$\hat{A}$, V	Jacobian Matrix and associated eigenvector/manifold

Table 1: Nomenclature

I. INTRODUCTION

Whenever an object starts moving in a given direction, a second object must be present which accepts the reaction of the force that accelerates the first, so says Newton's third law of motion. When a spacecraft moves through empty space, the accelerating forces act between the vehicle and the mass of the propellant expelled. In 1895, the distinguished Russian rocket pioneer Konstantin Eduarovitch Tsiolkovskii derived the famous "Tsiolkovskii equation," the basis of all theoretical work on rocket propulsion. Relating the burnout velocity of a rocket with its exhaust velocity and its mass ratio, this "rocket equation" shows how important it is for the exhaust velocity of a rocket motor to be as high as possible. [Ref. 1: pp. 2-3]

Since mankind's advent into space, several types of space flight propulsion systems have been developed to include chemical, nuclear, electric and solar propulsion devices with the majority of spacecraft to date employing chemical rockets. While the science and technology of chemical rockets developed at a rapid pace, the idea of using the benefits of Maxwell's relations to eject charged particles from a thrust chamber progressed slowly with long intervals between periods of creative thought. In 1945, Herbert Radd recommended the use of fast electrically accelerated particles to reduce fuel mass and in 1946, Jakob Ackeret analyzed the performance capability of a spacecraft by arguing that the total kinetic energy carried away by the exhaust beam corresponded to a reduction of the mass of the vehicle according to $E=mc^2$. Hence, assuming that a certain fraction of the vehicle mass is converted into kinetic beam energy, the total propellant mass can be calculated which in turn leads to a maximum terminal velocity of the spacecraft, a result which is independent of particle size, time of propulsion, conversion method and magnitude of the vehicle. In essence, the optimum exhaust velocity is determined simply by maximizing the terminal velocity. [Ref. 1: pp. 2-3]

Propulsive devices that use Maxwell's Law's differ from chemical systems: the latter is characterized by having the same energy and propulsive sources, while in the former the energy conversion method differs from that of propulsion. In essence, electric propulsion

systems allow greater carrying capacity with shorter flight times. For example, the Hohmann transfer time from a Low-Earth-Orbit (LEO) to the orbit of Pluto requires approximately 45 years if chemical means are considered; an electrically propelled vehicle, in comparison, requires approximately three years. [Ref. 1: p. viii]. The large difference in mass payload ratio (final mass/initial launch mass) obtained is highlighted by an analysis for a Mars mission: a chemical system using a high impulse Hohmann trajectory from LEO delivers approximately 10% to 18% of the launch mass to the Martian surface [Ref. 2: pp. 152], while an electric system using a low impulse spiral trajectory could deliver 20% to 60% of the launch mass, depending on the desired transit time. With effective exhaust velocities as high as 10,000 m/s, electric propulsion thus offers the performance envelope needed for manned interplanetary missions. [Ref. 2: pp. 37]

Electric propulsion systems are divided into three categories: 1) electrostatic, where acceleration is achieved through the interaction of coulombic fields with charged propellant particles, 2) electrothermal, where propellant heated electrically is expanded thermodynamically through a nozzle, and 3) electromagnetic, where acceleration is achieved through the interaction of the Lorentz force with highly ionized gases (plasma). Of the types of electric propulsive thrusters available, electrothermal devices include the resistojet and arcjet. It should be noted that the current necessary to form the plasma in these devices also allows the magnetic field to accelerate the gas. These systems (and for that matter, any device using a thermal nozzle) are, however, limited by the amount of heat that can be added to the flow and are thus ultimately dependent on the materials used. As electromagnetic (EM) thrusters rely on Lorentz interactions to accelerate the flow, these devices are not limited in the sense of electrothermal systems and therefore offer different operational characteristics. The various types of EM thrusters available include the ion engine and plasma thrusters (wide variety to include electrodynamic, magnetoplasma-dynamic or MPD, pulsed-plasma, Hall accelerator, Lorentz force accelerator, pulsed coaxial thruster, plasma arcjet, pulsed ablative thrusters, to name just a few). [Ref. 2: pp. 565-596] The MPD thruster is relevant to this work.

MPD systems are a relatively recent addition to the electric propulsion family,

originally discovered when peculiar behavior of an electrothermal arcjet thruster was investigated. Researchers found that without significant mass flow-rate applied, the arcjet continued to operate in a mode clearly unique: pressure within the thrust chamber was too low for the device to be choked, and so it was theorized that an induced magnetic field from the high arc current accelerated the plasma flow - the magnetoplasmadynamic thruster was "born." [Ref. 3]

The area of research to which MPD thrusters are applied is termed magnetohydrodynamics (MHD), the field of physics that investigates how moving conductive (electrolytic) fluids behave while subjected to applied electric or magnetic fields. The fluids involved must be conductive, or ionized sufficiently to pass a current, and in the case of an MPD, the fluid must reach a plasma state. MHD devices behave analogously to motors or generators and can either add or remove energy from the fluid in exchange for electrical energy; systems developed include the MHD tunnel drive for submarines and the MHD turbine. Magnetoplasmadynamic (MPD) thrusters are currently being considered for application to primary propulsion system on robotic and piloted interplanetary missions; the high specific impulses offered by MPD devices can reduce launch mass requirements by over a factor of two compared to chemical system if the power to thrust conversion efficiency is over 50%. [Ref. 4]

MPD thrusters are classified by considering two major features: 1) the power supply which defines the continuous, quasi-steady and pulsed MPD systems, and 2) the magnetic field which characterizes the self-field and applied-field MPD thrusters [Ref. 3]. A continuous, or steady-state, thruster is one in which the propellant flow and current throughout the device are continuous, thereby allowing the system to reach a high temperature equilibrium state. The quasi-steady thruster does not reach equilibria since it uses a continuous gas flow with rapidly pulsed current, through which high amounts of energy are provided in short bursts. The pulsed thruster is similar to the quasi-steady MPD system except it uses less frequent pulses; equilibrium flow is also not reached and consequently low temperature materials may be used for constructing such a device. The applied- and self-field thrusters define the way in which the primary accelerating field (magnetic) is affected. The

applied-field system employs a large current in an external coil, or large permanent magnets, to accelerate the plasma whereas in the self-field device the current not only ionizes the gas but also creates the field that accelerates the resulting plasma.

The magnetoplasmadynamic thruster was originally discovered in the 1960's, and yet much work remains to understand its fundamental operation. For example, the steady state, self-field MPD thruster operated by the University of Southampton, U.K., was originally developed to simulate the atmosphere effects on structures in LEO, an environment dominated by highly reactive atomic oxygen. The MPD is suited to simulate such conditions as it offers a unique combination of high thrust and high exit velocity. The Southampton MPD presently operates at power levels in the range 6-17 kW but suffers from electrode erosion, instabilities, a contaminated beam and short run-times. Work on this thruster has identified electrode erosion as a major problem, making the device unsuitable for its intended function. Specifically, the mode of erosion differs from that seen at other institutions and the levels of erosion are higher and exhibit a rate increase not seen with other devices. [Ref. 5] Electrode erosion, current spotting, frozen flow loses and electrode power deposition are just several factors that limit the performance of MHD devices [Ref. 6, 7]. Specifically, anode power deposition is the single largest power loss mechanism in MPD thrusters operating at sub-megawatt power levels. [Ref. 8, 9, 10, 11, 12]

To gain further insight to MPD phenomena, computer codes that accurately describe observed data from steady-state MPD thrusters have been developed [Ref. 13, 14, 15]. However, these codes do not adequately describe observed data from quasi-steady thruster experiments. It has been suggested that the lack of proper electrode modeling (i.e., sheaths and fall potentials) in these codes may explain this discrepancy [Ref. 16]; perhaps the difficult set of coupled, nonlinear partial differential equations involved has limited analytical work to model the anode sheath and ambipolar regions. For example, Hugel [Ref. 17] and Subramanian [Ref. 18] address the influence of the sheath region, but do not model the electric field, temperature or sheath fall voltage. Hence, the focus of this work: analysis of the anode voltage drop region.

II. LITERATURE REVIEW

The principal voltage loss mechanism near an electrode can be divided into two main classes: ohmic and sheath losses. Ohmic resistivity occurs because of the finite conductivity of a real plasma, particularly thermal boundary layers, degree and kinetics of ionization and Joule heating. Sheath drops are caused by Debye shielding which forms a space charge field adjacent to the electrode [Ref. 19: pp. 200-204]. Furthermore, material problems restrict the temperatures at which the electrodes can operate. In many cases cooling of the electrodes is required since the plasma, in order to maintain a high ionization, must be hotter than the working temperatures of most materials. This temperature difference between the electrodes and the plasma further aggravates the voltage losses because of the presence of the thermal boundary layers. As has been shown, voltage losses can exceed 50% of the total power output, with sheath drops accounting for a large fraction of this loss. [Ref. 6, 7]

The tool most commonly used for measurement of local plasma properties is the electrostatic probe, a small electrode which may be biased positively or negatively with respect to the plasma in which it is immersed. Such work is relevant to non-emitting anodes which, though heavily biased, also probe and disturb the plasma locally. As a result, most analytical work on sheath phenomena is embodied in probe theory investigations where the effects of an electrode (probe) locally disturb a quiescent plasma. [Ref. 20,21: pp. 1-7, pp. 8-9]

In 1924 Langmuir pioneered the use of electric probes, giving the first sound mathematical basis to this diagnostic technique. The analysis of electrostatic probes in collision-dominated (higher pressure) plasmas began with Davydov and Zmanovskaja [Ref. 22] who assumed that a quasi-neutral diffusion controlled region extended to within one mean free path of the probe where it was matched to the edge of a free-fall sheath; a transition region between the two regimes was not attempted, however. Ecker, et al. [Ref. 23] attempted matching the solution in the collision-dominated region directly to that in the free-fall sheath using variational principles, work which was criticized by Cohen [Ref. 24] based on mathematical grounds: something was forced to fit via some artificially imposed boundary;

matching between separate regions was accomplished through variational principles and consequently was not asymptotic in nature [Ref. 24].

Existing sheath solutions are limited to special case simplifications. Several solutions are available for spherical probes by Kiel [Ref. 25], whose analysis neglected diffusion, Barad and Cohen [Ref. 26], Su and Lam [Ref. 27], as well as by Cohen [Ref. 24, 28]. The latter group carried out the first completely systematic analyses of spherical probes in collision-dominated plasmas. These researchers assumed the continuum-equations valid everywhere in the plasma right up to the probe surface; their results showed both the sheath and the quasi-neutral regions appeared naturally from the diffusion equations. In these efforts, two major assumptions prevail: the plasma was assumed so lightly ionized that only charge-neutral interactions were accounted, and the continuum equations were postulated with an isothermal formulation. For cool, nonequilibrium plasmas, however, charge-charge collisions must be considered [Ref. 29: p. 165]. To that end, McKee and Mitchner [Ref. 30] investigated a collisionless sheath with constant transport properties that also included ionization as well as recombination effects in the ambipolar region. Exploring spherical probe theory further, Cohen and Schweitzer [Ref. 31] then extended Cohen's original asymptotic analysis [Ref. 24] for the entire region, an analysis which allowed for weak ionization and recombination effects while also assuming constant transport coefficients. Su and Sonin [Ref. 32] next formulated a spherical probe theory by considering the effects of electron-ion collisions by approximating diffusion coefficients as a function of the neutral particle density, a density assumed as constant. Barad and Cohen [Ref. 26] then presented a continuum theory (for spherical probes) in which non-constant transport coefficients were used, coefficients based on charge-charge collisional assumptions. This analysis, however, did not incorporate ionization or recombination effects. In work similar to Lam's original theory for flow of weakly ionized gases [Ref. 28], Stahl and Su [Ref. 33] use the same approach of separating the sheath, ambipolar region and free stream; their methods prove the existence of a sheath on a flat probe, yet plasma chemistry is not considered (ionization and recombination). It should be noted that both Su and Lam [Ref. 27], for spherical probes, and Stahl and Su [Ref. 33], for flat probes, consider transition regions to match the inner sheath to the outer quasi-neutral

or ambipolar zones - albeit both research groups neglected plasma reactivity in their formulations. In related work, Godyak and Sternberg [Ref. 34] applied the ionization potential as the boundary condition for both the plasma and the sheath in an effort to understand the electrodynamic properties of the plasma-sheath boundary for the cathode; their analysis, however, assumed constant ionization for the plasma reactivity with recombination neglected.

It may be inferred from these efforts that anode-voltage-drop-region analyses remain insoluble due not only to the nonlinear nature of the equations, but also to the transitional nature of particle motion in most sheaths. In an extensive review of probe theory, Chung, Talbot and Touryan [Ref. 20] state that a general solution for determining charge density and species temperature for probes small relative to boundary layer thicknesses is not available. Additionally, Nasser [Ref. 35] discusses an elementary theoretical approach to the glow discharge problem by introducing a set of one-dimensional governing equations (continuum) - the electron and ion current equations, the net production of electrons and ions, and the Poisson equation. According to Nasser, these equations should have a solution, but most attempts to achieve such have failed, with the difficulty lying in the boundary conditions [Ref. 35: p. 412]. Voltage losses at electrode boundaries and surface erosion, together with sheath effects which influence ionization, play an important role in plasma devices and must be controlled in designs of practical interest. Particularly, thermal arcjets and MPD accelerators deposit between 15% and 80% of the input power into the anode. This presents not only a severe performance penalty, but also introduces thermal design problems since the heat thus generated must be radiated away from the thruster surfaces [Ref. 7, 9].

Completely satisfactory solutions to the anode voltage drop phenomena do not exist for several plasma conditions; one such case involves steady, collisional, low-temperature isothermal discharges [Ref. 36]. For instance, the effect of several parameters on the region require further study, including the influence of temperature, the role of the problem dimensionality as well as the effect of plasma chemistry. It remains unclear, moreover, as to the exact cause of the anode spots which have been observed for various MPD thruster operating conditions, a behavior which appears roughly as periodic oscillations [Ref. 6, 7, 9].

A one-dimensional, collisional, equilibrium solution can satisfactorily reproduce the observed electric field and charge density distributions for the entire anode voltage drop region where the electron temperature equals that of the heavy species [Ref. 36]. However, this model cannot describe any decrease in current density away from the surface, or current constriction, at the anode surface which might be necessary in non-equilibrium. A two-dimensional model, developed by Biblarz and Dolson [Ref. 6], represents these phenomena, in the absence of species ionization and recombination, and predicts the voltage drop in the region: the sheath accounted for a majority of the anode voltage drop [Refs. 6, 7, 36].

Since the pioneering work of Tonks and Langmuir (relating to low-pressure discharges), the anode description has remained as one of the classic problems in plasma physics. In this work, the high density problem is generalized to any electrode surface in contact with a partially-ionized plasma when the current flow is sufficiently small: the problem of a non-emitting electrode (probe) in contact with a thermally generated plasma. An anode is explicitly considered along with a non-emitting cathode and the governing one-dimensional continuum equations are formulated. The electrodynamic behavior of plasma reactivity in the electrode regions is then discussed with considerations given to three distinct zones of the anode voltage drop regime: inner or space-charged sheath, transition and outer or quasi-neutral ambipolar zones.

III. GOVERNING EQUATIONS AND NUMERICAL DATA

A. GOVERNING EQUATIONS

A flat electrostatic probe immersed in a high-density, flowing, partially-ionized gas is considered. For plasmas of moderately high density and low degree of ionization (as applied to discharge lasers and MHD devices), the plasma region affected by an electrode, i.e., the electrode region, can be considered of the boundary-layer type with the transport of charges approximated as one-dimensional. Traditionally, the electrode region is further separated into two distinct zones, as delineated by the species densities: a sheath and an ambipolar region, both which may be of the order of tenths or even hundredths of a millimeter in extent [Ref. 6] where the sheath extent is driven by variation of the electric field and the quasi-neutral region extent is influenced by the influences of chemistry.

The problem is formulated by considering the hydrodynamic continuum equations for two species, ions and electrons. Induced and applied magnetic fields are neglected with energy conservation implicitly satisfied since heat transfer, radiation, Joule heating and surface emission effects are at first neglected (for example, $\mathbf{B}=\mathbf{0}$, $\nabla T_e=0$, $\nabla T_i=0$, $\mathbf{J}\cdot\mathbf{E}=0$).

The equations below are assumed valid throughout the entire domain of interest, to include the electrode (probe) surface. Table (1) lists the nomenclature used:

$$\frac{\partial (Mn_i v_i)}{\partial t} + Mn_i v_i \nabla v_i = qn_i E - kT_i \nabla n_i - Mn_i f_i v_i - F_i \qquad \text{Equation (1a)}$$

$$\frac{\partial (mn_e v_e)}{\partial t} + mn_e v_e \nabla v_e = -qn_e E - kT_e \nabla n_e - mn_e f_e v_e - F_e \qquad \text{Equation (1b)}$$

$$\nabla\cdot\boldsymbol{E} = \frac{q}{\epsilon_o}(n_i - n_e) \qquad \text{Equation (2)}$$

$$\nabla j_i = q\nabla(n_i v_i) \qquad \text{Equation (3a)}$$

$$\nabla j_e = q\nabla(n_e v_e) \qquad \text{Equation (3b)}$$

$$\nabla(n_i v_i) = \nu n_e - \alpha_2 n_i n_e \qquad \text{Equation (4a)}$$

$$\nabla(n_e v_e) = -\nu n_e + \alpha_2 n_i n_e \qquad \text{Equation (4b)}$$

$$\nabla\cdot\boldsymbol{J} = 0 \implies J = j_i + j_e \qquad \text{Equation (5)}$$

Equations (1a) and (1b) describe the momentum-transfer between the ions and electrons with neutrals: the left-hand side represents the unsteady and convective contributions, respectively, while the right-hand side symbolizes coulombic, pressure, collisional and frictional forces, respectively. Next, the electrode is considered as a positive, non-emitting surface (anode). Through this process, a flow of negative charges is induced toward the plate and a flow of positive charges is repelled away from the plate; the anode, in completing the arc current with the cathode, collects incoming electrons while driving all positive charges toward the negative surface. This separation of charge in the anode fall region produces a divergence of the electric field and a variation of potential away from the plate, as given by equation (2) (the variation of potential is readily deduced from Gauss's equation (2)). The current densities are denoted by equations (3a) and (3b) in terms of the species flux of charged particles per unit area. Equations (4a) and (4b) are then the continuity equations for the ion and electron flux as caused by the ionization and electron-ion (two-body) recombination processes: positive ions are produced within the anode fall region by electron impact with neutrals and conversely, positive ions combine with negative electrons to form neutrals. Equation (5) is the conservation of total charge; the sum of the species currents remains constant for a one-dimensional formulation. Hence, from set (1-5), the anode model presented in this work is developed with the following assumptions:

1. Steady state; free-stream plasma is neutral with uniform charge densities (Saha equilibrium).

2. Mean free path of the charged particles is small compared to the sheath thickness which in turn is much smaller than the dimensions of the body; the sheath is treated as a continuum.

3. Chemical equilibrium in the boundary layer; the two-body recombination coefficient is held constant over the entire anode fall region as a first approximation [Ref. 29: p. 238]. Further, the ionization coefficient is treated as Townsend's first coefficient.

4. There is no applied magnetic field and induced magnetic field effects are neglected (low Magnetic Reynolds number) - consequently no ion slip.

5. No continuum radiation losses, no ion emission, no significant Joule heating.

6. Isothermal: $\nabla T_e=\nabla T_i=\nabla T_o=0$ and $T_e=T_i=T_o$. The true electron temperature will either be close to the anode surface temperature or the free stream temperature since thermal equilibrium is assumed in the boundary layer. Because of the relatively small number of collisions that the electrons suffer in the boundary layer, it is frequently argued that the electron temperature is close to the free stream temperature [Ref. 37].

7. Diffusion velocities of the ions and electrons due to electric field interactions are small in comparison with their thermal velocities; diffusion coefficients are assumed constant.

8. End effects, in the case of a planar surface, are neglected.

9. Under the assumption of a highly biased probe, it is possible to ignore convection not only in the very thin transition region, but also in the sheath region, even for sheaths with the same order of thickness as the boundary layer [Ref. 33]. Assuming perfectly elastic collision between the species and neutrals, essentially a constant collisional frequency is assumed sufficiently large so that the convective derivative in (1) can be neglected.

10. With the assumptions of steady state and negligible convection, a spatially homogenous fluid results.

For a semi-infinite plane with coordinate outward from the planar positive surface so that $\nabla \equiv d/dy$, set (1-5) thus becomes:

$$0 = qn_i E - kT_i \frac{d(n_i)}{dy} - Mn_i f_i v_i$$

$$0 = -qn_e E - kT_e \frac{d(n_e)}{dy} - mn_e f_e v_e$$

$$\frac{d(E)}{dy} = \frac{q}{\epsilon_o}(n_i - n_e)$$

$$\frac{d(j_i)}{dy}\left(\frac{1}{q}\right) = \nu n_e - \alpha_2 n_i n_e$$

$$\frac{d(j_e)}{dy}\left(\frac{1}{q}\right) = -\nu n_e + \alpha_2 n_i n_e$$

$$\frac{d(J)}{dy} = 0 \implies J = j_i + j_e$$

Here, equations (3a) and (3b) have been incorporated with equations (4a) and (4b). Using species mobilities, $\mu_{i,e}=\frac{q}{m_{i,e}f_{i,e}}$ and the diffusion coefficients, $D_{i,e}=\frac{kT_{i,e}}{m_{i,e}f_{i,e}}$ (the Einstein relation $\mu_{i,e}=\frac{qD_{i,e}}{kT_{i,e}}$), species momentum conservation can be re-written in terms of species flux, $\Gamma_{i,e}$, where Fick's law of diffusion is a special case (E=0 so that $\mu_{i,e}$=0). Specifically, (1) and (2) become

$$\Gamma_{i,e}=n_{i,e}v_{i,e}=\pm\mu_{i,e}n_{i,e}E-D_{i,e}\nabla n_{i,e} \qquad \text{Equation (6)}$$

Essentially, diffusion is a random process in which a net flux from dense regions to less dense regions occurs simply because more particles begin their motion in the more dense area - the flux is proportional to the density gradient. [Ref. 38: pp. 135-138] But as the species travel toward the electrode, reactivity occurs - ions and electrons recombine while electron collision with neutrals breaks neutrality adding charges to the electrode region; flow neutrality is broken and the fluid is no longer a plasma. Thus, under constant-property conditions, the species continuity equations together with Gauss's equation describe the flux of charges in the vicinity of an electrode or plasma probe. [Ref. 33, 39] With the application of the Einstein relation, set (1-5) are re-cast to give the model used in this work, the geometry for which is shown in Figure (1):

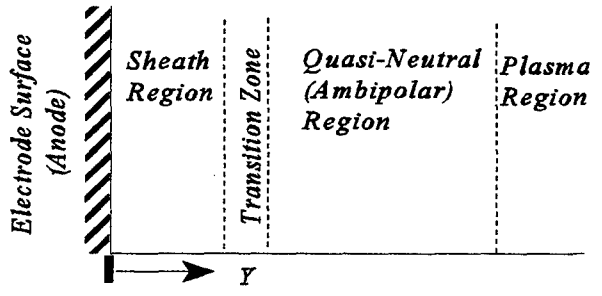

Figure 1: Geometry of Anode Fall Region

To obtain the mathematical model used in this work, the definition of the diffusion coefficient is used to re-write the species elastic collision frequencies, $f_s=[kT_o]/[D_s m_s]$ for isothermal conditions, and the current density is defined as $j_s=qn_s v_s$ where s=i, e. The resulting equations (1-5) are then solved for their highest derivative terms:

$$\frac{d(n_i)}{dy}=\left[\frac{q}{kT_o}\right]n_i E - \left[\frac{1}{q}\right]\frac{j_i}{D_i} \qquad \text{Equation (7a)}$$

$$\frac{d(n_e)}{dy}=-\left[\frac{q}{kT_o}\right]n_e E + \left[\frac{1}{q}\right]\frac{j_e}{D_e} \qquad \text{Equation (7b)}$$

$$\frac{d(E)}{dy}=\left[\frac{q}{\epsilon_o}\right](n_i-n_e) \qquad \text{Equation (8)}$$

$$\frac{d(j_e)}{dy}=-\left[q\right]\nu n_e + \left[q\alpha_2\right]n_i n_e \qquad \text{Equation (9a)}$$

$$\frac{d(j_i)}{dy}=\left[q\right]\nu n_e - \left[q\alpha_2\right]n_i n_e \qquad \text{Equation (9b)}$$

In the formulation of equations (7-9), 14 variables result (three universal constants included). Before analysis of this system, the equations must be written in terms of dimensionless variables and proper parameters. For this work, both the Buckingham Pi Theorem and Fractional Analysis techniques were applied (Appendix A). The Buckingham method, although a useful tool for revealing the dimensionality of the problem, does not bring forth the physical effects which influence system behavior. On the other hand, fractional analysis coupled with the use of the governing equations, begins to give physical meaning to the dimensionless parameters obtained.

Using undisturbed plasma values for normalizing the variables gives three primary length scales for the system modeled by equations (7-9) since $n_{o_i}=n_{o_e}=n_o$, $j_{o_i}=j_{o_e}=j_o$ for the undisturbed, neutral plasma: L_E, $L_{n_i}=L_{n_e}=L_n$, $L_{j_i}=L_{j_e}=L_j$. The results are summarized in Table 2 with

the length scales listed in Table 3:

Governing Equations [Equations (7-9)]	Non-dimensional Parameters via Buckingham Pi's	Non-dimensional Parameters via Undisturbed Plasma Values
$\frac{d(\bar{n}_i)}{d\bar{y}} = \left[a\right]\bar{n}_i\bar{E} - \left[b\right]\frac{\bar{j}_i}{D_i}$	$a = \left[\frac{q}{\pi_1\pi_6 kT_o}\right]$, $b = \left[\frac{\pi_2\pi_8}{\pi_5\pi_6 q}\right]$	$a = \left[\frac{qE_oL_{n_i}}{kT_o}\right]$, $b = \left[\frac{j_{o_i}L_{n_i}}{qn_{o_i}D_{o_i}}\right]$
$\frac{d(\bar{n}_e)}{d\bar{y}} = -\left[c\right]\bar{n}_e\bar{E} + \left[d\right]\frac{\bar{j}_e}{D_e}$	$c = \left[\frac{q}{\pi_1\pi_6 kT_o}\right]$, $d = \left[\frac{\pi_3\pi_7}{\pi_4\pi_6 q}\right]$	$c = \left[\frac{qE_oL_{n_e}}{kT_o}\right]$, $d = \left[\frac{j_{o_e}L_{n_e}}{qn_{o_e}D_{o_e}}\right]$
$\frac{d(\bar{E})}{d\bar{y}} = \left[e\right]\bar{n}_i - \left[f\right]\bar{n}_e$	$e = \left[\frac{\pi_1 q}{\pi_2\pi_6\epsilon_o}\right]$, $f = \left[\frac{\pi_1 q}{\pi_3\pi_6\epsilon_o}\right]$	$e = \left[\frac{qn_{o_i}L_E}{\epsilon_oE_o}\right]$, $f = \left[\frac{qn_{o_e}L_E}{\epsilon_oE_o}\right]$
$\frac{d(\bar{j}_e)}{d\bar{y}} = -\left[g\right]\bar{\nu}_i\bar{n}_e + \left[h\right]\bar{n}_i\bar{n}_e$	$g = \left[\frac{\pi_4 q}{\pi_3\pi_6\pi_9}\right]$, $h = \left[\frac{\pi_4 q\alpha_2}{\pi_2\pi_3\pi_6}\right]$	$g = \left[\frac{q\nu_o n_{o_e}L_{j_e}}{j_{o_e}}\right]$, $h = \left[\frac{q\alpha_2 n_{o_i}n_{o_e}L_{j_e}}{j_{o_e}}\right]$
$\frac{d(\bar{j}_i)}{d\bar{y}} = \left[i\right]\bar{\nu}_i\bar{n}_e - \left[j\right]\bar{n}_i\bar{n}_e$	$i = \left[\frac{\pi_5 q}{\pi_3\pi_6\pi_9}\right]$, $j = \left[\frac{\pi_5 q\alpha_2}{\pi_2\pi_3\pi_6}\right]$	$i = \left[\frac{q\nu_o n_{o_e}L_{j_i}}{j_{o_i}}\right]$, $j = \left[\frac{q\alpha_2 n_{o_i}n_{o_e}L_{j_i}}{j_{o_i}}\right]$
$where\ D_{i,e} \equiv \bar{D}_{i,e}D_{o_{i,e}}$		

Table 2: Non-dimensional Parameters

Sheath: Space-Charge Dominant	Transition Zone: Number Density Gradient Dominant	Ambipolar Region: Equilibrium Near Plasma Boundary
$L_E < L_{n_{i,e}} < L_{j_{i,e}}$	$L_E = L_{n_{i,e}} < L_{j_{i,e}}$	$L_E = L_{n_{i,e}} = L_{j_{i,e}}$
$L_E = \frac{\epsilon_o E_o}{qn_{o_{i,e}}}$, $L_{n_{i,e}} = \frac{kT_o}{qE_o}$, $L_{j_{i,e}} = \frac{j_{o_{i,e}}}{q\nu_o n_{o_{i,e}}}$	$L_{n_{i,e}} = \frac{kT_o}{qE_o} = L_E$, $L_{j_{i,e}} = \frac{j_{o_{i,e}}}{q\nu_o n_{o_{i,e}}}$	$L_{j_{i,e}} = \frac{j_{o_{i,e}}}{q\nu_o n_{o_{i,e}}}$

Table 3: Length Scales via Fractional Analysis

It should be noted that the length scales L_E, L_n and L_j are in agreement with reference 50 if the species conduction currents in the undisturbed plasma are written in terms of thermal velocities and the above electric field and number density scales are combined to form the Debye shielding length for planar surfaces ($L_E L_n = \lambda_D^{1/2}$).

B. NUMERICAL DATA

To gain further insight into the physical models presented, numerical analyses were conducted with data from reference 36 for 6000°K nitrogen; data for the ionization and two-body recombination coefficients are found in Appendix B.

	Data Value
Temperature (°K), T_o	6.0000e+03
Total Current (mA/cm^2), J: used for j_{oi}, j_{oe}	1.0000e+02
Undisturbed Plasma Charge Density (1/m^3), n_o: used for n_{oi}, n_{oe}	1.0000e+19
Undisturbed Plasma Total Density (1/m^3), N:	2.0000e+24
Undisturbed Plasma Electric Field (V/m), E_o	1.2000e+04
E/N (Vcm^2)	6.0000e-17
Pressure (N/m^2), p: from [p=NkT]	1.6560e+05
Two-body recombination coefficient (m^3/s), α_2: [Ref. 40]	1.0000e-13
Ionization coefficient (1/s), v: from [Ref. 41] with $\nu/N \approx 10^{-18}$ (m^3/s) for above E/N converted to Td (1Td=10^{-21}Vm^2)	1.0000e+06
Ion Diffusion Coefficient (m^2/s): $D_i N \approx 4.46(10^{18})T_o^{1/2}$ from [Ref. 42: pp. 2-28]	1.7274e-04
Electron Diffusion Coefficient (m^2/s): $D_i/D_e \sim m/M$	3.1665e-01

Table 4: Numerical Data for Analysis - Nitrogen

IV. PHYSICAL MODEL

A. SPACE-CHARGE REGION: SHEATH

Voltage losses at electrode boundaries, surface erosion and sheath effects play an important role in plasma devices and must be controlled in designs of practical interest. Particularly, thermal arcjets and MPD accelerators deposit between 15% and 80% of the input power into the anode. This presents not only a severe performance penalty, but also introduces thermal design problems since the heat thus generated must be radiated away from the thruster surfaces. [Ref. 7, 9] So a natural question: what happens at the anode?

Near a surface (anode) in contact with a plasma there is a region, the sheath, in which the electric field is strong and in which the electron number density is much larger than that of the ions (see Figures (2) and (3)).

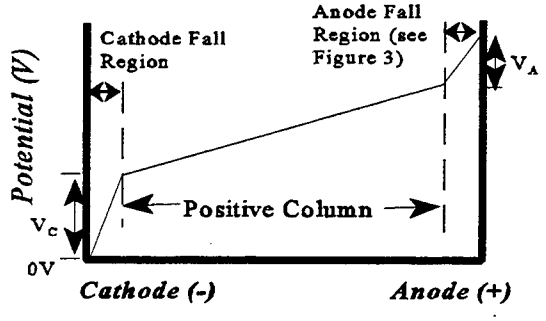

Figure 2: Axial Potential Profile for a High Current Arc Between Two Electrodes (not to scale) [after Ref. 3: p. 114]

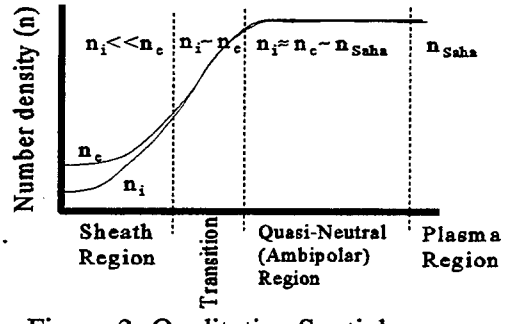

Figure 3: Qualitative Spatial Distribution of Species Densities - Anode Fall Region (not to scale)

Figure (3) shows the qualitative behavior, in the anode fall region, of the spatial distribution of species densities; it is expected that from the wall outward, the densities approach one-another, eventually reaching Saha equilibrium at the plasma boundary. The

overall shape of the curves (Figure (3)) stem purely from the density flux $\frac{dn}{dt} = \nu n - \alpha_2 n^2$,

in the absence of any other types of influences. However, it is usually the interaction of a systems' many parts, not the action of each piece independently, that determines the final system behavior.

The mathematical model developed for the sheath, whether anode or cathode, depends on the details desired: whether surface effects are considered, whether induced or external magnetic fields are included, as to how the flow chemistry is modeled, among others. For the cathode, sheath models usually adopt the assumptions that electrons are in equilibrium with the electric field and that the ionization in the sheath can be neglected [Ref. 34]. In comparison, the electrons in the anode fall must supply by ionization enough ions to account for the ion current that flows out of the positive column toward the cathode [Ref. 43: pp. 59-60]; electrons emerge from the column, are attracted by the anode, gain energy through the voltage drop and ionize neutrals. The extent of the anode sheath is then determined by the space charge distribution and by the magnitude of the gas ionization potential [Ref. 35: p. 420]; hence, the associated length scale for the sheath is governed by that which results from the dimensional analysis of the Gauss equation (8).

Moreover, after a current flow is established between the plates, the anode region may exist in a vapor that issues from the electrodes. In vacuum arcs, Miller [Ref. 44] characterizes the anode region as operating in one of five distinct modes, ranging from a passive, low current mode to a high current, fully developed spot mode. These observed instability phenomena are similar to those noted in MPD thrusters - anode spot formation at high current clearly limits anode lifetime [Ref. 6, 7, 9, 17]. What could cause such "spotting?"

In a comprehensive review of anode-spot phenomena, Miller suggests [Ref. 44] that a sudden increase in the voltage noise frequently indicates that an anode foot-print could be forming or that a transition into the anode-spot mode could be occurring. Further, this abrupt change in voltage has been associated with a sudden change of ion density in the region near the anode, a density decrease that would leave the local electron space charge uncompensated

and thus produce a low-conductivity region. The sudden increase in voltage would then reflect this local shortage of ions - an ion depletion region or ion starvation region. Even-though the most suitable model for the anode region is still actively debated, the general idea of the appearance of an ion deficiency region near the anode as triggering the transition into the anode-spot mode has been fairly supported. [Ref. 44] So, to better understand the processes involved within the anode fall, equations (7-9) are modified as follows:

Because the anode-spot instability is likely related to the species density distribution within the anode fall region, the role of net charge production, the chemistry, should be critical to the overall system behavior: from equations (7-9), the species densities are influenced by both coulombic interactions as well as by the currents and consequent production phenomena, the fine balance between ionization and recombination. Therefore, the current densities as given by equations (9a-9b) are combined with the species densities, equations (7a-7b): the latter are differentiated with respect to the spatial variable in this effort. The result gives for the space-charge region a system of two second order, ordinary, non-linear, coupled differential equations with one first order, coupled, ordinary differential equation. The non-dimensional parameters given in the bracket notation are listed in Tables 2 and 10:

$$\frac{d^2(\bar{n}_i)}{d\bar{y}^2} = \left[a\right]\bar{E}\,\frac{d(\bar{n}_i)}{d\bar{y}} + \left[\frac{bj}{D_i} - af\right]\bar{n}_i\bar{n}_e + \left[ae\right]\bar{n}_i^2 - \left[\frac{bi}{D_i}\right]\bar{n}_e\bar{\nu} \qquad \text{Equation (10a)}$$

$$\frac{d^2(\bar{n}_e)}{d\bar{y}^2} = -\left[c\right]\bar{E}\,\frac{d(\bar{n}_e)}{d\bar{y}} + \left[\frac{dh}{D_e} - ce\right]\bar{n}_i\bar{n}_e + \left[cf\right]\bar{n}_e^2 - \left[\frac{dg}{D_e}\right]\bar{n}_e\bar{\nu} \qquad \text{Equation (10b)}$$

$$\frac{d(\bar{E})}{d\bar{y}} = \left[e\right]\bar{n}_i - \left[f\right]\bar{n}_e \qquad \text{Equation (10c)}$$

Essentially, the conservation laws are combined: species momentum now reflects the influence of charge production terms. Here, the left-hand side of equations (10a-10b) is the rate of change of the number density gradient, an accelerating behavior. The gradient of the species number density is found in the first term on the right-hand side of set (10a-10b), a rate influenced by the strength of the electric field as measured by the imbalance between the species number densities, the Gauss equation (10c). The first term of the right-hand side of (10a-10b) describes the interaction of coulombic and gradient forces, the influence of the equation of motion as described in the earlier formulation of (1-5); the third term completes the formulation of motion in this model. The general concept of energy conservation begins to take shape with the second and fourth terms of (10a-10b): The former has included two-body recombination effects as diminished not only by coulombic interactions, but also by diffusion. The fourth term illustrates a source of energy to the system , ionization, again as influenced by diffusion. Essentially, the accelerating terms on the left-hand side of (10a) and (10b) are described by balances of motion (gradients) and energy (ionization, recombination) where the exchange of energies is brought about and influenced by diffusion processes. It should stand to reason that as the species density gradient increases, energy losses should become more dominant until the gradients diminish their contribution to the flow: recombination should begin to take hold until eventually equilibrium is restored, balancing diffusion with energy source and sink.

B. TRANSITION ZONE: QUASI-NEUTRALITY

In order to determine the behavior of the anode fall, boundary conditions have to be applied to equations (7-9) or to set (10). In the case of the positive column and the cathode fall region, it is known [Refs. 45, 46, 47, 48] that for the isothermal case, the spatial derivatives of the particle density and the drift velocity become singular if the drift velocity attains the ambipolar sound speed [Ref. 49, pp. 77-86; 50]. This apparent singularity appears near the wall, marking the end of the quasi-neutral region and the beginning of the space-charge sheath adjacent to the wall; the ambipolar solution breaks down because the space charge density cannot become larger than the local density of ions or electrons. [Ref. 50; 33; 52: pp. 202-204]. Hence, researchers have always chosen the ion sound speed as the

appropriate bound for the ion velocity. This condition seems a natural compromise between Bohm's criterion for the collisionless sheath which requires the ion velocity exceeds or is at least equal to the ion sound speed and Persson's criterion for an ambipolar flow at the plasma boundary, which states that the ion velocity is in fact less than the ion sound speed. However, these criteria are incompatible as was shown by Godyak and Sternberg. [Ref. 34] For example, in the numerical treatment of the plasma-wall problem without plasma-sheath separation, the ion velocity reaches ion sound speed in the region where plasma neutrality is violated [Ref. 51: p. 51].

It seems that since there is no strict boundary between the plasma and the sheath, it is not obvious which boundary conditions work the best; much controversy remains for the negative electrode. Attempts have been made to bridge or to remove these apparent discontinuities by introducing a transition layer [Ref. 27] or by choosing various plasma-sheath boundary conditions [Refs. 45, 34]. For example, Godyak and Sternberg [Ref. 34] show that the usual choice of choosing the ion sound speed as the boundary, leads to discontinuities of the potential, plasma density and velocity gradients. These workers therefore introduced as their boundary condition a specific value of the electric field that provides a breakdown of the neutrality at the plasma boundary and so treated the sheath and ambipolar model separately, attaining a smooth transition between sheath and plasma - for the cathode region. In their model, however, only constant ionization was assumed for species production.

Fundamentally, the issue of transition in the cathode region remains somewhat controversial, a subject even more unclear when the positive electrode is considered, where essentially scant information is available. But a transition to ambipolar diffusion must occur [Ref. 52: pp. 64-68], a transition where the electric field domination shifts to that of a density gradient driven region, an area where now the length scale for the number density becomes important.

To capture this effect and to retain the role of charge production in the dynamical behavior of the system, equations (7) are again differentiated allowing the species densities to be written in terms of the production terms. Applying the quasi-neutral condition,

$\bar{n}_i \sim \bar{n}_e$, then gives the transition model, equation (11) which can also be obtained from the sheath formulation, set (10).

$$\frac{d^2(\bar{n})}{d\bar{y}^2} = \left(\frac{D_i - D_e}{D_i + D_e}\right)\left[a\right]\bar{E}\frac{d(\bar{n})}{d\bar{y}} + \left(\frac{1}{D_i + D_e}\right)\left[bj + dh\right]\bar{n}^2 - \left(\frac{1}{D_i + D_e}\right)\left[bi + dg\right]\overline{nv}$$

Equation (11)

In comparison to equations (10a-10b), the space-charged model, the effects of diffusion are clearly seen not only on the rate of change of the number density or density gradient term (first term of (11)), but also on the energy balance terms, recombination (second term of (11)) and ionization (third term of 11). Furthermore, coulombic interactions are no longer evident in the energy balance, playing only a secondary role in the density gradient description (first term of (11)).

A key character of equation (11) is that ambipolar diffusion is not yet fully formed, a consequence of the transition region in which perhaps the instability of the sheath, electrostatic repulsion of ions, is carried forth by gradient effects so that ions are further pushed from the positive plate. The growth in densities away from the plate then affects their free diffusion, a process evolving into ambipolar diffusion.

C. AMBIPOLAR REGION

When the density of electrons and ions becomes large enough, their mutual Coulomb fields affect their free diffusion. This modification can be written in terms of the space charge field as given by:

$$\Gamma_{i,e} = n_{i,e} v_{i,e} = \pm \mu_{i,e} n_{i,e} E - D_{i,e} \nabla n_{i,e} \qquad \text{Equation (6)}$$

From (6), it is seen that should the species flux densities not be equal, a significant charge

imbalance would arise. For example, if the plasma is much larger than a Debye length, it must be quasi-neutral and the diffusion rates of the species would adjust themselves so that the same rate from the plasma into the region of quasi-neutrality is achieved: the electrons have a larger thermal velocity as compared to the ions and tend to leave the plasma first. A positive charge is thus left behind creating an electric field of such polarity as to retard the loss of electrons and to accelerate the loss of ions: the plasma, by its very definition, is a neutral fluid. [Ref. 38: p. 139] From this formulation, the ambipolar diffusion coefficient can be determined as $D_a = \frac{D_e \mu_i + D_i \mu_e}{\mu_i + \mu_e}$ where the Einstein relation may be applied to write mobilities in terms of diffusions. It should be pointed out that the ratio D/μ represents a measure of energy [Ref. 52: pp. 60-63], and that if $T_e = T_i$, as is assumed in this work, the ambipolar electric field tends to enhance the diffusion of ions by a factor of two, a diffusion that is primarily controlled by the slower species: $D_a \approx 2D_i$. The primary function of the ambipolar field is then to serve as an energy-exchange mechanism for transferring random kinetic energy from the electrons to the ions such that the ion diffusion continues away from the positive plate. [Ref. 45]

The model for the ambipolar region is thus formulated, again following naturally from equation (10) or from equations (7-9), the sheath model: proceeding as before, equations (7) are differentiated with respect to the spatial variable allowing set (9) to contribute to the densities. However, unlike previous, now set (7) is multiplied by the respective species diffusion coefficient, the result which gives one second order, ordinary differential equation for the density in terms of not only the necessary chemistry, but also in terms of the ambipolar diffusion, D_a:

$$2\frac{d^2(\bar{n})}{d\bar{y}^2} = \left[\frac{bj}{D_i} + \frac{dh}{D_e}\right]\bar{n}^2 - \left[\frac{bi}{D_i} + \frac{dg}{D_e}\right]\bar{n}\,\bar{v} \qquad \text{Equation (12)}$$

In comparison with equation (11), it is immediately seen that the density gradient

contribution, the rate of change of number density, is no longer evident. The only terms remaining in (12) are those of charge production; the system chemistry. As the flow approaches equilibrium near the plasma boundary, the number density must approach that of Saha so that the definition of "plasma" is upheld.

The physical model in summary: the electric field pushes the flow from the electrode surface toward the density gradient dominated region in which the density gradient pushes the system toward the plasma boundary where eventually energy conservation must be satisfied. Ionization must balance recombination such that Saha equilibrium is attained at the plasma boundary. It is in this region that the largest of the length scales has influence: the current or ionization scale. This last scale defines the extent of the anode fall region, a region where flow chemistry becomes paramount, determining plasma equilibrium.

But is the anode fall stable? Previous attempts [Ref. 53] at numerical analysis have proven challenging at best. So a better understanding of the nature of equations (7-9) and sets (10-12) is needed: in the next chapter, non-linear analysis techniques are applied to mathematical models presented previously.

V. ANALYSIS

A. LOCAL ANALYSIS

To begin the analysis of the anode fall, non-linear methods as briefly outlined in Appendix C are used: further information on particular ideas can be found in references 54 and 55, among others.

1. Space-Charge Region: Sheath

To begin an analysis of either equations (7-9) or equations (10), non-linear methods as outlined in Appendix C are used: first, equations (10) are written as a system of first order differential equations, then stagnation points within both systems, equations (7-9) and the first order formulation of equations (10), are determined. Next, the local behavior about these stagnation regions in terms of system characteristics is evaluated, leading to a qualitative stability picture of the system dynamics.

a. Equilibrium (Stagnation) Regions

First equations (7-9) and equations (10), the anode sheath models are analyzed (non-dimensional parameters are given in Table 2):

$$\frac{d(\bar{n}_i)}{d\bar{y}} = \left[a\right]\bar{n}_i\bar{E} - \left[b\right]\frac{\bar{j}_i}{D_i} \qquad \frac{d(\bar{n}_e)}{d\bar{y}} = -\left[c\right]\bar{n}_e\bar{E} + \left[d\right]\frac{\bar{j}_e}{D_e} \qquad \text{Equations (7a)-(7b)}$$

$$\frac{d(\bar{E})}{d\bar{y}} = \left[e\right]\bar{n}_i - \left[f\right]\bar{n}_e \qquad \text{Equations (8)}$$

$$\frac{d(\bar{j}_e)}{d\bar{y}} = -\left[g\right]\bar{\nu}_i\bar{n}_e + \left[h\right]\bar{n}_i\bar{n}_e \qquad \frac{d(\bar{j}_i)}{d\bar{y}} = \left[i\right]\bar{\nu}_i\bar{n}_e - \left[j\right]\bar{n}_i\bar{n}_e \qquad \text{Equations (9a)-(9b)}$$

where $D_{i,e} \equiv \bar{D}_{i,e} D_{o_{i,e}}$

$$\frac{d^2(\bar{n}_i)}{d\bar{y}^2} = \left[a\right]\bar{E}\,\frac{d(\bar{n}_i)}{d\bar{y}} + \left[\frac{bj}{D_i} - af\right]\bar{n}_i\bar{n}_e + \left[ae\right]\bar{n}_i^2 - \left[\frac{bi}{D_i}\right]\bar{n}_e\bar{\nu} \qquad \text{Equation (10a)}$$

$$\frac{d^2(\bar{n}_e)}{d\bar{y}^2} = -\left[c\right]\bar{E}\,\frac{d(\bar{n}_e)}{d\bar{y}} + \left[\frac{dh}{D_e} - ce\right]\bar{n}_i\bar{n}_e + \left[cf\right]\bar{n}_e^2 - \left[\frac{dg}{D_e}\right]\bar{n}_e\bar{\nu} \qquad \text{Equation (10b)}$$

$$\frac{d(\bar{E})}{d\bar{y}} = \left[e\right]\bar{n}_i - \left[f\right]\bar{n}_e \qquad \text{Equation (10c)}$$

The original model, equations (7-9) can immediately analyzed, whereas equations (10) have to be recast as a set of coupled, first-order differential equations.

$$\frac{d(\bar{n}_i)}{d\bar{y}} = x_1$$

$$\frac{d(x_1)}{d\bar{y}} = \left[a\right]\bar{E}\,x_1 + \left[\frac{bj}{D_i} - af\right]\bar{n}_i\bar{n}_e + \left[ae\right]\bar{n}_i^2 - \left[\frac{bi}{D_i}\right]\bar{n}_e\bar{\nu} \qquad \text{Equation (10a)}$$

$$\frac{d(\bar{n}_e)}{d\bar{y}} = x_2$$

$$\frac{d(x_2)}{d\bar{y}} = -\left[c\right]\bar{E}\,x_2 + \left[\frac{dh}{D_e} - ce\right]\bar{n}_i\bar{n}_e + \left[cf\right]\bar{n}_e^2 - \left[\frac{dg}{D_e}\right]\bar{n}_e\bar{\nu} \qquad \text{Equation (10b)}$$

$$\frac{d(\bar{E})}{d\bar{y}} = \left[e\right]\bar{n}_i - \left[f\right]\bar{n}_e \qquad \text{Equation (10c)}$$

To find the stagnation points within these first-order system, the derivative terms are each set to zero and non-dimensional parameters from Table 2 are applied. The results give for the equilibrium criteria:

1. From equations (8) and (10c), $\bar{n}_i^* = \bar{n}_e^* = \bar{n}^*$ as expected; this result is then incorporated into equations (9a-9b) as well as (10a-10b).

2. Similarly, from equations (9a-9b) and (10a-10b), $\bar{n}^* = 0$ or $\bar{n}^* = \dfrac{\nu_o \bar{\nu}}{\alpha_2 n_o}$; a stagnation point appears when $\bar{n}_e^* = \bar{n}_i^* = \bar{n}^* = 0$ and when the plasma boundary is approached. The latter condition immediately emphasizes the flow chemistry, ionization and recombination. Without recombination, the second stagnation would not be present, as seen from either equations (9a-9b) or equations (10a-10b) with d/dy[ ]=0. The former equilibrium, on the other hand, seems artificial at first, unless the species densities behave such that they cross when $\bar{n}_e^* = \bar{n}_i^* = \bar{n}^* = 0$, immediately implying a quasi-neutral condition since equation (8) or equation (10c) require $\bar{n}_i^* = \bar{n}_e^* = \bar{n}^*$ at stagnation. In general, the fixed points found stem purely from the chemistry behavior, equations (9a-9b) and consequently (10a-10b) in which ionization and two-body recombination are the only processes included. If, on the

other hand, three-body recombination is added to the equations, then additional stagnation regions become evident since equations (9a-9b) are now cubic. The equilibrium region near $\bar{n}_e^* = \bar{n}_i^* = \bar{n}^* = 0$ still remains, however. Similarly, if ionization is the only production term considered in the sheath model, then the stagnation region near the plasma boundary "disappears." The condition $\bar{n}_e^* = \bar{n}_i^* = \bar{n}^* = 0$ remains for all cases: ionization only, ionization with two-body recombination, ionization with two- and three-body recombination. So it appears that continuity (equations (9)) requires flow equilibrium when perhaps quasi-neutral conditions are initially met, at the sheath boundary, and when the plasma interface is approached. It is recombination that establishes the latter while the presence of ionization stipulates the former.

3. The current densities at the equilibrium position can be found by using $\bar{n}^* = 0$ or $\bar{n}^* = \dfrac{\nu_o \bar{\nu}}{\alpha_2 n_o}$ with equations (7a-7b): if $\bar{n}^* = \dfrac{\nu_o \bar{\nu}}{\alpha_2 n_o}$, then

$$\bar{j}_i^* = \left[\frac{q^2 E_o D_i \nu_o}{k T_o \alpha_2 j_{o_i}}\right] \bar{E}^* \bar{\nu}^* \quad and \quad \bar{j}_e^* = \left[\frac{q^2 E_o D_e \nu_o}{k T_o \alpha_2 j_{o_e}}\right] \bar{E}^* \bar{\nu}^*$$

since $n_{o_i} = n_{o_e} = n_o$ when $\bar{n}_i^* = \bar{n}_e^* = \bar{n}^*$. Here, the influence of not only ionization and recombination, but also of diffusion on the current density distributions are clearly seen. Similarly, from equations (7a-7b), $\bar{j}_{i,e}^* = 0 \ \forall \bar{n}^* = 0$.

4. Charge conservation is used to isolate the value of the electric field at stagnation near the plasma boundary, where $\bar{n}^* = \dfrac{\nu_o \bar{\nu}}{\alpha_2 n_o}$. That is,

$$\nabla \cdot \boldsymbol{J} = 0 \Rightarrow J = j_e + j_i = J_o \quad or \quad \bar{j}_e + \bar{j}_i = 1 \quad gives$$

$$\bar{j}_e^{\,*} + \bar{j}_i^{\,*} = 1$$

$$\left[\frac{q^2 E_o D_e \nu_o}{kT_o \alpha_2 j_{o_e}}\right] \bar{E}^{\,*} \bar{\nu}^{\,*} + \left[\frac{q^2 E_o D_i \nu_o}{kT_o \alpha_2 j_{o_i}}\right] \bar{E}^{\,*} \bar{\nu}^{\,*} = 1 \quad or$$

$$\bar{E}^{\,*} \bar{\nu}^{\,*} = \frac{1}{\left[\frac{q^2 E_o D_e \nu_o}{kT_o \alpha_2 j_{o_e}}\right] + \left[\frac{q^2 E_o D_i \nu_o}{kT_o \alpha_2 j_{o_i}}\right]}$$

from which $\bar{E}^{\,*}$ is obtained graphically since the right-hand side of this expression simply represents a constant. Applying the Arrhenius function [Ref. 52: pp. 94-109] for the ionization, $\bar{\nu} \sim e^{\left[\frac{-1}{\bar{E}}\right]} = \frac{\nu}{\nu_o}$ and using numerical data for nitrogen yields $\bar{E}^{\,*} \approx 0.54$. From this, $\bar{j}_e^{\,*} \approx 0.99816$, $\bar{j}_i^{\,*} \approx 0.0005445$, $\bar{n}^{\,*} \approx 0.15695$. These results show the relative magnitude of the electron and ion currents within the anode fall, $j_e \gg j_i$ as expected. If, on the other hand, $\bar{j}_{i,e}^{\,*} = 0 \;\; \forall \bar{n}^{\,*} = 0$ is used, an inconclusive result is obtained: $\bar{E}^{\,*}$ cannot be isolated from either equations (7-9) or equations (10). Further, $\bar{\nu} \sim e^{\left[\frac{-1}{\bar{E}}\right]} = \frac{\nu}{\nu_o}$ does not permit zero field. Therefore, it seems reasonable that a finite field should exist over the entire range of the anode sheath. Von Engel [Ref. 56: pp. 12-20] highlights such arguments: a finite field must be allowed, which could then introduce a potential trough. A virtual anode is thought to exist if the space charges have the same sign as the nearby electrode, with the emitting surface located at the potential minimum [Ref. 56: pp. 14-17].

The fixed points found in the model represented by equations (7-9) and in part by set (10) are listed in Table 5 below, featuring the role of ionization, recombination and diffusion in the

existence of the fixed point near the plasma boundary. Again, continuity (equations (9)) seems to require flow equilibrium when perhaps quasi-neutral conditions are initially met, the sheath boundary, and when the plasma interface is reached. It is the recombination phenomena that establishes the latter stagnation region while the presence of ionization stipulates the former.

Variable	$\bar{n}_1^*$ Near the Sheath Boundary	$\bar{n}_2^*$ Near the Plasma Interface	$\bar{n}_2^*$ Numerical Value for Nitrogen
$\bar{n}^*$	0	$\frac{v_o \bar{v}}{\alpha_2 n_o}$	0.15695
$\bar{E}^*$	$\bar{E}^*$ finite	$\bar{E}^* \bar{v}^* = \frac{1}{\frac{q^2 E_o v_o D_i}{kT_o \alpha_2 j_{o_i}} + \frac{q^2 E_o v_o D_e}{kT_o \alpha_2 j_{o_e}}}$	0.54
$\bar{j}_e^*$	0	$\bar{j}_e^* = \left[\frac{q^2 E_o D_e v_o}{kT_o \alpha_2 j_{o_e}}\right] \bar{E}^* \bar{v}^*$	0.99816
$\bar{j}_i^*$	0	$\bar{j}_i^* = \left[\frac{q^2 E_o D_i v_o}{kT_o \alpha_2 j_{o_i}}\right] \bar{E}^* \bar{v}^*$	0.0005445

Table 5: Stagnation Regions in General Sheath Model - Ionization with Two-body Recombination

b. Jacobian at the Equilibrium Positions

To determine the system characteristics about its fixed points, a local Taylor series expansion is carried out about the equilibrium of interest (Appendix C); the rate of change of the flow is given in terms of the Jacobian, which for equations (7-9) becomes:

$$\hat{A}_{inner} = \begin{bmatrix} [a]\bar{E} & 0 & [a]\bar{n}_i & 0 & -\left[\frac{b}{D_i}\right] \\ 0 & -[c]\bar{E} & -[c]\bar{n}_e & \left[\frac{d}{D_e}\right] & 0 \\ [e] & -[f] & 0 & 0 & 0 \\ [h]\bar{n}_e & -[g]\bar{v}+[h]\bar{n}_i & \frac{-[g]\bar{n}_e\bar{v}}{\bar{E}^2} & 0 & 0 \\ -[j]\bar{n}_e & [i]\bar{v}-[j]\bar{n}_i & \frac{[i]\bar{n}_e\bar{v}}{\bar{E}^2} & 0 & 0 \end{bmatrix}$$

Here, six variables affect the system dynamics: ion and electron number densities, electric field, species diffusivities, and ionization. Of these, the diffusion coefficients are assumed constants, so essentially four variables drive the behavior: species densities, electric field and consequently ionization. If $\hat{A}_{inner}$ is evaluated at the stagnation points, the resulting eigenvalues describe the dynamics in the neighborhood of the fixed point (Appendix C). Specifically, at the plasma boundary equilibrium with nitrogen data:

$$\lambda_1 = 1.376704 \quad \lambda_2 = 0$$
$$\lambda_3 = 0.630455 \quad \lambda_4 = -1.37437$$
$$\lambda_5 = -0.63279$$

For this case, the eigenvalues are real and distinct, leading to a multi-dimensional type of "saddle" behavior (Appendix C). The stagnation region near the plasma boundary is unstable: the largest eigenvalue is positive, indicative of exponential growth. Appendix D lists the roots

of the characteristic polynomial of $\hat{A}_{inner}$. It appears λ_1 gives exponential growth - the process of ion repulsion from the positive plate forces the instability of the sheath. The sheath drives the system toward the first stagnation criterion, toward quasi-neutrality.

Provided a finite field exists when $\bar{n}_e^* = \bar{n}_i^* = \bar{n}^* = 0$, then the fixed point in its vicinity gives a similar qualitative behavior: the eigenvalues of the resulting Jacobian are given by

$$\lambda_1 = [a]\bar{E} \qquad \lambda_{2,3} = 0$$

$$\lambda_{4,5} = -\frac{[c]\bar{E}}{2} \pm \frac{\sqrt{\left([c]\bar{E}\right)^2 - 4\left[\frac{dg}{D_e}\right]\bar{\nu}}}{2} \qquad where \qquad \bar{\nu} \sim e^{\left[\frac{-1}{\bar{E}}\right]} = \frac{\nu}{\nu_o}$$

These eigenvalues are always real with two characteristics equal while the remaining are distinct: Table 6 lists some numerical examples for nitrogen data.

	$\bar{E}$ 0.04	$\bar{E}$ 3.00	$\bar{E}$ 10.00
$\lambda_1 = [a]\bar{E}$	0.04	3.00	10.00
λ_2=0	0	0	0
λ_3=0	0	0	0
$\lambda_4 = -\frac{[c]\bar{E}}{2} - \frac{\sqrt{\left([c]\bar{E}\right)^2 - 4\left[\frac{dg}{D_e}\right]\bar{v}}}{2}$	-0.04	-2.9986	-9.99947
$\lambda_5 = -\frac{[c]\bar{E}}{2} + \frac{\sqrt{\left([c]\bar{E}\right)^2 - 4\left[\frac{dg}{D_e}\right]\bar{v}}}{2}$	~0	-0.0014	-0.00053

Table 6: Eigenvalues of Stagnation Region n_i=n_e=n=0 with Finite Field - Numerical Values for Nitrogen

Again, the essential feature of the sheath is instability: ions are driven from the positive wall as required by electrostatics. The stagnation region near $\bar{n}_e^* = \bar{n}_i^* = \bar{n}^* = 0$ is unstable, perhaps pushing the system away toward the recombination induced equilibrium near the plasma boundary. It is the strength of the initially applied electric field that imposes the stability characteristics for the fixed point $\bar{n}_e^* = \bar{n}_i^* = \bar{n}^* = 0$. This leads to the following question: is the sheath model, as presented by either equations (7-9) or set (10), an example of a system in which a certain type of "fixed point" is always present, a stagnation region satisfying quasi-neutrality and thereby representing the sheath boundary? If so, does this equilibrium present a type of transcritical bifurcation (see Appendix C) whose stability perhaps depends on the initially applied electric field? The foregoing does suggest so.

The precarious nature of the fixed points found in the sheath model suggest that numerical integration methods will not prove fruitful over the entire domain of the anode fall.

However, by exploring the various regimes of equations (7-9) in the form of the second order differential equations given by equations (10), further insight into the anode fall could be expected.

2. Transition Zone: Quasi-Neutrality

Previously, it has been shown that the sheath is inherently unstable, that the ions are electrostatically repelled from the electrode (anode) surface. If through that process quasi-neutrality occurs, then for steady-state conditions either density gradients or diffusive processes have to drive the system toward the plasma boundary since the condition of $\bar{n}_i \sim \bar{n}_e$ stipulates the electric field be constant; so something else has to continue driving the ions away from the anode wall. Equation (11) highlights the density gradient and is considered next as a set of coupled first-order differential equations:

$$\frac{d^2(\bar{n})}{d\bar{y}^2} = \left(\frac{D_i - D_e}{D_i + D_e}\right)\left[a\right]\bar{E}\frac{d(\bar{n})}{d\bar{y}} + \left(\frac{1}{D_i + D_e}\right)\left[bj + dh\right]\bar{n}^2 - \left(\frac{1}{D_i + D_e}\right)\left[bi + dg\right]\overline{nv}$$

Equation (11)

which give

$$\frac{d(\bar{n})}{d\bar{y}} = x_1$$
$$\frac{d(x_1)}{d\bar{y}} = \left(\frac{D_i - D_e}{D_i + D_e}\right)\left[a\right]\bar{E}x_1 + \left(\frac{1}{D_i + D_e}\right)\left[bj + dh\right]\bar{n}^2 - \left(\frac{1}{D_i + D_e}\right)\left[bi + dg\right]\overline{nv}$$

Equation (11)

where the electric field is constant due to quasi-neutral conditions, $\bar{n}_i \sim \bar{n}_e$.

a. Equilibrium (Stagnation) Regions

To find the stagnation points within these first-order system, the derivative terms are each set to zero and non-dimensional parameters from Table 2 are applied. The results gives for the equilibrium criteria:

1. Setting d [ ]/dy=0 in equation (11) immediately gives the previously found stagnation condition near the plasma boundary: $\bar{n}^* = \frac{\nu_o \bar{v}}{\alpha_2 n_o}$. The fixed point $\bar{n}^* = 0$ again seems to present a mathematical phenomenon since equation (11) does not describe the sheath condition. If quasi-neutral arguments are again used, then perhaps the condition $\bar{n}^* = 0$ may have meaning - the plasma shields itself against external influences (electric field), and so, quasi-neutral characteristics are fundamental to its definition. The stagnation region at $\bar{n}^* = 0$ does, perhaps, present a physical phenomenon: the onset of quasi-neutrality or the sheath boundary, found as a consequence of ionization present in the sheath model and in equations (11), the "transition" model.

2. The magnitude of the constant electric field, and therefore constant ionization, at the start of the quasi-neutral transition is determined by the matching conditions when $\bar{n}_i \sim \bar{n}_e$. These criteria are either found through analytically matching equations (10) with equations (11) for some small parameter(s), or numerically. Numeric methods will be considered later in this work. Suggestions toward an analytic matching attempt are provided in paragraph B below.

b. Jacobian at the Equilibrium Positions

To determine the system characteristics about its fixed points, a local Taylor series expansion is carried out about the equilibrium of interest (Appendix C); the rate of change of the flow is given in terms of the Jacobian, which for equation (11) becomes:

$$\hat{A}_{transition} = \begin{bmatrix} 0 & 1 \\ \frac{1}{D_i+D_e}\left[2\left(bj+dh\right)\bar{n}-\left(bi+dg\right)\bar{v}\right] & \left(\frac{D_i-D_e}{D_i+D_e}\right)a\bar{E} \end{bmatrix}$$

Since the electric field becomes constant at the onset of quasi-neutrality at the sheath boundary, the electric field thus locks in the behavior of the transition region. To determine these stability characteristics, the general eigenvalues of $\hat{A}_{transition}$ are determined:

$$\lambda_{1,2} = \frac{a\bar{E}(D_i-D_e)}{2(D_i+D_e)} \pm \frac{\sqrt{a^2\bar{E}^2(D_i-D_e)^2-4\bar{v}(D_i+D_e)(bi+dg)+8\bar{n}(D_i+D_e)(bj+dh)}}{2(D_i+D_e)}$$

where the non-dimensional parameters are listed in Tables 2 and 10. These eigenvalues determine the dynamical behavior of the transition when $\hat{A}_{transition}$ is evaluated at a fixed points, albeit the electric field strength is determined from the sheath as the system reaches $\bar{n}_i \sim \bar{n}_e$. By inspection of the first term found in these eigenvalues, the following is observed:

1. If the field is positive, then the system displays exponential decay, stability; but electrostatics demands that ions be repelled from the positive plate. This leads to the expectation that the transition zone is also unstable, similar to the sheath. Consequently, the field should be negative at the point of quasi-neutrality.

2. Using the stagnation criteria for $\bar{n}^* = 0$ with finite field indicates that the characteristics should display stable behavior for positive field, the diffusion difference

$(D_i\text{-}D_e)$ is negative, and unstable behavior for negative field. The initially applied electric field strength then does determine the stability of the fixed point $\bar{n}^* = 0$, an equilibrium which appears when ionization is present in the model.

3. To find the behavior near the plasma boundary when $\bar{n}^* = \frac{\nu_o \bar{v}}{\alpha_2 n_o}$, nitrogen data along with an arbitrary selected field strength, $\bar{E}(\bar{y}_{\bar{n}_i \sim \bar{n}_e}) = -5.00$ are used to give the eigenvalues λ_1=-0.041 and λ_2=5.026: the eigenvalues are real, distinct and predict a saddle-type behavior near the plasma boundary - a robust linearization (see Appendix C). For this case, the flow field, locally, is characterized by a very strong unstable manifold corresponding to λ_2. A similar result was found by analyzing the sheath model presented by either equations (7-9) or equations (10).

4. On the other hand, if the sheath behavior at quasi-neutral formation gives a positive field, e.g., $\bar{E}(\bar{y}_{\bar{n}_i \sim \bar{n}_e}) = 5.00$, then the Jacobian eigenvalues predict stability locally about the fixed point: λ_1=0.021 and λ_2=-5.013 where now the saddle behavior is marked with a strong, stable manifold, contrary to the sheath analysis earlier.

Thus, the criteria found at the onset of quasi-neutrality at the sheath boundary form the initial conditions imposed upon the transition zone and hence govern the stability characteristics of the fixed points at $\bar{n}^* = 0$ and $\bar{n}^* = \frac{\nu_o \bar{v}}{\alpha_2 n_o}$.

3. Ambipolar Region

In the sheath, ions are repelled electrostatically until quasi-neutrality occurs, where chemical processes balance such that the ion density approaches that of the electrons - the electric field becomes constant. If this balance does not reflect total charge neutrality, i.e., Saha equilibrium, then other processes (the field is now constant) must drive the system toward such equilibrium; however, a stabilizing mechanism must be available once the

densities are near the plasma boundary. So as the species density gradient increases, energy losses should become more dominant until the gradients diminish their contribution to the flow: recombination should begin to take hold until eventually equilibrium is restored, balancing diffusion with energy source and sink - ambipolar diffusion becomes the vehicle which takes the flow density toward the plasma stagnation. To translate these physical processes to a mathematical model, quasi-neutral conditions, $\bar{n}_i \sim \bar{n}_e$, are applied to the sheath equations (10) from which equation (12) results naturally, highlighting the ambipolar diffusion in its full form:

$$2\frac{d^2(\bar{n})}{d\bar{y}^2} = \left[\frac{bj}{D_i}+\frac{dh}{D_e}\right]\bar{n}^2 - \left[\frac{bi}{D_i}+\frac{dg}{D_e}\right]\bar{n}\,\bar{v} \qquad \text{Equation (12)}$$

or

$$2\frac{d(\bar{n})}{d\bar{y}} = x_1$$
$$\frac{d(x_1)}{d\bar{y}} = \left[\frac{bj}{D_i}+\frac{dh}{D_e}\right]\bar{n}^2 - \left[\frac{bi}{D_i}+\frac{dg}{D_e}\right]\bar{n}\,\bar{v} \qquad \text{Equation (12)}$$

where the electric field is constant due to quasi-neutral conditions, $\bar{n}_i \sim \bar{n}_e$.

a. Equilibrium (Stagnation) Regions

To find the stagnation points within this first-order system, the derivative terms are each set to zero and non-dimensional parameters from Table 2 are applied. The results gives for the equilibrium criteria:

1. Setting d [ ]/dy=0 in (12) immediately gives the previously found stagnation condition near the plasma boundary: $\bar{n}^* = \dfrac{\nu_o \bar{v}}{\alpha_2 n_o}$.

2. Similar to the transition zone, the fixed point $\bar{n}^* = 0$ again presents a mathematical phenomenon until physical arguments are applied as before. $\bar{n}^* = 0$ perhaps indicates the onset of quasi-neutral conditions.

The magnitude of the constant electric field, and therefore constant ionization, at the start of the quasi-neutral ambipolar region continues from the transition zone and again locks in the behavior of the ambipolar region: the initial field strength determines the initial conditions for, and consequently the stability of, the transition zone. The way in which the density gradient then develops influences the initial conditions to the ambipolar region. All in all, the initially applied electric field strength impacts the stability of the anode fall, in entirety - the electric field directly influences ionization and hence the stagnation found near the onset of quasi-neutrality.

b. Jacobian at the Equilibrium - Analysis

To determine the system characteristics about its fixed points, a local Taylor series expansion is carried out about the equilibrium of interest (Appendix C); the rate of change of the flow is given in terms of the Jacobian, which for equation (12) becomes:

$$\hat{A}_{ambipolar} = \begin{bmatrix} 0 & 1 \\ \left(\frac{bj}{D_i} + \frac{dh}{D_e}\right)\bar{n} - \frac{1}{2}\left(\frac{bi}{D_i} + \frac{dg}{D_e}\right)\bar{v} & 0 \end{bmatrix}$$

with general eigenvalues

$$\lambda_{1,2} = \pm \frac{\sqrt{-2D_iD_e\left[-2\bar{n}(D_e bj + D_i dh) + \bar{v}(D_e bi + D_i dg)\right]}}{2D_iD_e}$$

If the stagnation conditions near the plasma boundary are applied, it can be easily be seen that the ambipolar eigenvalues are always real and distinct, again predicting the saddle-type

behavior (Appendix C). In comparison to both the sheath and the transition zone, the electric field no longer is found explicitly part of the Jacobian eigenvalues, however an implicit role is still evident in terms of the ionization. Furthermore, diffusion and chemistry are part in all eigenvalues, from sheath to ambipolar.

Proceeding as before, the Jacobian is evaluated at the plasma boundary stagnation, $\bar{n}^* = \frac{v_o \bar{v}}{\alpha_2 n_o}$, using nitrogen data. The initial field strength is chosen arbitrarily; "initial" is defined as that condition found at the onset of the ambipolar region as determined by matching criteria between sheath and transition, at the beginning of quasi-neutrality. The resulting Jacobian eigenvalues or characteristics are again robust (system non-linearities do not change the qualitative nature of the flow) [Ref. 54: p. 163]. That is, if $\bar{E}(\bar{y}_{\bar{n}_i \sim \bar{n}_e}) = -5.00$, $\lambda_{1,2} = \pm 37.13$, whereas if $\bar{E}(\bar{y}_{\bar{n}_i \sim \bar{n}_e}) = 5.00$, $\lambda_{1,2} = \pm 30.4$. Although the eigenvalues are real and distinct, they are of the same magnitude: exponential growth is exactly offset by exponential decay - a hallmark of energy conservation or homoclinic behavior (see Appendix C). The phase portrait for equations (12), $\bar{n}(\bar{y})$ vs $\frac{d[\bar{n}(\bar{y})]}{d\bar{y}}$, using nitrogen data, is shown in Figure (4).

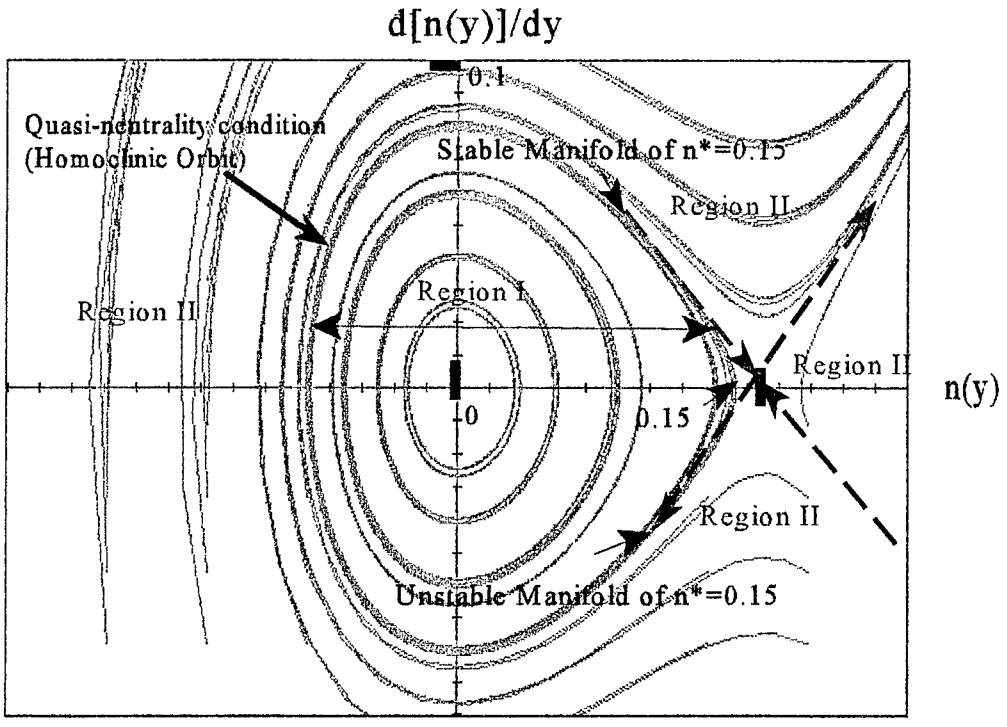

Figure 4: Phase Portrait for Ambipolar Region, Equation (12), with Nitrogen Data for 64 Different Initial Conditions using Ionization and Two-Body Recombination

Can the stagnation near the plasma boundary be reached? Is this region stable? The behavior of the ambipolar region is driven by the initial conditions as applied to equations (12) as shown by figure (4): if the initial conditions are such that region I is dominant, then the manifolds of the stagnation near the plasma boundary, the saddle behavior (see Appendix C), confine the system trajectories. If, on the other hand, the initial conditions are such that region II is dominant, then the system will become unstable. The manifolds of this linearization form the threshold, at least locally, which perhaps determines the requirements for quasi-neutrality - the homoclinic trajectories, as given below:

$$V_{saddle\ \ manifold} = \begin{bmatrix} \bar{n} \\ \dfrac{d(\bar{n})}{d\bar{y}} \end{bmatrix} = \begin{bmatrix} \pm\sqrt{\dfrac{-2D_iD_e}{\left[-2\bar{n}(D_ebj+D_idh)+\bar{v}(D_ebi+D_idg)\right]}} \\ 1 \end{bmatrix}$$

Here, the contributions of ambipolar diffusion, ionization and two-body recombination are clearly seen; two-body recombination is found in the non-dimensional parameters [h] and [j]. More often than not, these homoclinic trajectories can be volatile: any numeric round-off error incurred through whatever computational algorithm used, will induce sufficient non-linearities that will prevent the solution from being "pinned" to these manifolds, the manifolds will break. Even if it were possible to achieve this exact trajectory, the initial conditions imposed by matching the transition region to the ambipolar equation will most likely make such efforts challenging. That is, the initial conditions provided to the quasi-neutral region by the sheath determine the behavior of the ambipolar evolution: either stable periodicity as shown by region I in Figure (4), or exponential growth as indicated by region II. In either case, the behavior of the sheath ultimately determines the behavior of the outer regions and therefore the anode fall, in general.

4. Comments/Observations

The preceding suggests that:

1. Ions, created through electron bombardment of neutral atoms throughout the anode fall region, are repelled electrostatically from the positive electrode toward a location of quasi-neutrality at the sheath boundary as well as toward an unstable stagnation region near the plasma interface. These equilibria form as a result of the chemistry present. That is, continuity (equations (9)) seems to require flow equilibrium when quasi-neutral conditions are initially met within the sheath, and when the plasma boundary is reached. It is recombination that establishes the latter while the presence of ionization stipulates the former. Fundamentally, the sheath as formulated is inherently unstable - ions are driven out of the system, toward the

negative electrode: it is the role of the anode, after all, to provide the positive current to the cathode [Ref. 43: p. 59].

2. At the moment of quasi-neutrality, when $\bar{n}_i \sim \bar{n}_e$, there appears a conservative phenomenon, such that the energy growth is matched by the energy loss - a chemical balance. Is the sheath model as presented, an example of a system in which a certain type of "fixed point" is always present, a stagnation region satisfying quasi-neutrality? If so, does this equilibrium present a type of transcritical bifurcation whose stability depends on the initially applied electric field? The brief analysis given in this chapter does suggest such behavior - the onset of quasi-neutral characteristics, the sheath boundary, might be indicative of a transcritical bifurcation.

3. The quasi-neutral balance, however, is insufficient to provide the necessary stability condition to ensure the system progresses toward, and remains in the close vicinity of, the plasma boundary fixed point. As such, any numeric solutions will most likely be difficult to achieve. That is, the initial conditions provided to the quasi-neutral region by the sheath determine the behavior of the ambipolar evolution: either stable periodicity as shown by region I in Figure (4), or exponential growth as indicated by region II. In either case, the behavior of the sheath ultimately determines the behavior of the outer regions and therefore the anode fall, in general.

B. ANALYTICAL MATCHING - SUGGESTIONS

The analytic analysis presented in this chapter suggests that the anode fall model used in this work does not represent sufficient dissipation, preventing the system from adjusting itself, to adhere, to the "stable manifold" of the stagnation region near the plasma boundary. The model is most likely incomplete in its physical representation. Perhaps analytically matching the second order sheath equations to the transition set which are then matched to the ambipolar equation, may reveal an inconsistency between some of the physically represented terms. Albeit this process seems challenging at first, perhaps some of the ideas suggested next could be applied:

1. Three length scales have been found when equations (7-9) were non-dimensionalized (Appendix A and Table 3). Three "small" parameters could then be used to match equations (10-12) as follows: Assume the sheath equations (10) behave rapidly over a very small distance, hence a fast changing parameter should be applied, $1/\delta \approx O(L_E)$. Further, assume the ambipolar model (12) as varying slowly in comparison, $\varepsilon \approx O(L_n \text{ or } L_j)$. In between is a region of transition where $\eta = \varepsilon/\delta$. But

where are these equations matched?

3. To determine the location of matching, the fixed points found from equations (7-9) could be used as a starting point. The linearization of equations (10-12) about these stagnation regions, then provides the criteria for matching: the respective manifolds describe the number density and the density gradients evident near these fixed points. The interpretation: the manifolds given by the linearization about the fixed points gives the conditions for matching, criteria which must be met by the preceding region as the system is driven into the next zone. The manifolds for the fixed point near the plasma boundary have already been presented in section A.3. above. The manifolds for the fixed point near the sheath boundary can be found from $\hat{A}_{transition}$ by using any symbolic mathematic utility such as MAPLE or MATHCAD. The following is an illustration of the above concept:

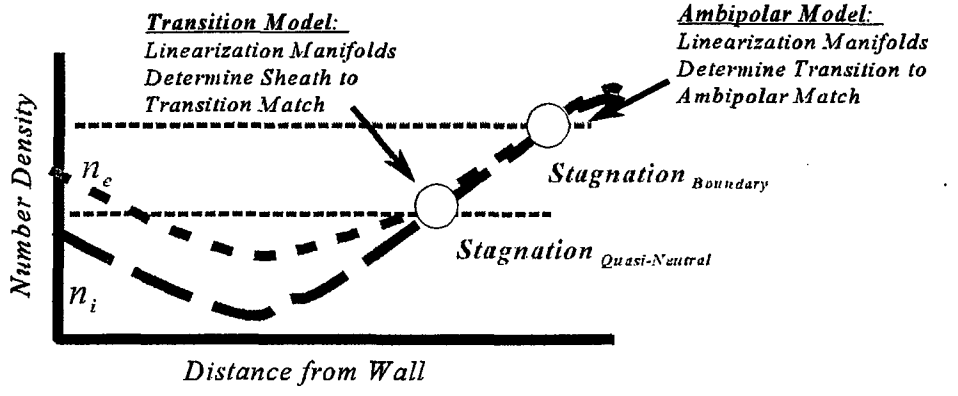

3. The initial conditions that are used for the sheath, however, remain a "shooting" problem. Perhaps a numeric iteration scheme where many initial conditions are tested might reveal some pattern for better selecting these conditions.

VI. NUMERICAL RESULTS FOR NITROGEN

Using available MATLAB 4-5-stage Runge-Kutta algorithms, both equations (7-9) and equations (10), as first order differential equations, are integrated numerically. The data thus obtained were then exported into a Quattro-Pro spreadsheet for plotting and easier analysis.

1. Length scales (Table 3) to determine the non-dimensional parameters:

$$L_E < L_{n_{i,e}} < L_{j_{i,e}}$$

$$L_E = \frac{\epsilon_o E_o}{q n_{o_{i,e}}},\ L_{n_{i,e}} = \frac{kT_o}{qE_o},\ L_{j_{i,e}} = \frac{j_{o_{i,e}}}{q v_o n_{o_{i,e}}}$$

2. Non-dimensionalized initial conditions (Table 4 lists the numerical data for nitrogen):

$$\bar{n}_i(\bar{y}=0) = \frac{10^8}{n_{o_i}},\ \bar{n}_e(\bar{y}=0) = \frac{10^{12}}{n_{o_e}},\ \bar{E}(\bar{y}=0) = \frac{E_{IC}(10^4)}{E_o}$$

$$\bar{j}_e(\bar{y}=0) = \frac{q^2 D_e \bar{E}(\bar{y}=0)\bar{n}_e(\bar{y}=0)}{kT_o},\ \bar{j}_i(\bar{y}=0) = \frac{q^2 D_i \bar{E}(\bar{y}=0)\bar{n}_i(\bar{y}=0)}{kT_o}$$

The drift currents are used to generate the appropriate initial conditions at the electrode wall since at the wall, the field induced motion will exceed that induced thermally; it is assumed that initially any density gradients are zero. To gain insight as to the impact of initial conditions on the system, the initial electric field is varied from 0.01 to 20(10^4) V/m. The results are given below. Of note, the method used to non-dimensionalize the variables (see Appendix A) gives rather small "non-dimensional numbers" in terms of magnitude, especially when the integration results shown are "close" to the electrode wall.

A. SPACE-CHARGE REGION, SHEATH

In overview: For $\bar{E}(0) < \bar{E}_{threshold} = 0.04$, the ion density behaves as expected, increasing monotonically, being primarily influenced by its gradient. Both the low initial field strength and the ion density gradient are insufficient, however, to push the species toward quasi-neutrality when $n_i \sim n_e$. When $\bar{E}(0) \geq \bar{E}_{threshold} = 0.04$, the initial field becomes strong enough to affect the ion density as compared to its gradient; the ions are pushed toward what appears as a density trough. Furthermore, for certain initial values of $\Delta n = |n_i - n_e|$ vs $E(0)$, the ions are pushed past their minimum density point, eventually approaching the electron density distribution, after which both densities remain close in magnitude for a short distance; essentially, for adequately strong initial electric field, quasi-neutrality is formed for a brief distance. The quasi-neutral characteristic is inherent within the energy balance found in the ions, the balance between ionization and recombination; without this balance, the space-charge region remains.

1. Varying Initial Conditions: Impact on System Behavior

To gauge the impact of various initial conditions, specifically combinations of species density and electric field, on the sheath dynamics, equations (10) were integrated for $n_i(0)=10^8$ [1/m^3], $n_e(0)=10^{12}$ [1/m^3] and $E(0)=6(10^4)$ [V/m] using the length scales as given in Table 3. These conditions were chosen after varying the initial conditions as will be described below.

Specifically for the ion density in the sheath:

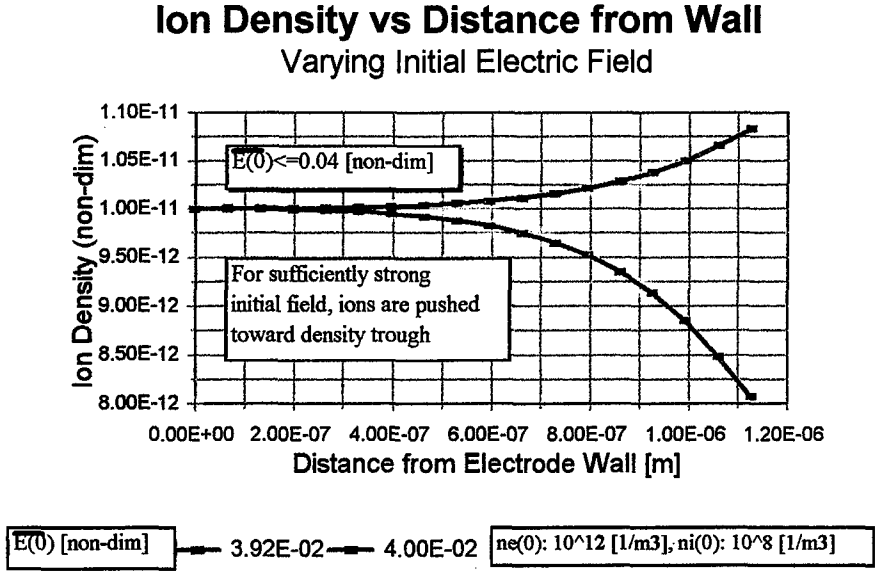

Figure 5: Ion Density vs Distance - $E(0) \leq E_{threshold}$

Figure (5) shows the ion density vs distance from the electrode wall for distances very close to the electrode surface - in comparison, see Figure (8) given later in this chapter. Again, the non-dimensionalization used makes the magnitudes for the density rather small, but these magnitudes represent non-dimensional quantities and so should be multiplied by n_o (see Table 4).

At the electrode wall, in its immediate vicinity, there are at least two major vehicles which drive the system away from the wall in steady-state: the initial electric field strength and the density gradient, such that if the field strength is low enough, the gradient dominates the system whereas if the field strength is high enough, the gradient influence becomes secondary in nature. Figures (6)-(7) depict the magnitude of the ion density gradient vs distance from the electrode wall and the electric field vs distance, respectively. Comparison with Figure (5) leads to the speculation that for low electric field strength, $\bar{E}(0) < \bar{E}_{threshold} = 0.04$, the

ion density is governed by its gradient, whereas when $\bar{E}(0) \geq \bar{E}_{threshold} = 0.04$, the electric field drives the ions from the wall. When $\bar{E}(0) = 0.04$ the boundary is reached where initial density gradient effects are surpassed by those of the field (Figures (5) and (6)) . As shown in Figure (5), the ion density appears to increase from the electrode wall for low initial field; yet this growth does not continue for very long. Essentially, the field strength is insufficient to drive the density further while the density gradient is too weak to provide the necessary impetus for the ion and electron densities to match. In general, Figures (5)-(7) show results for integrated variables in close vicinity of the electrode surface - in comparison, see Figure (8).

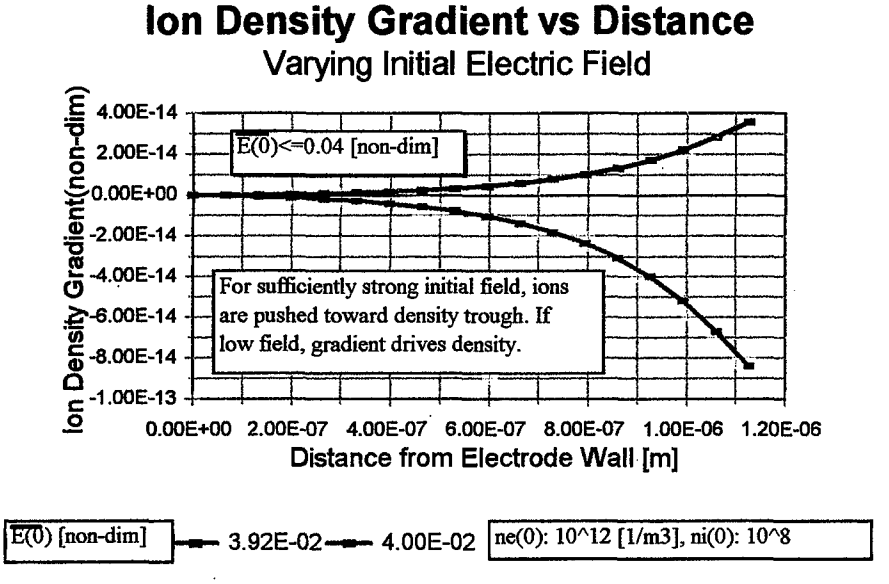

Figure 6: Ion Density Gradient vs Distance - $E(0) \leq E_{threshold}$

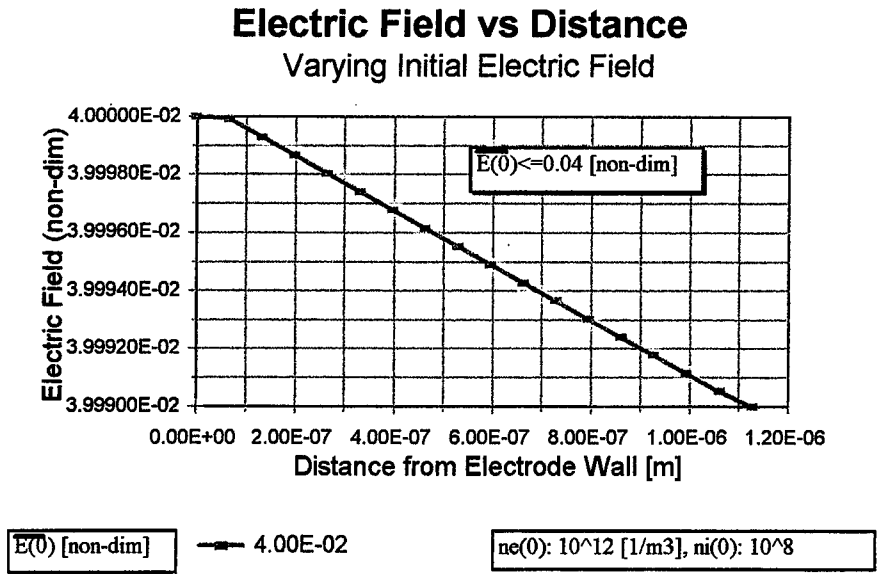

Figure 7: Electric Field vs Distance: $E(0) \leq E_{threshold}$

A density minimum occurs whith the initial electric field strength increases (Figure (8)). Moreover, the density decline reaches a minimum according to the electric field strength imposed. A constriction is suggested where the location and magnitude of these minima appear affected by the initial field strength as shown in Figure (8).

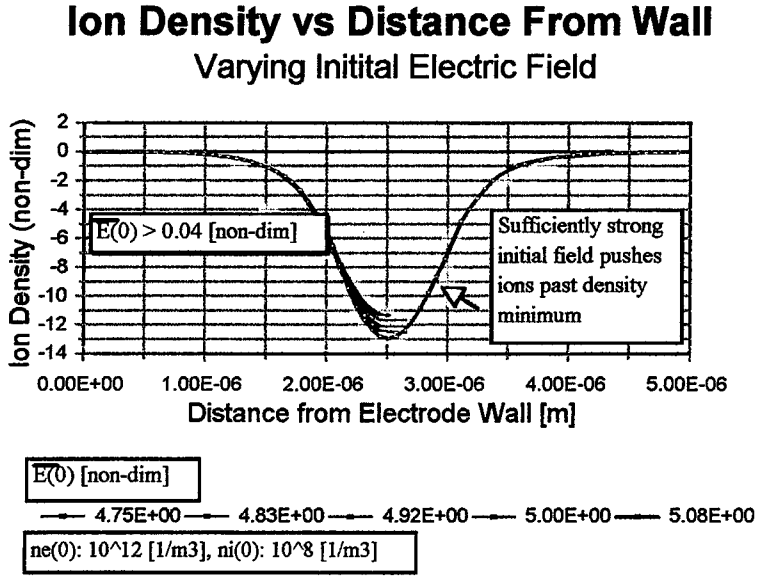

Figure 8: Ion Density vs Distance - $E(0) > E_{threshold}$

Figure (8) suggests the extent of the sheath as order $10^{(-6)}$, in agreement with the theory which requires the shielding to be of Debye length: $\lambda_D=[\epsilon_o kT_o/q^2n_o]^{1/2}$. But only sufficiently strong initial electric field intensities are able to push the ion densities past their wells, past their constriction (Figure (8)).

In comparison, the electrons in the anode sheath behave as expected, being less influenced by electrostatic repulsion than the ions. Figure (9) shows that for very low initial field strength, the electron density increases monotonically, but only very slightly.

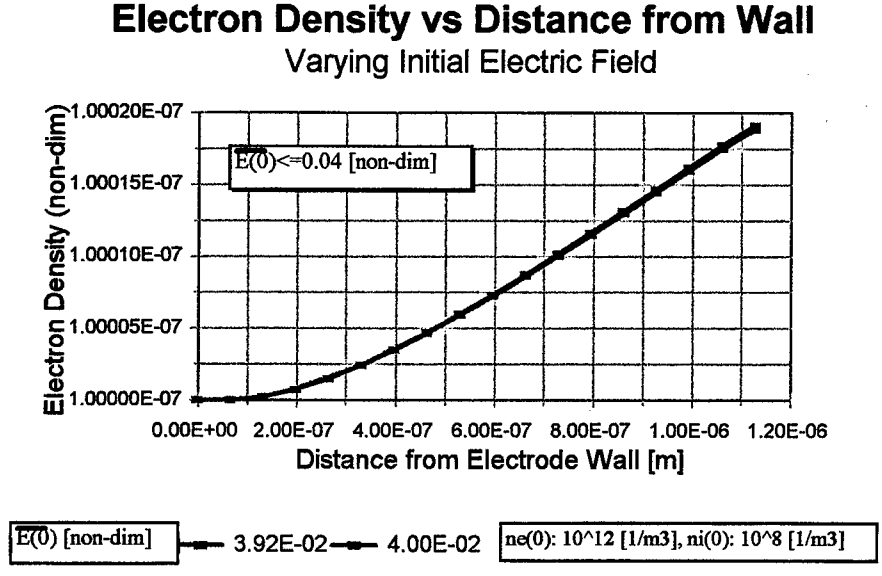

Figure 9: Electron Density vs Distance - $E(0) \leq E_{threshold}$

So, it is expected that increasing initial field strength should give rise to increasing electron density - this is the general case (Figure (10)). The electron density does decrease very slightly before the location of ion minimum is reached as illustrated by Figures (10)-(11); Figure (11) represents a more detailed view of Figure (10) in the region before ion minimum. Similar to the ion density, only sufficiently large initial field magnitudes push the electron density past the location of ion well (Figure (10)). From a physical standpoint, it should be remembered that both species are affected by electrostatic forces: the ions, however, are influenced to a much greater extent due to the electrostatic repulsion required when like charges are sufficiently close; qualitatively, these are the observations found in the preceding

analysis (Chapter V).

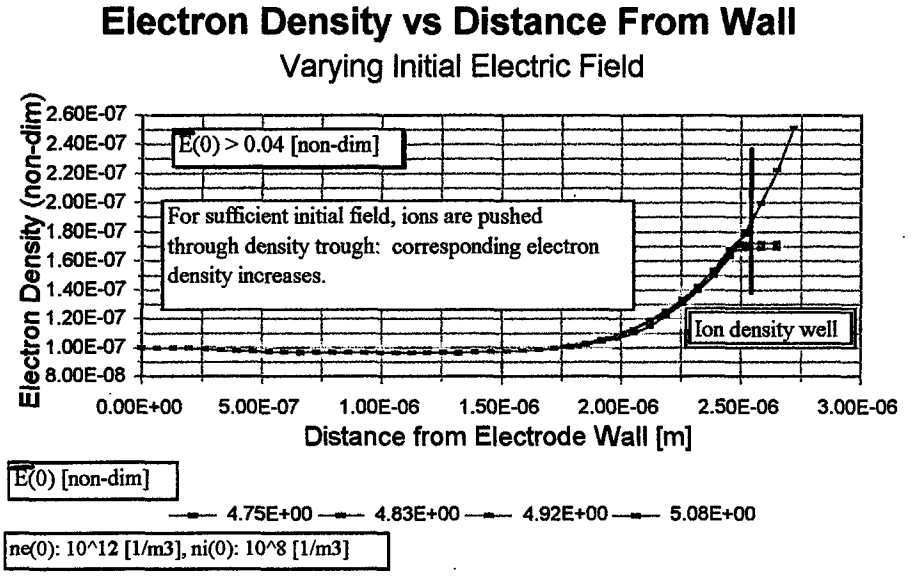

Figure 10: Electron Density vs Distance - Near and Past Density Minimum $E(0) > E_{threshold}$

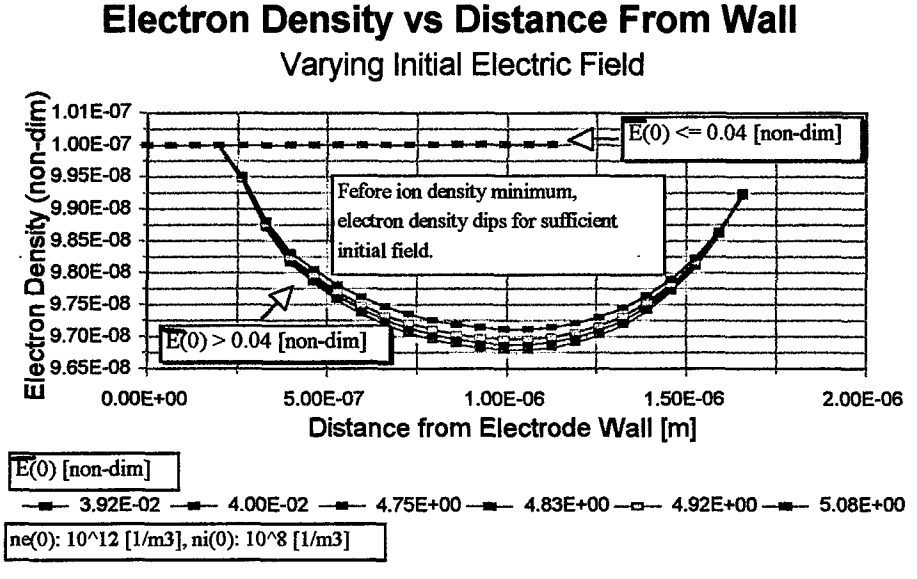

Figure 11: Electron Density vs Distance - $E(0) \leq E_{threshold}$, $E(0) > E_{threshold}$ (Expanded View)

If the initial field is sufficiently strong to push the ion density past its minimum, the minimum occurs when the electric field curvature changes: that is, the field curvature as written in terms of its potential $\frac{d^2}{d\bar{y}^2}(\bar{V})$ changes signs. Shown in Figure (12) are the results for

$$\bar{E}(0)=5.08 \quad \text{with} \quad n_i(0)=10^8\left[\frac{1}{m^3}\right],\ n_e(0)=10^{12}\left[\frac{1}{m^3}\right] \quad :$$

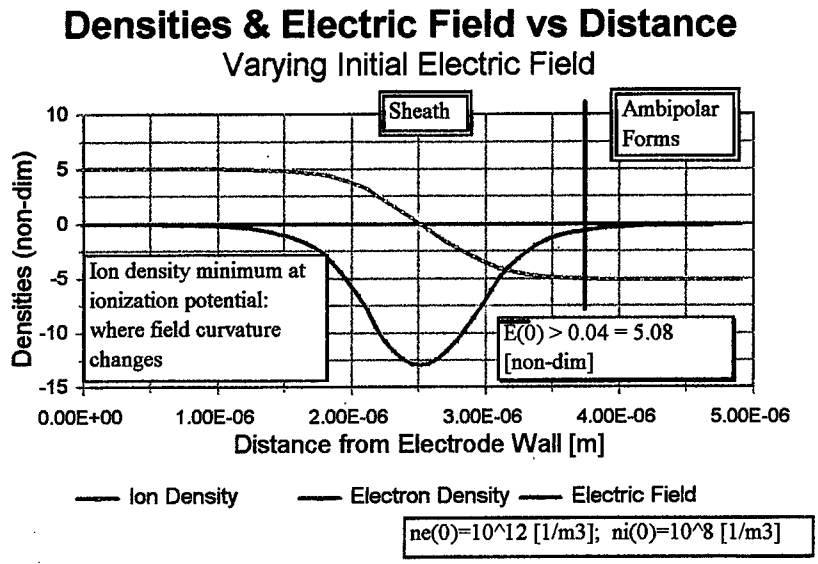

Figure 12: Densities & Electric Field vs Distance - $E(0) > E_{threshold}=5.08$

Although a quasi-neutral region forms when the initial electric field is sufficiently strong so as to push the ions past their well, the number density near the plasma boundary is not reached: $\bar{n}^*=0.15695$ as compared to the maximum density achieved when $\bar{n}_i \sim \bar{n}_e$ where $\bar{n}$ is on the order of 10^{-3}. Since $\bar{n}_i \sim \bar{n}_e$ requires $\bar{E}$ = constant, something else is needed to drive the system toward the plasma stagnation - some form of

transition. To summarize the effect of initial conditions:

It appears that the anode fall is comprised of diverse behavior, in part determined by the initial conditions chosen: there appear ranges of $\Delta n = |n_i - n_e|$ vs $E(0)$ for which both equations (7-9) and equations (10) naturally form a region of quasi-neutrality whereas for other ranges of $\Delta n = |n_i - n_e|$ vs $E(0)$, there seems insufficient initial energy to push the ion density past its minimum. To gauge this effect, equations (10) were integrated again but now E(0) was varied from 0.01 to 20(10^4) [V/m] for fixed Δn ranging between 10^9 to 10^{16} [1/m^3]. Figure (13) shows the results in semi-logarithmic format: the data points are plotted for which E(0) is sufficient to drive the ion density past the minimum, toward the electron density. From this plot, a type of "cut-off" region seems to form: to the left, the ions remain locked in their density well, to the right, the ions are driven past this minimum toward $\bar{n}_i \sim \bar{n}_e$:

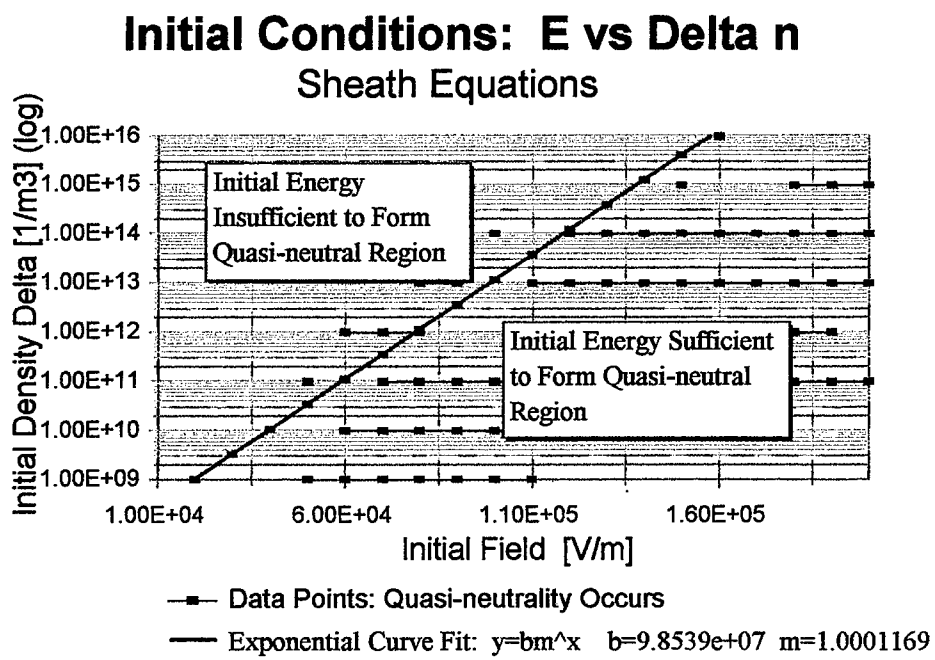

Figure 13: How to Begin Selecting Initial Conditions E vs Δn: $\Delta n = |n_i - n_e|$

For the region of initial conditions for which $\bar{n}_i \sim \bar{n}_e$ is reached, an interesting result appears when the ion density is plotted against the corresponding ion density: a type of phase portrait for the ions. Specifically, a multi-dimensional homoclinic-behavior results (see Appendix C), a characteristic commonly associated with energy conservation: for sufficient initial field, energy requires a balance between gains and losses, between ionization and recombination. So, if the initial conditions are such that the ion density is pushed past its well toward quasi-neutrality, the event of $\bar{n}_i \sim \bar{n}_e$ closes the homoclinic orbit and energy is balanced: a comparison between the case $\bar{E}(0) = 5.00$ and $\bar{E}(0) = 4.17$ is shown in Figure (14).

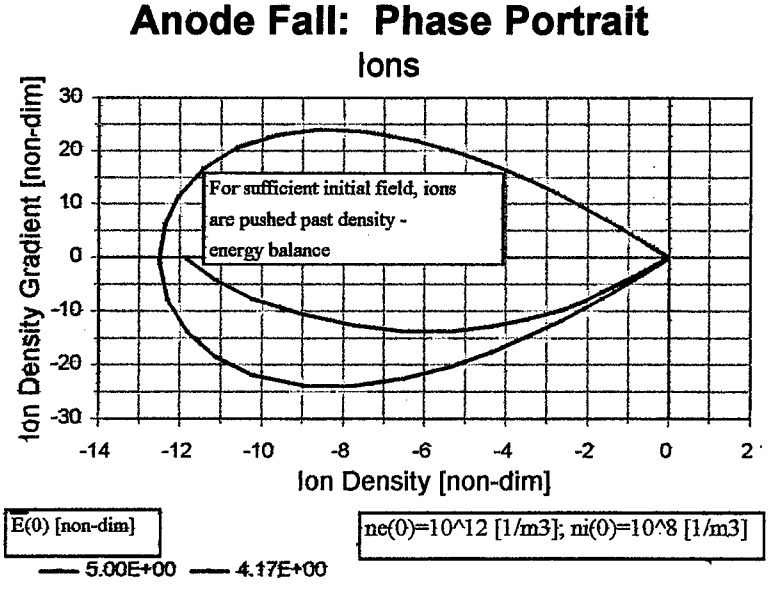

Figure 14: Anode Fall with Sufficient Initial Field - Phase Portrait for Ions

The integrated results of equations (10) not only provide the species density behavior, but also their gradients. As such, a natural question arises as to the behavior of species drift and random currents: the behavior of the species under the influences of an electrostatic field (potential) as compared to the behavior in an environment free of potential.

2. Drift and Random Currents

The species densities are not constant throughout a region which is influenced by an electric field; a uniform electric field applied to a cloud of constant charge q will produce a directed motion along with a variation of the concentration. From this principle, the species drift currents are found [Ref. 57: pp. 53-55]:

$$\begin{aligned} j_{o_{i,e}}\bar{j}_{drift_{i,e}} &= \pm q n_{o_{i,e}} \bar{n}_{i,e} \bar{v}_{avg\ drift_{i,e}} \\ &= \pm q n_{o_{i,e}} \bar{n}_{i,e} \left[\mu_{i,e} E_o \bar{E} - \frac{D_{i,e}}{n_{o_{i,e}} \bar{n}_{i,e}} \frac{d}{L_E d\bar{y}} \left(n_{o_{i,e}} \bar{n}_{i,e} \right) \right] \\ &= \pm q n_{o_{i,e}} \bar{n}_{i,e} \left[\frac{D_{i,e} q}{kT_o} E_o \bar{E} - \frac{D_{i,e}}{n_{o_{i,e}} \bar{n}_{i,e}} \frac{d}{L_E d\bar{y}} \left(n_{o_{i,e}} \bar{n}_{i,e} \right) \right] \end{aligned} \qquad \text{Equation (13)}$$

where the Einstein relation for mobility has been applied. To obtain the random current, the thermal velocity is used such that

$$j_{o_{i,e}}\bar{j}_{random_{i,e}} = \pm \left(\frac{1}{4} \right) q n_{o_{i,e}} \bar{n}_{i,e} v_{thermal_{i,e}} = \pm \left(\frac{1}{4} \right) q n_{o_{i,e}} \bar{n}_{i,e} \sqrt{\frac{2kT_o}{m_{i,e}}} \qquad \text{Equation (14)}$$

The effect of varying initial conditions, Δn vs $E(0)$, are again determined in similar procedures as for the species densities above as shown next. First, the ion currents are considered:

For field strengths $\bar{E}(0) < \bar{E}_{threshold} = 0.04$, the random ion current increases,

following the tendencies of the ion density (see Figure (5)). When the initial field is increased such that $\bar{E}(0) \geq \bar{E}_{threshold} = 0.04$, the random and drift currents intersect as a function

of the rate of decrease or strength of initial field. Again, the random current (equation (14)) follows the density distribution for isothermal conditions. Figure (15) summarizes these results for locations "close" to the electrode surface.

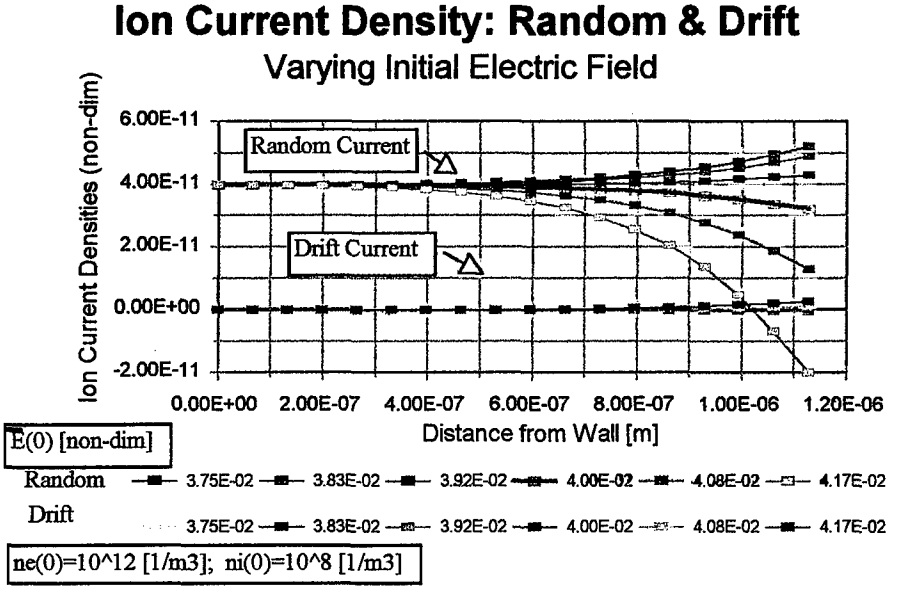

Figure 15: Random & Drift Ion Current Density vs Distance - $E(0) \leq E_{threshold}$

If the initial electric field is sufficiently large so as to push the ions past their density well, the drift current follows accordingly. Furthermore, the random current follows the ion density as shown in Figure (16).

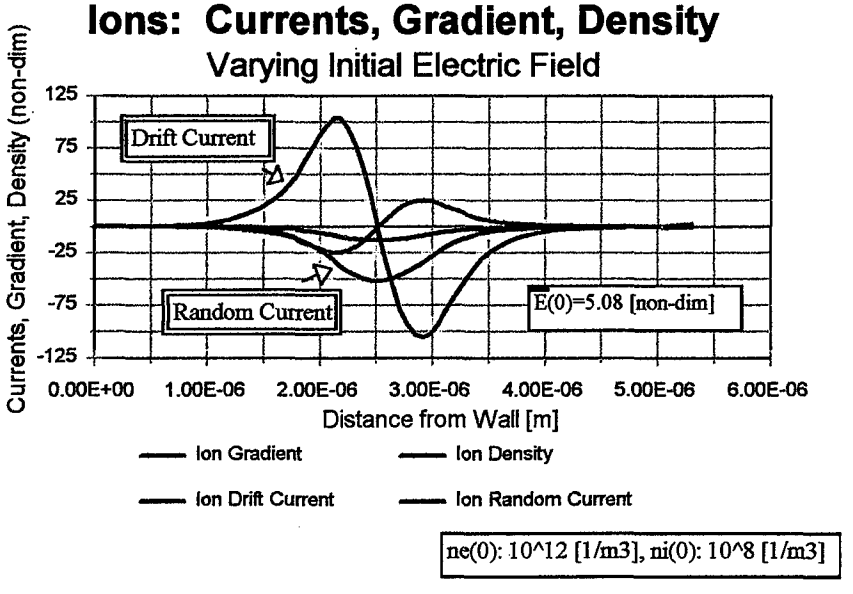

Figure 16: Ions - Drift & Random Currents, Density & Gradient vs Distance - E(0)=5.08

Of note is that ion both the drift and random currents seem to approach a limiting value as the realm of quasi-neutrality is approached; perhaps the saturation current as theorized by Child and Langmuir [Ref. 58: p. 238]. Next, the electron currents are considered:

For sufficiently large initial field, the rapid variation in the electron density gradient (see Figure (11)) is markedly observed in the corresponding electron drift current - Figure (17). Additionally, the electron random current does not intersect the electron drift current, in comparison to that of the ions. Instead, the random electron current follows the tendencies of the electron density (Figure (18)) where the negative charge of the electron reverses the magnitude of the electron density plot (see Figure (11)), in comparison to the ion results. Furthermore, when a sufficiently large initial field is applied, the electron drift current increases past the point (spatial coordinate) of the density minimum, diverging spatially from the random current (Figure (19)).

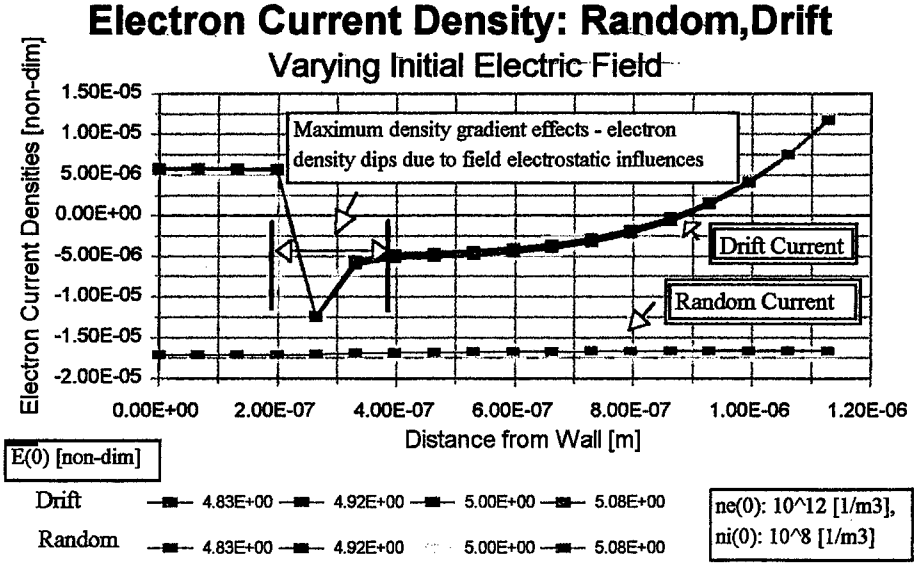

Figure 17: Random & Drift Electron Current Densities vs Distance - Before Ion Density Minimum, $E(0)>E_{threshold}$

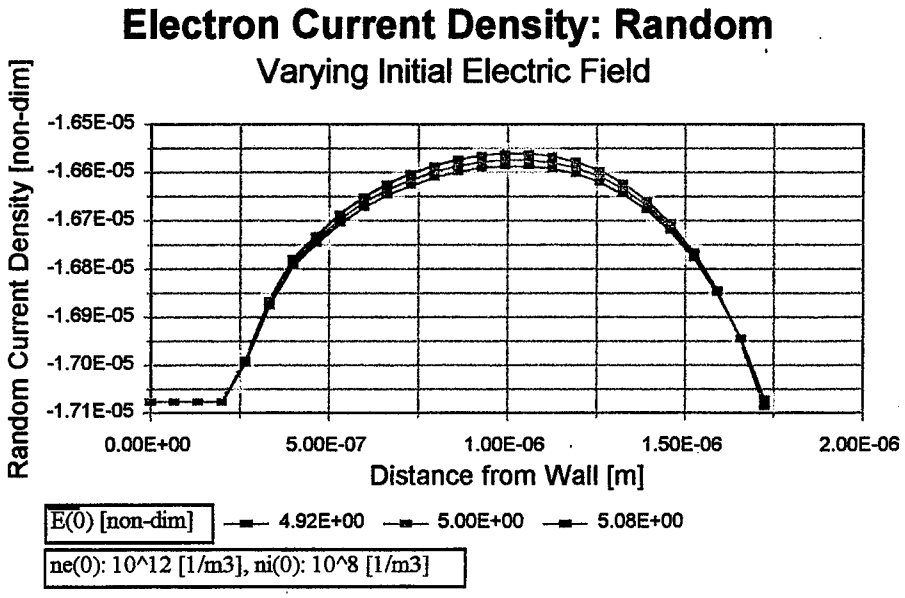

Figure 18: Random Electron Current Density vs Distance - Before Ion Density Minimum, $E(0)>E_{threshold}$

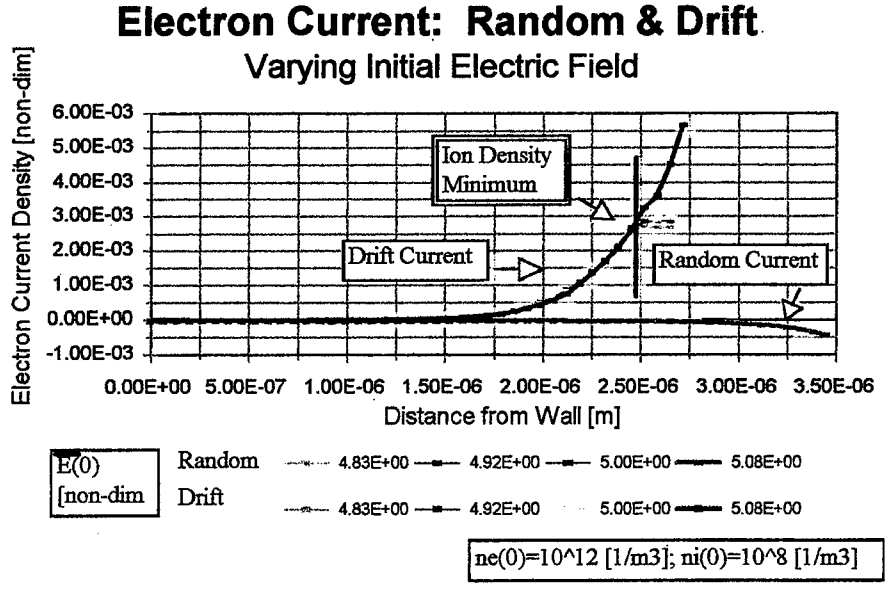

Figure 19: Random & Drift Electron Current Densities vs Distance - Near and After Ion Density Minimum, $E(0)>E_{threshold}$

B. NUMERICALLY MATCHING

Although a quasi-neutral region forms when the initial electric field is sufficiently strong so as to push the ions past their well, the number density near the plasma boundary is not reached: $\bar{n}^* = 0.15695$ as compared to the maximum density achieved when $\bar{n}_i \sim \bar{n}_e$ where $\bar{n}$ is on the order of 10^{-3}. Since $\bar{n}_i \sim \bar{n}_e$ requires $\bar{E}$ = constant, something else is needed to drive the system toward the plasma stagnation - some form of transition, for without it, the species densities diverge (Figure (20, 21)).

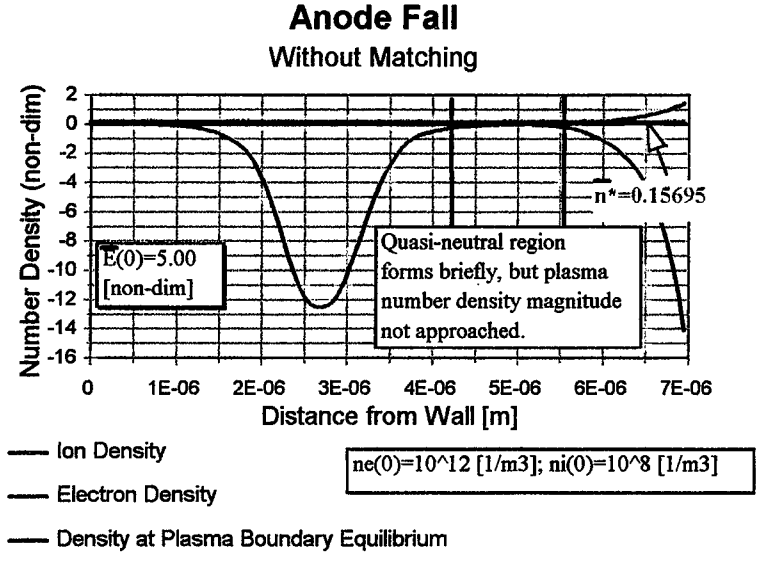

Figure 20: Anode Fall - Without Numeric Matching

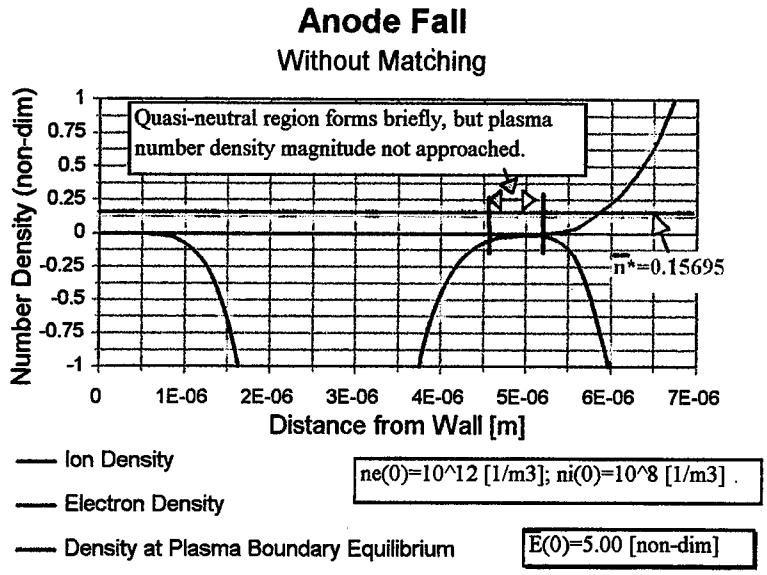

Figure 21: Anode Fall - Without Numeric Matching (Expanded View)

In steady-state with isothermal conditions, with the electric field constant when $\bar{n}_i \sim \bar{n}_e$, there remain two primary phenomena which could drive the density toward the plasma equilibrium: density gradient or ambipolar diffusion. To obtain the overall effect, first the sheath equations as given by set (10) are matched numerically to the final ambipolar equations, (12) using for the matching conditions $\bar{n}_i \sim \bar{n}_e$ that result from equations (10) provided the initial field is sufficiently strong to allow the ions to proceed past their density well; the results for $E(0)=6.1(10^4)$ [V/m] and $n_i(0)=10^8$ [$1/m^3$] with $n_e(0)=10^{12}$ [$1/m^3$] are shown in Figure (22).

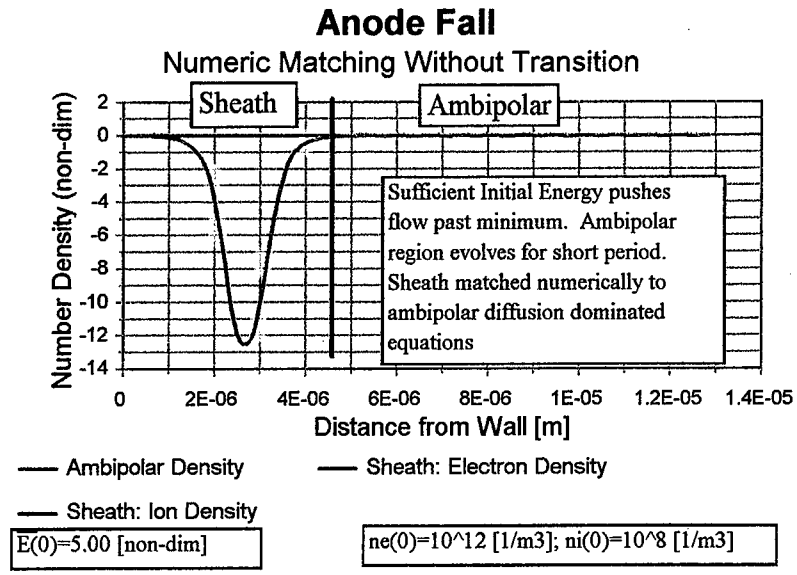

Figure 22: Anode Fall - Numeric Matching without Transition

The density remains below the plasma boundary stagnation (Figures (22, 23))- ambipolar diffusion is insufficient to drive the density toward the plasma boundary. The cosinusoidal behavior shown is determined by the matching conditions imposed by the sheath equations (10) upon the ambipolar equation (12) - Chapter V.

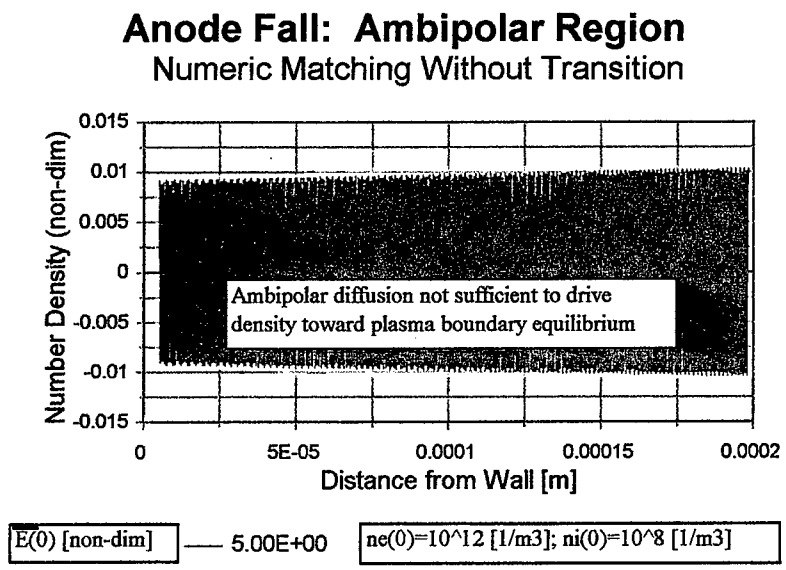

Figure 23: Anode Fall - Numeric Matching without Transition (Expanded View)

If, on the other hand, a full transition region is considered in which the density gradient is the primary source to drive the system, then the plasma boundary density is approached. The transition equations do not, however, reflect the impact of the density growth on free diffusion - the formation of ambipolar diffusion. Hence, using the plasma boundary stagnation, $\bar{n}^* = 0.15695$, along with the electric field intensity at the onset of $\bar{n}_i \sim \bar{n}_e$ as initial conditions (or matching conditions) to equations (12), the transition equations (11) are numerically matched to the ambipolar formulation, set (12). Figure (24, 25) illustrates the results for E(0)=6.1(10^4) [V/m] and $n_i(0)=10^8$ [$1/m^3$] with $n_e(0)=10^{12}$ [$1/m^3$].

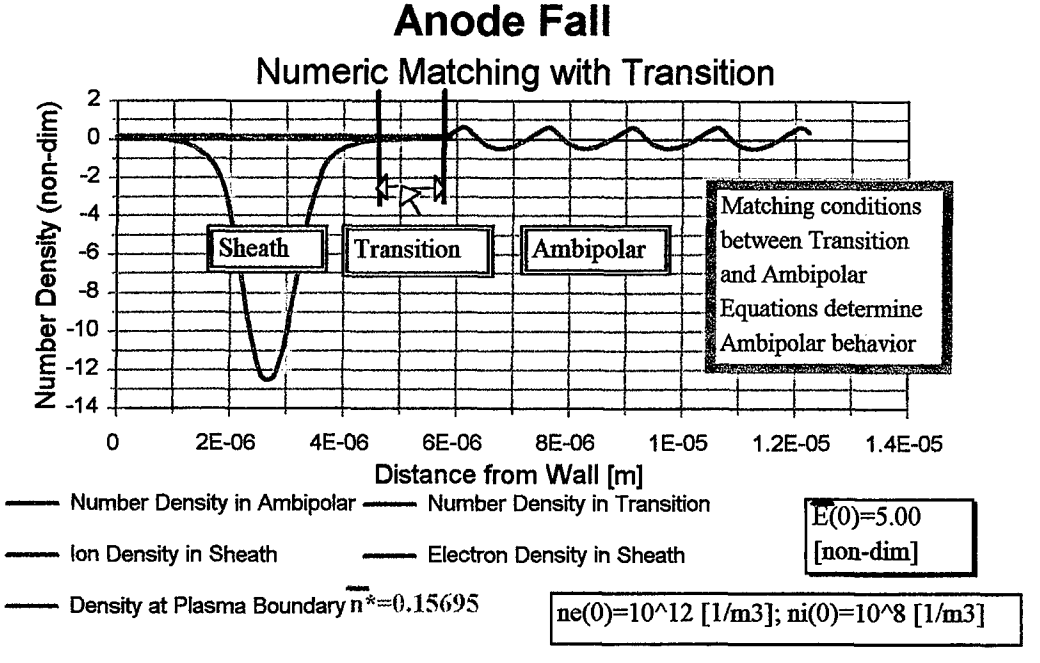

Figure 24: Anode Fall - Numeric Matching with Transition

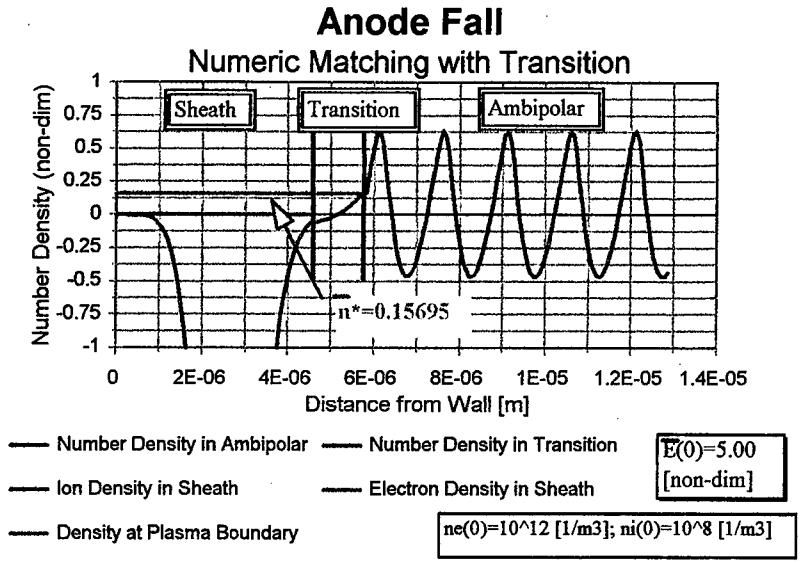

Figure 25: Anode Fall - Numeric Matching with Transition (Expanded View)

The ambipolar region shown in Figures (24, 25) clearly shows the very sensitive nature of this zone; the initial conditions to the transition region the consequent matching to the ambipolar zone determine the characteristics of this latter region (see Chapter V, Figure (4)). Specifically, the behavior of the anode fall region, as modeled by equations (7-9) and equations (10-12), is governed by the initial conditions imposed to the transition by the sheath. The ultimate condition that determines the anode fall characteristics, however, is the initial field strength imposed upon the region: if the field is sufficiently strong, the ion density is pushed past its well toward quasi-neutrality - these matching conditions, for the transition equations, determine the rate of density increase and consequently the initial conditions for the ambipolar equations. These criteria will then impose the behavior for the ambipolar region, whether the manifolds of the plasma boundary stagnation restrict the system characteristics, or whether the realm of instability is entered (see Chapter V and Figure (4)).

VII. SUMMARY, CONCLUSIONS AND RECOMMENDATIONS

A. SUMMARY

Voltage losses at electrode boundaries, surface erosion and sheath effects play an important role in plasma devices and must be controlled in designs of practical interest. Particularly, thermal arcjets and MPD accelerators deposit between 15% and 80% of the input power to the anode. This presents not only a severe performance penalty, but also complicates the thermal design problems since the heat thus generated must be radiated away from the thruster surfaces. [Ref. 7, 9] A natural question arises: what is the behavior found in the anode region? Perhaps a restatement of the qualitative picture of the anode, as offered by Ingold [Ref. 43: pp.59-63], serves as an answer:

> 1. The anode fall voltage is on the order of the ionization potential of the gas since electrons must be accelerated to an energy sufficiently high so that an ion current for the positive column is provided.
>
> 2. The anode fall region is determined primarily by space-charge and secondly by the ionization requirements.

Moreover, in a comprehensive review of anode-spot phenomena, Miller [Ref. 44] suggests that a sudden increase in the voltage noise frequently indicates that an anode foot-print could be forming or that a transition into the anode-spot mode could be occurring. Further, this abrupt change in voltage has been associated with a sudden change of ion density in the region near the anode, a density decrease that would leave the local electron space charge uncompensated and thus produce a low-conductivity region. The sudden increase in voltage would then reflect this local shortage of ions - an ion depletion region or ion starvation region. Even-though the most suitable model for the anode region is still actively debated, the general idea of the appearance of an ion deficiency region near the anode as triggering the transition into the anode-spot mode has been fairly supported.

So to expand these qualitative portraits of the anode fall, this work investigated the nature of the voltage drops in the vicinity of a non-emitting, positive electrode. The selected

approach involves non-linear analysis techniques of the continuum governing equations for steady-state, isothermal conditions in one dimension, where both ionization and two-body recombination processes are considered. The following conclusions and observations are offered:

B. CONCLUSIONS

Ions, created through electron bombardment of neutral atoms throughout the anode fall region, are repelled electrostatically from the positive electrode toward a location of quasi-neutrality at the sheath boundary, as well as toward an unstable stagnation region near the plasma interface. These equilibria form as a result of the chemistry present. That is, continuity (equations (9)) seems to require flow equilibrium when quasi-neutral conditions are initially met within the sheath and when the plasma boundary is reached. It is recombination that establishes the latter while the presence of ionization stipulates the former. Fundamentally, the sheath, as formulated, is inherently unstable - ions are driven out of the system, toward the negative electrode. The stagnation regions were obtained analytically, through non-linear analysis techniques; to test these results, nitrogen data were used in a numerical algorithm from which the following observations are made:

At the electrode wall, in its immediate vicinity, at least two major processes repel the positive ions away from the wall in the isothermal, steady-state case: the initial electric field strength and the initial density gradient. If the field strength is low enough, the gradient dominates the system and the ion density behaves as expected, increasing monotonically for a short distance. If the field strength is high enough, the gradient influence becomes secondary in nature, the field then driving the species densities. However, the low initial field strength and ion density gradient are insufficient to push the species toward quasi-neutrality, when $n_i \sim n_e$. On the other hand, when the initial field becomes sufficiently strong as compared to the species density gradient, the ions are pushed toward what appears as a density trough. Furthermore, for certain initial values of $\Delta n = |n_i - n_e|$ vs $E(0)$, the ions are pushed past their well, eventually approaching the electron density in magnitude but not merging: for sufficiently strong initial field, quasi-neutrality forms in a self-consistent way. Further, if

conditions permit the ions to traverse their density well, their constriction, then at the moment of quasi-neutrality, when $\bar{n}_i \sim \bar{n}_e$, there appears a conservative phenomenon for the ions, where energy growth is matched by energy loss - a chemical balance.

At the onset of quasi-neutrality, however, the ensuing species densities do not match the plasma neutrality requirements (Saha). Thus, a transition region must drive the system toward the plasma boundary: for steady-state conditions, the primary mechanism is the density gradient. When the species density becomes large enough, mutual Coulomb fields affect free diffusion and ambipolar diffusion results. The ambipolar field then continues to drive the ions away from the positive plate; the initial conditions to the transition region, the consequent matching to the ambipolar zone, determine the characteristics of this latter region. Specifically, the behavior of the anode fall region, as modeled by equations (7-9) and equations (10-12), is governed by the initial conditions imposed to the transition by the sheath. The ultimate condition that determines the anode fall characteristics, however, is the initial field strength imposed upon the region: if the field is sufficiently strong, the ion density is pushed past its well toward quasi-neutrality - these matching conditions for the transition equations determine the rate of density increase and consequently the initial conditions for the ambipolar equations. These criteria then determine whether the manifolds of the plasma boundary stagnation restrict the system, or whether the realm of instability is entered. As such, any numeric solutions will most likely be challenging, a result observed when, using nitrogen data, the various anode fall regions are numerically matched.

Both the analysis and the numerical results suggest that the anode fall model used in this work does not represent sufficient dissipation, preventing the system from adjusting itself, to adhere, to the "stable manifold" of the stagnation region near the plasma boundary. The model is most likely incomplete in its physical representation: either temperature gradients, diffusion written in terms of the electric field, full time dependencies or quasi-steady formulation, magnetic field effects and/or three-body recombination effects may provide the necessary dissipation.

C. RECOMMENDATIONS

To improve upon the results obtained in this work, further considerations should be given to:

1. Species temperature variation throughout the fall region, specifically in the sheath.

2. Diffusion perhaps written as a function of the electric field instead of as assumed constant for each species.

3. Full time-dependent and/or quasi-steady formulations for the anode fall.

4. The effect of three-body recombination on the stagnation regions found, as well as the influences of magnetic fields on the system behavior.

This work presents a broad overview of many subjects, many of which really need further investigation, among them:

1. Analytically matching the second order sheath equations to the transition set and to the ambipolar equation; essentially, the analytic analog of the numeric matching ideas presented in this work. The results of such mathematical treatment might reveal that, in fact, more physics is needed in equations (7-9).

2. Further investigation of the sensitivity to initial conditions for the ion density well as well as quasi-neutral zone formation; a wider range of initial conditions should be tested in the hopes of finding some better relation between Δn versus E which would be of aid in any numeric endeavor. Such analysis should also focus on a variety of gases, not be limited to nitrogen; possible candidates include xenon and argon.

3. Generation of a current versus voltage curve, I-V curve, by integrating the electric field data and using the current calculations given in this work. Does the result match the literature?

APPENDIX A. NON-DIMENSIONALIZATION

Mathematical derivations are frequently burdened by complicated functions of the constants in the problems. Before the mathematical analysis is carried out, a preliminary dimensional analysis may not only reveal the ways in which some of the constants enter into the final solution, but also unveil significant dimensionless products of a problem. Then the original differential equations may be expressed in terms of dimensionless notation, a method particularly useful since model laws are usually derived from the differential equations that govern phenomena. [Ref. 59: p. 144] Dimensional analysis is a process in as much influenced by art as it is by scientific methods: two principles were applied to this work - the Buckingham Pi Theorem and Fractional Analysis coupled with the physical requirements brought by the governing equations themselves.

A. BUCKINGHAM PI THEOREM

The Pi Theorem may be stated as "The number of dimensionless products in a complete set is equal to the total number of variables minus the rank of their dimensional matrix." [Ref. 59: p. 31] In using the Pi Theorem, the following conditions should be fulfilled: [Ref. 60: p. 20]

1. The list of dimensional parameters must contain all of the parameters of physical significance including all independent parameters and one dependent parameter.

2. The non-dimensional pi's as finally composed should contain, at least once, each of the parameters in the original list.

3. The list of dimensions used to compose the physical parameters must be independent, or else provision must be made to compensate for the redundancy.

There are infinitely many different complete sets of dimensionless products that can be formed from a given set of variables. Insofar as Buckingham's theorem is concerned, any such complete set is admissible, with some sets more useful than others. So how may a complete set of dimensionless products be most advantageously selected at the outset?

1. Arrangement of Variables and Terminology

As Buckingham has pointed out, the maximum amount of experimental control over the dimensionless variables is obtained if the dependent variable does not occur in more than one dimensionless product, a product referred to as the "dependent dimensionless variable or pi" [Ref. 59]. Using a dimensional matrix as outlined in reference 59, the preceding condition will be realized, as nearly as possible, if in the dimensional matrix the first variable is the dependent variable, the second variable is that which is easiest to regulate experimentally, the third variable is that which is next easiest to regulate experimentally, and so on. [Ref. 59: p. 39] Consequently, the variables describing equations (7-9) are arranged as follows: $E=x_1$, $n_i=x_2$, $n_e=x_3$, $j_e=x_4$, $y=x_5$, $D_e=x_6$, $\nu=x_7$, $j_i=x_8$, $D_i=x_9$, $k=x_{10}$, $T_o=x_{11}$, $\alpha_2=x_{12}$, $\epsilon_o=x_{13}$, and $q=x_{14}$ where E represents the electric field, $n_{i,e}$ characterize the ion and electron number densities, respectively, $j_{i,e}$ are the ion and electron current densities, respectively, y is the geometry coordinate length, $D_{i,e}$ characterize the ion and electron diffusivities, respectively, and ν is the ionization coefficient. Universal constants and those variables held constant are entered last in the matrix since these are not deemed "experimentally controllable": k is the Boltzmann constant, α_2 the two-body recombination coefficient, and ϵ_o the permittivity of free space with q as the charge. The entries of the matrix are next made: the dependent variable, i.e., the first entry in the matrix, is the electric field, since in terms of voltage applied, it governs the space charge development. The second and third entries into this matrix represent the number density distributions and govern the current development. All other variable entries are made arbitrarily, the only requirement being that arrangement which gives a linearly independent solution for $x_{10}...x_{14}$. To complete the dimensional matrix, each variable and constant is written in terms of the fundamental units of mass (M), length (L), time (t), charge (Q) and temperature (θ); the matrix outlining the coefficients of these units for each variable becomes:

	E	n_i	n_e	j_e	y	D_e	v	j_i	D_i	k	T_o	α_2	ϵ_o	q
[M]	1	0	0	0	0	0	0	0	0	1	0	0	-1	0
[L]	1	-3	-3	-2	1	2	0	-2	2	2	0	3	-3	0
[t]	-2	0	0	-1	0	-1	-1	-1	-1	-2	0	-1	2	0
[Q]	-1	0	0	1	0	0	0	1	0	0	0	0	2	1
[θ]	0	0	0	0	0	0	0	0	0	-1	1	0	0	0

Table 7: Variables in Terms of Fundamental Units

There will be 14-5=9 dimensionless pi's (number of variables minus the number of units necessary to describe them). In fact the rank of this matrix is five which not only reflects the number of fundamental units necessary, but also the five constants of the problem: k, T_o, q, ϵ_o, α_2. Solving for the variables x_i for i=10..14, in terms of the variables x_j for j=1..9 results in the homogenous, linear, algebraic equations. By taking this equation set into matrix format and solving for each variable x_i where i=1..9, the homogeneous, linearly independent non-dimensional pi's can be determined:

$$x_{10} = -2\,x_1 - 3\,x_2 - 3\,x_3 - 5\,x_4 + x_5 - x_6 - 3\,x_7 - 5\,x_8 - x_9$$
$$x_{11} = -2\,x_1 - 3\,x_2 - 3\,x_3 - 5\,x_4 + x_5 - x_6 - 3\,x_7 - 5\,x_8 - x_9$$
$$x_{12} = -x_4 - x_6 - x_7 - x_8 - x_9$$
$$x_{13} = -x_1 - 3\,x_2 - 3\,x_3 - 5\,x_4 + x_5 - x_6 - 3\,x_7 - 5\,x_8 - x_9$$
$$x_{14} = 3\,x_1 + 6\,x_2 + 6\,x_3 + 9\,x_4 - 2\,x_5 + 2\,x_6 + 6\,x_7 + 9\,x_8 + 2\,x_9$$

x_1 (E)	x_2 (n_i)	x_3 (n_e)	x_4 (j_e)	x_5 (y)	x_6 (D_e)	x_7 (v)	x_8 (j_i)	x_9 (D_i)	x_{10} (k)	x_{11} (T_o)	x_{12} (α_2)	x_{13} (ϵ_o)	x_{14} (q)
1	0	0	0	0	0	0	0	0	-2	-2	0	-1	3
0	1	0	0	0	0	0	0	0	-3	-3	0	-3	6
0	0	1	0	0	0	0	0	0	-3	-3	0	-3	6
0	0	0	1	0	0	0	0	0	-5	-5	-1	-5	9
0	0	0	0	1	0	0	0	0	1	1	0	1	-2
0	0	0	0	0	1	0	0	0	-1	-1	-1	-1	2
0	0	0	0	0	0	1	0	0	-3	-3	-1	-3	6
0	0	0	0	0	0	0	1	0	-5	-5	-1	-5	9
0	0	0	0	0	0	0	0	1	-1	-1	-1	-1	2

Table 8: Buckingham Pi's - Matrix Formulation

Non-dimensional Variables	Relationship Between Non-dimensional Variables, Buckingham Pi's and Undisturbed Plasma Values	Buckingham Pi's
$\overline{E}$	$\overline{E} = \pi_1 E = \frac{E}{E_o}$	$\pi_1 = \frac{q^3}{(kT_o)^2 \epsilon_o}$
$\overline{n_i}$	$\overline{n_i} = \pi_2 n_i = \frac{n_i}{n_{o_i}}$	$\pi_2 = \left[\frac{q^2}{(kT_o)\epsilon_o}\right]^3$
$\overline{n_e}$	$\overline{n_e} = \pi_3 n_e = \frac{n_e}{n_{o_e}}$	$\pi_3 = \left[\frac{q^2}{(kT_o)\epsilon_o}\right]^3$
$\overline{j_e}$	$\overline{j_e} = \pi_4 j_e = \frac{j_e}{j_{o_e}}$	$\pi_4 = \frac{q^9}{(kT_o)^5 \epsilon_o^5 \alpha_2}$
$\overline{j_i}$	$\overline{j_i} = \pi_5 j_i = \frac{j_i}{j_{o_i}}$	$\pi_5 = \frac{q^9}{(kT_o)^5 \epsilon_o^5 \alpha_2}$
$\overline{y}$	$\overline{y} = \pi_6 y = \frac{y}{L}$ L are characteristic length scales	$\pi_6 = \frac{(kT_o)\epsilon_o}{q^2}$
$\overline{D_e}$	$\overline{D_e} = \pi_7 D_e = \frac{D_e}{D_{o_e}}$	$\pi_7 = \frac{q^2}{(kT_o)\epsilon_o \alpha_2}$
$\overline{D_i}$	$\overline{D_i} = \pi_8 D_i = \frac{D_i}{D_{o_i}}$	$\pi_8 = \frac{q^2}{(kT_o)\epsilon_o \alpha_2}$
$\overline{v_i}$	$\overline{v_i} = \pi_9 v_i = \frac{v_i}{v_{i_o}}$	$\pi_9 = \frac{q^6}{(kT_o)^3 \epsilon_o^3 \alpha_2}$

Table 9: Relationship Between Non-dimensional Variables, Buckingham Pi's and Undisturbed Plasma Values

When these pi's are inserted into the appropriate governing equations, each term in the equation will have a non-dimensional parameter affecting it. For example, the dimensional

Gauss $\frac{dE}{dy} = \frac{q}{\epsilon_o}(n_i - n_e)$ written with Buckingham Pi's gives

$$\frac{\pi_6}{\pi_1}\frac{d\bar{E}}{d\bar{y}} = \left[\frac{q}{\pi_2 \epsilon_o}\right]\bar{n}_i - \left[\frac{q}{\pi_3 \epsilon_o}\right]\bar{n}_e \quad or$$

$$\frac{d\bar{E}}{d\bar{y}} = \left[\frac{\pi_1 q}{\pi_2 \pi_6 \epsilon_o}\right]\bar{n}_i - \left[\frac{\pi_1 q}{\pi_3 \pi_6 \epsilon_o}\right]\bar{n}_e$$

It is the constants and pi's within the brackets that form the non-dimensional parameters.

2. Pi Theorem - Results and Conclusions

Although the Pi Theorem forms a good framework for discussing the nature of units, dimensions and related topics, the theorem, when used as the only means toward analysis, suffers from several deficiencies:

1. No direct means for finding the pertinent pi's is available and dimensional analysis itself provides little framework for incorporating relevant physical information.

2. The theorem alone does not provide conditions under which one or more pi's can be neglected or for which sets of dimensionless groups may be combined.

So another method must be used to make the problem non-dimensional.

B. FRACTIONAL ANALYSIS

There is another common method of dimensional analysis that is intrinsically the same as the foregoing technique but differs from it in that the differential equations are expressed in dimensionless forms by applying, among others, a characteristic length L and/or a characteristic time period τ, such that $\bar{x} = \frac{x}{L}$, $\bar{T} = \frac{t}{\tau}$; that is, all variables are non-dimensionalized by introducing appropriate characteristic values - fractional analysis. [Ref. 59] A fractional analysis is any procedure for obtaining some information about the answer to a problem in the absence of methods or time for finding a complete solution, a method from which an approximate analytical or numerical solution can be obtained [Ref. 60]. Specifically:

1. What is the physical meaning of each of the governing parameters and variable? What are the qualitative effects of an increase or decrease in any given parameter or variable?

2. Can we find the conditions under which the effects of certain parameters can be neglected either in a given region or for a particular problem? If so, does this lead to governing equations that are more tractable so that they can be solved even though the general equations cannot be solved?

3. Are there any combinations of two or more non-dimensional parameters or variables, or transformations of variables, which lead to fewer independent quantities or which simplify the correlations achieved?

To answer these questions, the confines of traditional dimensional analysis, as a tool by itself, are exceeded and other methods must be employed. One such method incorporates dimensional analysis with governing equations as advocated by Sedov [Ref. 61]. Sedov has clearly shown that important information can be obtained by simultaneous use of the governing equations together with dimensional analysis. Consequently a systematic methodology is needed to obtain information directly from the governing equations without actually solving them, a methodology involving three primary ideas: [Ref. 60: p. 66-70]

1. Normalization based on governing equations; making equations and conditions non-dimensional in terms of non-dimensional variables of standard magnitude.

2. Absorption of parameters.

3. Combination of variables.

To carry out such procedures, a clear understanding of the physical information inherent in the equations is essential. Of equal importance is using a standard procedures for transforming the variables to non-dimensional form and standard magnitude; it is not sufficient to make governing equations non-dimensional in any arbitrary way. So of the three processes stated above, normalization is the most important. [Ref. 60]

Here, normalization is defined as making the governing equations and conditions non-

dimensional in terms of non-dimensional variables of standard magnitude. To carry out a normalization, two steps are usually required: 1) making all the variables non-dimensional in terms of the appropriate scales of the problem; 2) dividing through the equation by the coefficient of one term to make the equation dimensionless (unit-free) term by term. Further, the method for choosing the scaling is critical as this choice will permutate throughout the ensuing analysis. To this end, the following procedure is used (after Kline):

1. Define all dependent non-dimensional variables so that they are approximately unity over a finite distance and nowhere exceed approximately unity in the domain of concern; in this work, the undisturbed plasma values are used, denoted by a "o" subscript.

2. Define all independent non-dimensional variables so that their increment is approximately unity over the same domain of concern (0 to 1, 1 to 2, etc, in the new variables).

As a result, the dimensionless groups formed are usually composed from the boundary conditions; from the characterizing sizes or scales of the body; and from the physical constraints of the original equation such as system properties, physical constants or both. In general, it is not known in advance, which choice of pi's gives the most useful set of parameters but it is obvious that the fewer pi's required to specify the behavior, the more useful the result will be. So, how to reduce the number of pi's and consequently parameters? [Ref. 60: pp. 75-94] The choice of length or time-scales coupled with physical insight are the first step in this effort, an effort leading to a "modified fractional analysis."

C. MODIFIED FRACTIONAL ANALYSIS: ANODE FALL

1. Non-dimensional Parameters

The derivative term found in the governing equations for the anode fall, equations (7-9), is important since without which the conditions at the plasma boundary could not be satisfied. So to make all the variables non-dimensional in terms of the appropriate scale, the equations are divided through by the coefficients of the derivative terms to form the necessary system parameters where both Buckingham Pi's and undisturbed plasma values were used to normalize the variables. Following is a list of the results obtained:

Governing Equations [Equations (7-9)]	Non-dimensional Parameters via Buckingham Pi's	Non-dimensional Parameters via Undisturbed Plasma Values
$\frac{d(\bar{n}_i)}{d\bar{y}} = \left[a\right]\bar{n}_i\bar{E} - \left[b\right]\frac{\bar{j}_i}{D_i}$ $\frac{d(\bar{n}_e)}{d\bar{y}} = -\left[c\right]\bar{n}_e\bar{E} + \left[d\right]\frac{\bar{j}_e}{D_e}$ $\frac{d(\bar{E})}{d\bar{y}} = \left[e\right]\bar{n}_i - \left[f\right]\bar{n}_e$ $\frac{d(\bar{j}_e)}{d\bar{y}} = -\left[g\right]\bar{\nu}_i\bar{n}_e + \left[h\right]\bar{n}_i\bar{n}_e$ $\frac{d(\bar{j}_i)}{d\bar{y}} = \left[i\right]\bar{\nu}_i\bar{n}_e - \left[j\right]\bar{n}_i\bar{n}_e$ *where* $D_{i,e} \equiv \bar{D}_{i,e}D_{o_{i,e}}$	$a = \left[\frac{q}{\pi_1\pi_6 kT_o}\right]$, $b = \left[\frac{\pi_2\pi_8}{\pi_5\pi_6 q}\right]$ $c = \left[\frac{q}{\pi_1\pi_6 kT_o}\right]$, $d = \left[\frac{\pi_3\pi_7}{\pi_4\pi_6 q}\right]$ $e = \left[\frac{\pi_1 q}{\pi_2\pi_6\epsilon_o}\right]$, $f = \left[\frac{\pi_1 q}{\pi_3\pi_6\epsilon_o}\right]$ $g = \left[\frac{\pi_4 q}{\pi_3\pi_6\pi_9}\right]$, $h = \left[\frac{\pi_4 q\alpha_2}{\pi_2\pi_3\pi_6}\right]$ $i = \left[\frac{\pi_5 q}{\pi_3\pi_6\pi_9}\right]$, $j = \left[\frac{\pi_5 q\alpha_2}{\pi_2\pi_3\pi_6}\right]$	$a = \left[\frac{qE_oL_{n_i}}{kT_o}\right]$, $b = \left[\frac{j_{o_i}L_{n_i}}{qn_{o_i}D_{o_i}}\right]$ $c = \left[\frac{qE_oL_{n_e}}{kT_o}\right]$, $d = \left[\frac{j_{o_e}L_{n_e}}{qn_{o_e}D_{o_e}}\right]$ $e = \left[\frac{qn_{o_i}L_E}{\epsilon_oE_o}\right]$, $f = \left[\frac{qn_{o_e}L_E}{\epsilon_oE_o}\right]$ $g = \left[\frac{q\nu_o n_{o_e}L_{j_e}}{j_{o_e}}\right]$, $h = \left[\frac{q\alpha_2 n_{o_i}n_{o_e}L_{j_e}}{j_{o_e}}\right]$ $i = \left[\frac{q\nu_o n_{o_e}L_{j_i}}{j_{o_i}}\right]$, $j = \left[\frac{q\alpha_2 n_{o_i}n_{o_e}L_{j_i}}{j_{o_i}}\right]$

Non-dimensional Parameters

2. Estimate of the Length Scales

In the above, the variables where normalized using undisturbed plasma values since the Buckingham's Theorem does not reflect the physics at hand: for example, the process of ionization affects the number density distribution in the sheath resulting in electric field variations and consequently influencing the current distribution. It would be difficult for one length scale to capture each of these behaviors. Consequently physical reasoning must be the foundation from which to estimate the length scales of the problem.

The neutral plasma is shielded from the space-charge region through coulombic effects, effects which should drive the length scales affecting the associated momentum exchange processes. The first term on the right-hand side of equations (7a) and (7b) model these effects and are used to estimate the length scale affecting the number density distribution: L_{n_i}, L_{n_e} . Specifically,

$$\frac{d(\bar{n}_i)}{d\bar{y}} = \left[a\right]\bar{n}_i\bar{E} - \left[b\right]\frac{\bar{j}_i}{D_i} \qquad \text{Equation (7a)}$$

$$\frac{d(\bar{n}_e)}{d\bar{y}} = -\left[c\right]\bar{n}_e\bar{E} + \left[d\right]\frac{\bar{j}_e}{D_e} \qquad \text{Equation (7b)}$$

where [a] and [c] are the coefficients for the coulombic terms summarized in Table 2 (main body of this work). Through the process of non-dimensionalization, the parameters are O(1) and the length scales become: $L_{n_i} = \frac{kT_o}{qE_o}$, $L_{n_e} = \frac{kT_o}{qE_o}$. Similarly, the length scale for the electric field comes strictly from Gauss, equation (8), where either term can be used to estimate the electric field length scale since the undisturbed plasma value for n_o is the same for both ions and electrons:

$$\frac{d(\bar{E})}{d\bar{y}} = \left[e\right]\bar{n}_i - \left[f\right]\bar{n}_e \qquad \text{Equation (8)}$$

Using the non-dimensionalization result that all parameters are O(1), $L_E = \frac{\epsilon_o E_o}{q n_{o_i}}$ where the parameters [e] and [f] are again given in Table 2.

Within the sheath, the ionization process outweighs the recombination loss, so in equations (9a) and (9b) the ionization term, the first term on the right-hand side of the equations, is used to estimate the current density length scales:

$$\frac{d(\bar{j}_e)}{d\bar{y}} = -\left[g\right]\bar{\nu}_i\bar{n}_e + \left[h\right]\bar{n}_i\bar{n}_e \qquad \text{Equation (9a)}$$

$$\frac{d(\bar{j}_i)}{d\bar{y}} = \left[i\right]\bar{\nu}_i\bar{n}_e - \left[j\right]\bar{n}_i\bar{n}_e \qquad \text{Equation (9b)}$$

That is, the non-dimensional parameters [g] and [i] (Table 2) estimate the length scales for

the appropriate current density: $L_{j_e} = \frac{j_{o_e}}{q v_o n_{o_e}}$, $L_{j_i} = \frac{j_{o_i}}{q v_o n_{o_e}}$. Essentially, the current scale reflects the influence of ionization.

3. Dimensionless Products - Groupings

Occasionally transforming dimensionless products to achieve greater control of the variables is desired or may form a useful grouping: the various results formed through non-dimensionalizing the Navier-Stokes equations are examples. The following combination of parameters have been found from equations (10-12):

Parameter Groupings from Equations (10-12)	Groupings in Terms of Problem Constants
$\left[\frac{bi}{D_i}\right]$	$\left[\frac{bi}{D_i}\right] = \frac{L_{n_i} L_{j_i} \nu_o n_{o_e}}{D_i n_{o_i}}$
$\left[\frac{bj}{D_i}\right]$	$\left[\frac{bj}{D_i}\right] = \frac{L_{n_i} L_{j_i} \alpha_2 n_{o_e}}{D_i}$
$\left[\frac{dg}{D_e}\right]$	$\left[\frac{dg}{D_e}\right] = \frac{L_{n_e} L_{j_e} \nu_o}{D_e}$
$\left[\frac{dh}{D_e}\right]$	$\left[\frac{dh}{D_e}\right] = \frac{L_{n_e} L_{j_e} \alpha_2 n_{o_i}}{D_e}$
$\left[ae\right]$	$\left[ae\right] = \frac{L_{n_i} q^2 L_E n_{o_i}}{kT_o \epsilon_o} = \frac{L_{n_i} L_E}{\lambda_D^2}$
$\left[cf\right]$	$\left[cf\right] = \frac{L_{n_e} q^2 L_E n_{o_e}}{kT_o \epsilon_o} = \frac{L_{n_e} L_E}{\lambda_D^2}$
$\left[af\right]$	$\left[af\right] = \frac{L_{n_i} q^2 L_E n_{o_e}}{kT_o \epsilon_o} = \frac{L_{n_i} L_E}{\lambda_D^2}$
$\left[ce\right]$	$\left[ce\right] = \frac{L_{n_e} q^2 L_E n_{o_i}}{kT_o \epsilon_o} = \frac{L_{n_e} L_E}{\lambda_D^2}$

Table 10: Non-dimensional Parameter Groupings

4. Summary

Fractional analysis coupled with the use of the governing equations indicates that potentially five length scales are present, one for each of the governing equations; however, by using undisturbed plasma values for the normalization, three length scales result: a scale reflecting the conservation of momentum, one for the variation of the electric field, and the third for charge conservation. Of these three lengths, the electric field scale is the smallest, indicating the extent of the sheath as the space-charge region defines this region. The number density scale, on the other hand, acts over the entire range of the anode fall and so should be larger in magnitude than that for the electric field scale. The largest of the length scales is the current scale since the current follows the variation in species density according to $j_s=qn_sv_s$ where s=i,e:

Sheath: Space-Charge Dominant	Transition Zone: Number Density Gradient Dominant	Ambipolar Region: Equilibrium Near Plasma Boundary
$L_E<L_{n_{i,e}}<L_{j_{i,e}}$ $L_E=\frac{\epsilon_o E_o}{qn_{o_{i,e}}}$, $L_{n_{i,e}}=\frac{kT_o}{qE_o}$, $L_{j_{i,e}}=\frac{j_{o_{i,e}}}{qv_o n_{o_{i,e}}}$	$L_E=L_{n_{i,e}}<L_{j_{i,e}}$ $L_{n_{i,e}}=\frac{kT_o}{qE_o}=L_E$ $L_{j_{i,e}}=\frac{j_{o_{i,e}}}{qv_o n_{o_{i,e}}}$	$L_E=L_{n_{i,e}}=L_{j_{i,e}}$ $L_{j_{i,e}}=\frac{j_{o_{i,e}}}{qv_o n_{o_{i,e}}}$

Length Scales via Fractional Analysis

APPENDIX B. IONIZATION AND TWO-BODY RECOMBINATION DATA

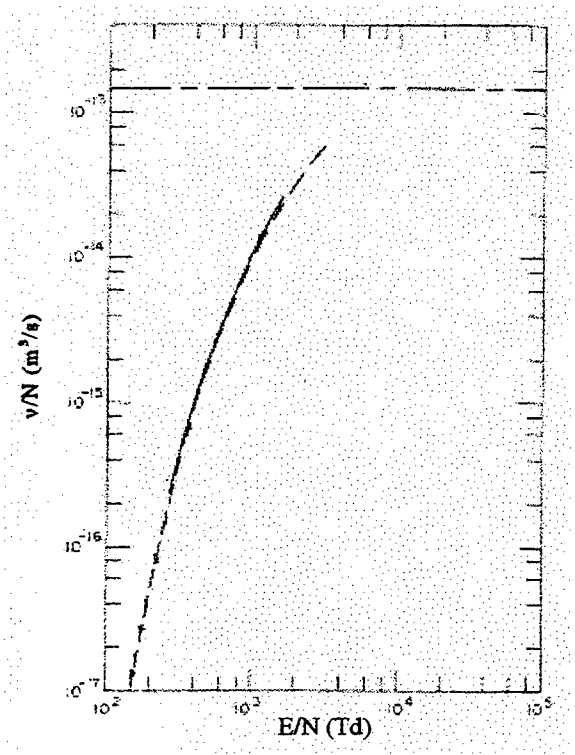

Figure 26: Ionization Coefficient ν/N as Function of E/N for N_2 [after Ref. 41]

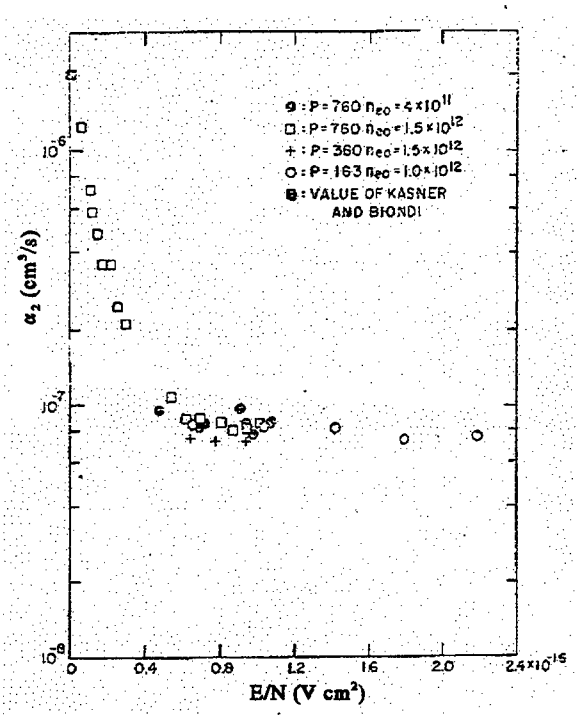

Figure 27: Two-Body Recombination Coefficient as Function of E/N for N_2 [Ref. 40]

Note: 1 Td=10^{-21} [Vm^2]

APPENDIX C. NON-LINEAR DYNAMICS - AN OVERVIEW

When exact closed-form solutions of a physical system as modeled by appropriate differential equations are difficult to obtain, or when the exact solution is too complicated to be useful, then the first step toward an approximate solution is local analysis. The results of such analysis are valid only in a sufficiently small neighborhood of a point, so ultimately a uniform approximation to the behavior of the solution over an entire interval may be found by piecing together regions where the local behavior is known through global analysis techniques involving perturbative and asymptotic methods. The following is a brief overview and adaptation of references 55 and 54 as well as class notes, reference 62.

A. LOCAL ANALYSIS: THE BASICS

If the general system given by

$$\dot{x}_1 = f_1(x_1,\ldots,x_n)$$
$$\vdots$$
$$\dot{x}_n = f_n(x_1,\ldots,x_n)$$

is visualized as trajectories flowing through an n-dimensional phase or velocity space with coordinates $(x_1,..,x_n)$, differential equations can be interpreted geometrically as vector fields, where now the velocity of the flow, the rate of change of the system behavior, can be plotted and the corresponding equilibria (stagnation or fixed points) of the system determined where the flow velocity is zero: the fixed points are calculated when the first variation tends to zero - calculus of variations. Linearization techniques, local Taylor series expansion about the stagnation, can now be used to find the stability about these points. Such analysis contains qualitative information about the dynamical behavior of the system leading to an overall explanation as to "why things happen the way they do."

In general, the behavior of a one-dimensional dynamical system $\dot{x}=f(x)$ is considered as a fluid flowing along the real line with local velocity f(x). This imaginary fluid is referred to as the phase fluid and the real line is the phase space. In higher dimensions, a similar situation occurs. The solution to $\dot{x}_i=f_i(x_1,\ldots,x_n) \quad \forall \quad i=1,2,\cdots,n$ given an arbitrary initial condition x_0 is then represented by the trajectory of the flow in *n*-dimensional space as determined by the function under investigation. The collection of these trajectories are referred to as a phase portrait whose appearance is controlled by the fixed points (stagnation, equilibria or zeros) x* as defined by f(x*)=0. This fixed point is defined as stable if all sufficiently small disturbances away from it dampen out as t→∞. Conversely, unstable equilibria are those for which disturbances grow in time.

B. LINEAR STABILITY ANALYSIS

An *n*-th order differential equation can be expressed as a system of *n* first-order equations by appropriate changes in the variables. To determine the rate of decay to a stable fixed point, linearization techniques about the equilibria are applied. For example, let x* be a fixed point and let η(t)=x(t)-x* be a small perturbation away from x*. To see whether the perturbation grows or decays, a differential equation for η is formed:

$\dot{\eta}=\frac{d}{dt}(x-x^*)=\dot{x}$ since x* remains constant by definition of stagnation points.

Consequently,

$$\dot{\eta}=\frac{d}{dt}(x-x^*)=\dot{x}=f(x)=f(x^*+\eta) \quad where \quad f(x^*+\eta)\approx f(x^*)+\eta f'(x^*)+O(\eta^2) \quad .$$

Noting that $f(x^*)=0$, $\dot{\eta} = \eta f'(x^*) + O(\eta^2)$. Moreover, if $f'(x^*)\neq 0$, then

$\dot{\eta} = \eta f'(x^*)$ is the linearization about x* where the perturbation $\eta(t)$ grows exponentially if $f'(x^*)>0$ and decays exponentially provided $f'(x^*)<0$. In essence, the slope or the rate of change of $f'(x^*)$ at the fixed point determines the stability of the stagnation.

If the dimension of the dynamical system is more than one dimensional, the procedure for stability analysis is similar but now a multi-variable Taylor series expansion is used for the linearization technique. Consider a two-dimensional non-linear system where the general form of a vector field on the phase plane is given by

$$\dot{x}_1 = f_1(x_1, x_2)$$
$$\dot{x}_2 = f_2(x_1, x_2)$$

with f_1 and f_2 as given functions. In vector notation, $\mathbf{x}=(x_1,x_2)$ and $f(\mathbf{x}) = [f_1(\mathbf{x}), f_2(\mathbf{x})]$. Here, $\mathbf{x}$ represents a point in the phase plane and $\dot{\mathbf{x}}$ is the velocity vector at that point. By flowing along the vector field, a phase point traces out a solution $\mathbf{x}(t)$, corresponding to a trajectory winding through the phase plane. Essentially the entire phase plane is filled with trajectories since each point can play the role of an initial condition. For nonlinear systems, however, it remains a challenging task to find these trajectories, the solutions, analytically. Even when explicit solutions are available, their form is often intractable and provide limited insight: the importance of a qualitative analysis to understand the characteristics, the dynamical behavior, of a system becomes apparent.

Consider the system

$$\dot{x} = f(x,y)$$
$$\dot{y} = g(x,y)$$

and suppose that (x*,y*) represents an equilibrium position, i.e., f(x*,y*)=0 and g (x*,y*)=0. To begin linearization, let u=x-x* and let w=y-y* be components of small perturbations away from the stagnation. To see whether the disturbance grows or decays, a differential equation for u and w must be found similarly to the one-dimensional method above (noting that x* and y* remain constant by definition of equilibrium):

$$\begin{aligned}\dot{u}=\dot{x}&=f(x^*+u,y^*+w)\\&=f(x^*,y^*)+u\frac{\partial}{\partial x}(f)+w\frac{\partial}{\partial y}(f)+O(u^2,w^2,uw)\\&=u\frac{\partial}{\partial x}(f)+w\frac{\partial}{\partial y}(f)+O(u^2,w^2,uw)\end{aligned}$$

and

$$\begin{aligned}\dot{w}=\dot{y}&=g(x^*+u,y^*+w)\\&=g(x^*,y^*)+u\frac{\partial}{\partial x}(g)+w\frac{\partial}{\partial y}(g)+O(u^2,w^2,uw)\\&=u\frac{\partial}{\partial x}(g)+w\frac{\partial}{\partial y}(g)+O(u^2,w^2,uw)\end{aligned}$$

where partial derivatives in the preceding are all evaluated at (x*,y*). That is, the effects of the perturbations (u,w) evolve according to the linearized system:

$$\begin{bmatrix}\dot{u}\\\dot{w}\end{bmatrix}=\begin{bmatrix}\frac{\partial}{\partial x}(f) & \frac{\partial}{\partial y}(f)\\\frac{\partial}{\partial x}(g) & \frac{\partial}{\partial y}(g)\end{bmatrix}_{(x^*,y^*)}\begin{bmatrix}u\\w\end{bmatrix}+O(u^2,w^2,uw)$$

The matrix of partial derivatives evaluated at the stagnation (x*,y*) is termed the Jacobian matrix, the multi-variable analogue of the derivative f'(x*) developed for the one-dimensional system. Furthermore, if the quadratic terms found in O(u^2,w^2,uw) are sufficiently small, then the behavior of the linearized system can be analyzed through study of the Jacobian matrix alone.

C. CLASSIFICATIONS OF FIXED POINTS

To classify all possible phase portraits that can occur given an arbitrary Jacobian matrix, it should be noted that the coordinate axes play a critical geometric role; they determine the direction of the flow as $t \to \pm\infty$, containing straight-line trajectories. A trajectory starting on one of these axes stays on that axis forever and exhibits simple exponential growth or decay along it. For the general case, however, the analog of these straight-line trajectories has to be found, so trajectories of the form $x(t) = e^{\lambda t} V$, where $\mathbf{V} \neq 0$ is some fixed vector, are sought with λ as a growth rate, also to be determined. If such solutions exist, they correspond to exponential motion along the line spanned by the vector **V**. The conditions on λ and **V** are determined by the eigenvalues and corresponding eigenvectors of the Jacobian matrix, respectively. That is, the characteristics of the linearized system are determined by the nature of the Jacobian eigenvalues.

1. Robustness of Linearization

The stability of a fixed point can be classified in terms of robust or marginal cases. Robust cases are those for which the stability does not change under the influence of small non-linear terms such as repellers (sources), attractors (sinks) or saddles. Specifically, repellers are those fixed points for which the Jacobian displays positive real parts for all eigenvalues, attractors are those characteristics which display negative real parts for all eigenvalues. Saddles occur when one eigenvalue is real and positive while the other is real and negative. Marginal stability results when both eigenvalues are imaginary (centers) or when at least one of the eigenvalues is zero. For marginal stability, then, at least one of eigenvalues satisfies $\mathrm{Re}(\lambda)=0$ whereas for robust stability, $\mathrm{Re}(\lambda)\neq 0$; that is, for marginal stability, the trace of the Jacobian matrix is zero or the flow divergence is zero, implying that the flow volume is preserved.

2. Real, Distinct Eigenvalues

In general, trajectories approach the origin of the phase portrait tangent to the slow eigendirection, the direction spanned by the eigenvector with the smaller $|\lambda|$. If $|\lambda_2| < |\lambda_1|$, then the trajectories approach λ_2 as $t \to \infty$:

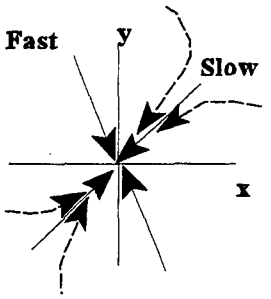

Real, Distinct Eigenvalues -
$0<|\lambda_2|<|\lambda_1|$ and $\lambda_1, \lambda_2<0$
"Node"

If all eigenvalues are positive and distinct, then the behavior locally about the respective stagnation is termed "unstable node", whereas if all eigenvalues are negative and distinct, then the dynamics about the fixed point is called "stable node".

What happens when one of the eigenvalues is positive while the other is negative? If $\lambda>0$, the corresponding eigensolution grows exponentially; if $\lambda<0$, the eigensolution decays exponentially. The stable manifold corresponds to the line spanned by the eigenvector formed by $\lambda<0$, whereas the unstable manifold corresponds to the line spanned by the eigenvector formed by $\lambda>0$. The combination of such behavior forms the "saddle" where trajectories are attracted toward the stable manifold and repelled as the unstable manifold is approached:

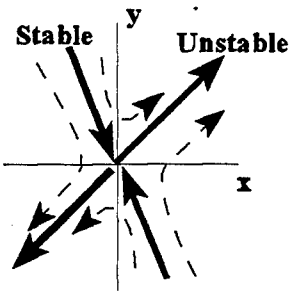

Real, Distinct Eigenvalues -
$\lambda_1<0, \lambda_2>0$ "Saddle"

3. Complex Eigenvalues

The eigenvalues of the Jacobian determine the local dynamical behavior of the system: the eigensolution $x(t) = c_1 e^{\lambda_1 t} V_1 + c_2 e^{\lambda_2 t} V_2$ is affected by the eigenvalues according to the behavior of $e^{\lambda t}$. If $\lambda_{1,2}=\alpha\pm i\omega$, then the system is influenced by $e^{\alpha t}e^{i\omega}$ where α is the real component of the complex eigenvalue (damping) and ω is the imaginary component, $\omega\neq 0$. By Euler's formula, $e^{i\omega t}=\cos(\omega t)+i[\sin(\omega t)]$ and so $\mathbf{x}(t)$ becomes a cosinusoidal function with exponential growth, instability, according to $e^{\alpha t}$ if $\alpha>0$, or with exponential decay, stability, if $\alpha<0$. Such behavior is termed "spiral", unstable or stable depending on whether energy is supplied to the flow or taken from the flow.

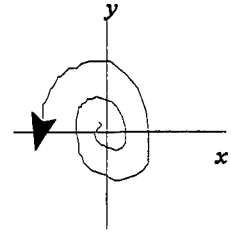

Complex Eigenvalues:
$\lambda_{1,2}=\alpha\pm i\omega t$ "Spiral"

If, on the other hand, the eigenvalues are purely imaginary, $\alpha=0$, then all solutions are periodic with period $T=2\pi/\omega$ where the oscillations have constant amplitude.

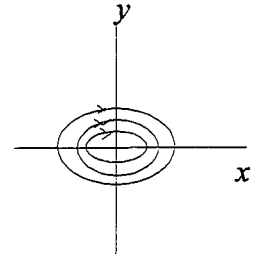

Imaginary Eigenvalues:
$\lambda_{1,2}=\pm i\omega t$ "Center"

Centers, or systems with purely imaginary eigenvalues, occur generally where energy is conserved, corresponding to a state of neutrally stable equilibrium, or a position of minimum energy, although the linearization represented is not robust. Small non-linear terms can change the characteristics from periodicity to exponential growth or decay (see below).

4. Real, Equal Eigenvalues

Suppose that $\lambda_1=\lambda_2=\lambda$, the eigenvalues of the system are equal. Two possibilities now exist: either there are two independent manifolds corresponding to λ, or there is only one.

If two independent manifolds exist, then they span the plane and so every vector forms a manifold with this same eigenvalue λ. If $\lambda\neq 0$, all trajectories are straight lines through the corresponding equilibrium position which is now termed a "star", stable or unstable if $\lambda<0$ or if $\lambda>0$, respectively:

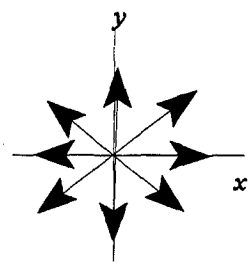

Real, Equal Eigenvalues:
$\lambda_1=\lambda_2=\lambda>0$ "Star"

If the eigenspace corresponding to the eigenvalue λ is one dimensional, i.e., there is only one manifold corresponding to λ, the corresponding fixed point is a "degenerate node": as $t\to\pm\infty$ where all trajectories become parallel to the one available eigendirection. Essentially, this behavior results when two distinct manifolds are scissored together with some of the trajectories becoming trapped in the collapsing region between the two eigendirections, while the surviving trajectories are pulled around to form the degenerate node with stability determined according to $\lambda<0$ or $\lambda>0$. The degenerate node is a borderline case between a spiral and a node; the trajectories are trying to wind around in a spiral (complex eigenvalues), but insufficient energy is present to complete the winding:

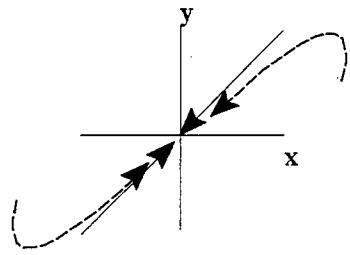

Real, Equal Eigenvalues with One Manifold: $\lambda_{1,2} = \lambda$

5. Miscellaneous

a. Small Non-linear Terms Change Linearization Stability-Sometimes

In the presence of non-linear terms, the character of marginally stable fixed points can change: centers, stars and degenerate nodes all satisfy the criterion $Re(\lambda)=0$. For example, if the linearization predicts a center, the influence of non-linear effects causes the phase portrait to show a stable or unstable spiral, a stable or unstable node; the presence of non-linear terms violate $Re(\lambda)=0$ by either adding or removing energy from the system, driving it away from the conserved state (center). Similarly, stars and degenerate nodes can also change their character, but unlike centers, non-linear effects change only the character of the star or degenerate node, not their stability: stable star to stable spiral or stable node, for example.

The phase portrait is structurally stable if its topology is not changed by arbitrary small perturbations to the vector field: the phase portrait of a saddle point is structurally stable, but that of a center is not since an arbitrary small amount of damping converts the center to a spiral. Essentially, if the phase portrait changes its topological structure as a parameter is varied, a bifurcation is in progress.

b. Example: A Glider

Consider a glider flying at speed v at an angle θ to the horizontal. Its motion is governed approximately by the dimensionless equations

$$\frac{dv}{dt} = -\sin(\theta) - Dv^2$$
$$v\frac{d\theta}{dt} = -\cos(\theta) + v^2$$

where the trigonometric terms represent the effects of gravity and the v^2 terms represent the effects of drag and lift. Here, it is desired to find the effects on the glider performance as the drag parameter, D, is varied.

To begin the analysis, first a local analysis is performed about any stationary points (fixed points) that occur when the derivative terms are set to zero. These fixed points are then used to evaluate the linearization (Jacobian) so that the system characteristics about the stagnation can be determined in terms of eigenvalues and eigenvectors. The results are summarized:

Fixed Point	Comments	Jacobian Eigenvalues
(nπ,1)	n=0,2,4,6,...	$\lambda_{1,2} = \frac{2D \pm \sqrt{4D^2 - 8}}{2}$
(nπ,-1)	n=0,2,4,6,...	$\lambda_{1,2} = \frac{2D \pm \sqrt{4D^2 - 8}}{2}$

From the preceding, it is seen that if the drag D>2 in non-dimensional terms, the eigenvalues of both fixed points will always be real and distinct. The associated dynamical behavior, locally, can therefore be characterized as a stable node for the fixed point (nπ,1) and as an unstable node for (nπ,-1). If D≥0, then the trace of the Jacobian (sum of respective eigenvalues) will always be less than zero for the fixed point (nπ,1), while the instability for (nπ,-1) is shown by the exponential growth of the oscillation component of the associated

system eigenvalues (trace>0).

If $2 \geq D \geq 0$, the eigenvalues are complex and hence the local dynamics of the system is represented by stable spirals for $(n\pi,1)$ and an unstable spiral for $(n\pi,-1)$. Similarly, the stability/instability is evident through the exponential decay/growth of the oscillations characterized by the real component of the respective eigenvalues. It should be noted that when D=2, the eigenvalues are real and equal, however. Consequently, the system behavior should be that of a star or a degenerate node: a spiral (unstable or stable, depending on the eigenvalues), is found instead. Here is evidence that nonlinear terms in the system can change the local behavior from that which is predicted by the linearization analysis.

If D=0, the case of no drag, then the eigenvalues for the fixed point $(n\pi,1)$ with n=0 will be imaginary, reflecting pure oscillation of the system and consequently periodic solutions with period $T=2\pi/\omega$. The resulting equilibria are characterized as centers and describe the lowest energy or power state of the system, the glider moving in a potential field, gravity, without any other influences. That is, the glider moves along lines of constant energy, along a curved flight path with a radius of curvature equal to the absolute altitude, experiencing the standard "fictitious" forces due to relative motion (centripetal acceleration, for example).

In general, for D>0, the case of increasing drag, the centers at $(n\pi,1)$ transition to stable spirals/nodes, whereas the centers at $(n\pi,-1)$ transition to unstable spirals/nodes. From an eigenvalue consideration, both dampening and oscillations are now evident; the eigenvalues are complex with exponential decay for the stable spiral/node and exponential growth for the unstable spiral/node. In essence, drag tends to offset the lift generated, as expected. This example shows that if the phase portrait changes its topological structure as a parameter is varied, a bifurcation is in progress.

D. BIFURCATIONS

As indicated, the stability of a fixed point can change; such qualitative changes in dynamics are referred to as bifurcations. Bifurcations provide models of transitions and instabilities as some control parameter is varied, the onset of coherent radiation in a laser, for example. Of the many types of bifurcations possible, only Saddle-node and Transcritical, are outlined here.

The saddle and transcritical bifurcations occur when one of the eigenvalues equals zero, involving the collision of two or more fixed points. These types of bifurcations have analogs in one, two and higher dimensions since the important behavior for these dynamics are confined to a one-dimensional subspace along which the bifurcation occurs, when $\mathrm{Re}(\lambda)=0$, while in the extra dimensions the flow is either simple attraction or repulsion from that subspace.

1. Saddle-Node Bifurcations

The saddle-node bifurcation is the basic mechanism by which fixed points are created and destroyed. For instance, as a parameter is varied, two fixed points move toward each other, collide and mutually annihilate. The prototypical example of a saddle-node bifurcation is given by the system $\begin{matrix}\dot{x}=r\pm x^2\\ \dot{y}=-y\end{matrix}$ where r is a small parameter determined by the problem at hand. Here, the motion is decoupled with the y-direction assumed arbitrarily as exponentially decaying. The fixed points for this system are $(x^*,y^*)=(\pm\sqrt{r},0)$, stagnation points which exist in the x,y plane when r>0, coalesce when r=0 and do not exist (in x,y space) when r<0. Upon further analysis, it is seen that the bifurcation is fundamentally one-dimensional, with the fixed points sliding toward each other along the unstable manifold of the saddle point at $(x^*,y^*)=(-\sqrt{r},0)$ where r>0.

For two-dimensional system, and for higher-dimensional systems, the flow is limited not only by fixed points (stagnation), buts also by closed orbits and the unions of fixed points and the trajectories connecting them. The latter are referred to as heteroclinic orbits when

they connect distinct points and homoclinic orbits when they connect a point to itself. For example, if the physical system is such that the unstable manifold of a saddle node intersects with its stable manifold, the resulting orbit is called "homoclinic:" the connection of the unstable manifold ($\lambda>0$) and the stable manifold ($\lambda<0$) of the saddle point is common in conservative systems but can also occur in non-conservative systems. When the system dynamics are such that additional damping is introduced, the tendency is for the homoclinic orbit to break, causing the unstable manifold to have components which approach the fixed point at the origin of the phase portrait as $t\rightarrow\infty$. This fixed point is then a sink, with eigenvalues $-\alpha\pm i\lambda$ where α is the damping. [Ref. 55: p. 45]

2. Transcritical Bifurcation

There are certain scientific situations where a fixed point (stagnation) must exist for all values of a parameter and can never be destroyed. For example, in the logistic equation there is a fixed point at zero population, regardless of the value of the growth rate; the laser rate equation (classical) is another example for which a fixed point always exists. However, such a fixed point may change its stability as the parameter is varied. The transcritical bifurcation is the standard mechanism for such changes in stability, with normal form given by: $\dot{x}=rx\pm x^2$, $\dot{y}=-y$ where r is control parameter determined by the problem. The difference between the saddle-node and transcritical bifurcations is that in the latter, the fixed points do not "disappear," their stability changes instead. Consider, for example, the laser rate equation [Ref. 54: p. 54]:

$$\begin{aligned}\frac{dn}{dt} &= gain - loss = GnW - kn \\ &= Gn(W_o - \alpha n) - kn = GW_o n - \alpha G n^2 - kn \\ &= (GW_o - k)n - (\alpha G)n^2\end{aligned}$$

where n(t) represents the number of photons, W characterizes the rate with which a single excited atom spontaneously generates a photon per second offset by the number of photons

per second that drop back to the ground state, α; W_o is the pump strength. G is the gain coefficient, and $-\kappa$ shows the rate at which photons are lost in the laser by scattering or impurities. For the laser rate equation shown, two equilibria exist: $n_1^*=0$ and $n_2^* = \frac{GW_o - k}{\alpha G}$. But what does this mean? Shown below are the phase portraits with the fixed points indicated:

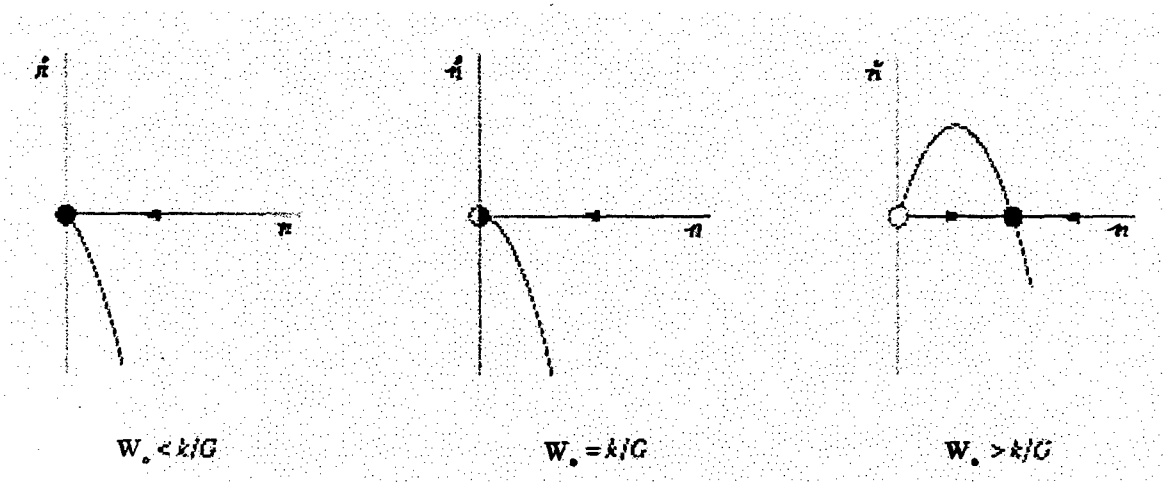

When $W_o < k/G$, $GW_o - k < 0$, $n_1^*=0$ is stable and for low levels of incident energy (weak pumping) the solution $n_1^*=0$ must be valid since n(t), the number of photons generated, must always be positive. Consequently, there can be no laser action - the laser acts like a lamp. When the laser is pumped at a greater intensity such that now $(GW_o - k)>0$ or $W_o > k/G$ holds, the solution with $n>0$ becomes possible and laser action is attained. The system undergoes a transcritical bifurcation when $W_o = k/G$, the laser threshold for this model. When $W_o > k/G$ the lamp becomes a laser and the fixed point $n_1^*=0$ loses stability, driving the system toward n_2^*. The pumping intensity elevates the inversion population: a critical threshold exists when $W_o = k/G$ below which laser action cannot occur (insufficient pumping energy and consequently insufficient inversion) and the laser acts like a lamp. Above the threshold, laser action occurs since sufficient energy is now available to raise the atoms to higher energy

levels so that the number of photons generated are enough to cause lasing. At the threshold, at the transcritical bifurcation point, the stability of the system origin becomes unstable, driving the dynamics toward greater population inversion and consequently toward the second fixed point. In fact, there are certain scientific situations where a fixed point (stagnation) must exist for all values of a parameter and can never be destroyed although it changes its stability character; the laser is such an example, for it is the stagnation at the origin that drives the system toward the lasing threshold at the bifurcation point. [Ref. 63]

APPENDIX D. CHARACTERISTICS OF SHEATH EQUATIONS

The Jacobian to equations (7-9),

$$\hat{A}_{inner} = \begin{bmatrix} [a]\bar{E} & 0 & [a]\bar{n}_i & 0 & -\left[\frac{b}{D_i}\right] \\ 0 & -[c]\bar{E} & -[c]\bar{n}_e & \left[\frac{d}{D_e}\right] & 0 \\ [e] & -[f] & 0 & 0 & 0 \\ [h]\bar{n}_e & -[g]\bar{v}+[h]\bar{n}_i & \frac{-[g]\bar{n}_e\bar{v}}{\bar{E}^2} & 0 & 0 \\ -[j]\bar{n}_e & [i]\bar{v}-[j]\bar{n}_i & \frac{[i]\bar{n}_e\bar{v}}{\bar{E}^2} & 0 & 0 \end{bmatrix}$$

has the following characteristic polynomial:

$$characteristic\ \ polynomial = \alpha\lambda^5 + \beta\lambda^4 + \gamma\lambda^3 + \zeta\lambda^2 + \eta\lambda + \epsilon = 0$$

where

$$\alpha = D_i D_e \bar{E}^2 \qquad \beta = D_i D_e \bar{E}^3 \left[c - a \right]$$

$$\gamma = \bar{E}^2 D_i \left\{ -\left[dh \right] \bar{n}_i + \left[dg \right] \bar{\nu} \right\} -$$
$$\bar{E}^2 D_e \left[bj \right] \bar{n}_e + \bar{E}^2 D_i D_e \left\{ -\left[ea \right] \bar{n}_i - \left[cf \right] \bar{n}_e \right\} -$$
$$\bar{E}^4 D_i D_e \left[ac \right]$$

$$\zeta = \bar{E}^3 D_e \left[bjc \right] \bar{n}_e + \bar{E}^3 D_i \left\{ \left[adh \right] \bar{n}_i - \left[adg \right] \bar{\nu} \right\} +$$
$$\bar{E}^3 D_i D_e \left\{ -\left[eac \right] \bar{n}_i + \left[afc \right] \bar{n}_e \right\} +$$
$$\bar{n}_e D_e \left[ebi \right] \bar{\nu} - \bar{n}_e D_i \left[fgd \right] \bar{\nu}$$

$$\eta = \bar{E} \bar{n}_e D_e \left[ecbi \right] \bar{\nu} +$$
$$\bar{E}^2 \bar{n}_e \left\{ \left[dhbi \right] \bar{\nu} - \left[bjdg \right] \bar{\nu} \right\} +$$
$$\bar{E} \bar{n}_e D_i \left[afdg \right] \bar{\nu} +$$
$$\bar{n}_e^2 \bar{E}^2 D_e \left[bjcf \right] +$$
$$\bar{E}^2 D_i \left\{ \bar{n}_i \bar{n}_e \left[dhaf \right] - \bar{n}_i \left[aedg \right] \bar{\nu} + \bar{n}_i^2 \left[aedh \right] \right\} +$$
$$\bar{E}^2 D_e \left\{ \bar{n}_i \bar{n}_e \left[cebj \right] - \bar{n}_e \left[cebi \right] \bar{\nu} \right\}$$

$$\epsilon = \bar{n}_i \bar{n}_e \left\{ \left[ebjgd \right] \bar{\nu} - \left[edhib \right] \bar{\nu} - \bar{n}_e^2 \left[hdfib \right] \bar{\nu} - \left[jbfgd \right] \bar{\nu} \right\}$$

To find the solutions to the characteristic polynomial, at least one of the roots has to be known apriori. To this end, the Jacobian is evaluated for the fixed point found when $\bar{n}_e^* = \bar{n}_i^* = \bar{n}^* = 0$ (see Table 5 in the main body of this work) but with $\bar{E}$ retained as a non-zero variable (see Chapter V). The resulting Jacobian eigenvalues for the fixed point for this condition become:

$$\lambda_1 = [a]\bar{E} \qquad \lambda_{2,3} = 0$$

$$\lambda_{4,5} = -\frac{[c]\bar{E}}{2} \pm \frac{\sqrt{\left([c]\bar{E}\right)^2 - 4\left[\frac{dg}{D_e}\right]\bar{v}}}{2D_e}$$

To find the general eigenvalues of the Jacobian then, the characteristics $\lambda_1 = [a]\bar{E}$ *and* $\lambda_2 = 0$ are assumed as solutions. By factoring the characteristic polynomial with these results and neglecting any remainder terms gives the approximate and complicated solutions to the characteristic polynomial:

$$\lambda_1 = [a]\bar{E} \quad \lambda_2 = 0$$

$$\lambda_3 = \left\{1 + \frac{\sqrt{y^3 + x^2}}{x}\right\}^{\frac{1}{3}} + \left\{1 - \frac{\sqrt{y^3 + x^2}}{x}\right\}^{\frac{1}{3}} - z$$

$$\lambda_4 = -\frac{1}{2}\left\{1 + \frac{\sqrt{y^3 + x^2}}{x}\right\}^{\frac{1}{3}} - \frac{1}{2}\left\{1 - \frac{\sqrt{y^3 + x^2}}{x}\right\}^{\frac{1}{3}} - \frac{1}{2}I\sqrt{3}\left\{\left\{1 + \frac{\sqrt{y^3 + x^2}}{x}\right\}^{\frac{1}{3}} - \left\{1 - \frac{\sqrt{y^3 + x^2}}{x}\right\}^{\frac{1}{3}}\right\} + z$$

$$\lambda_5 = -\frac{1}{2}\left\{1 + \frac{\sqrt{y^3 + x^2}}{x}\right\}^{\frac{1}{3}} - \frac{1}{2}\left\{1 - \frac{\sqrt{y^3 + x^2}}{x}\right\}^{\frac{1}{3}} + \frac{1}{2}I\sqrt{3}\left\{\left\{1 + \frac{\sqrt{y^3 + x^2}}{x}\right\}^{\frac{1}{3}} - \left\{1 - \frac{\sqrt{y^3 + x^2}}{x}\right\}^{\frac{1}{3}}\right\} + z$$

with

$$x = \frac{1}{6}\gamma_1\left(\frac{\beta}{\alpha}+\kappa\right) - \frac{1}{2}\gamma_2 - \frac{1}{27}\left(\frac{\beta}{\alpha}+\kappa\right)^3$$

$$y = \frac{1}{3}\gamma_1 - \frac{1}{9}\left(\frac{\beta}{\alpha}+\kappa\right)^2$$

$$z = \frac{1}{3}\left(\frac{\beta}{\alpha}+\kappa\right)$$

where

$$\kappa = \left[a\right]\bar{E}, \qquad \gamma_1 = \left(\frac{\beta}{\alpha}+\kappa\right)\kappa + \frac{\gamma}{\alpha}, \qquad \gamma_2 = \gamma_1\kappa + \frac{\zeta}{\alpha}$$

If numeric data nitrogen is applied to the stagnation region near the plasma boundary (Tables 4, 5) and the results substituted into these roots, an order of magnitude comparison can be performed with the actual results obtained (the exact evaluation of Jacobian at the fixed point in question):

	λ_1	λ_2	λ_3	λ_4	λ_5
Jacobian Evaluated at Plasma Boundary Stagnation	1.376704	0	0.630455	-1.37437	-0.63279
Approximate Solutions to Jacobian at Plasma Boundary Stagnation	1.41467	0	0.54	-1.41262	-0.54205

Table 11: Sheath Equations - Jacobian Characteristics Evaluated at Plasma Boundary Equilibrium

It seems that λ_1 dominates the exponential growth seen during any numeric simulation - the process of ion repulsion from the positive plate forces the instability of the sheath.

LIST OF REFERENCES

1. Stuhlinger, E., *Ion Propulsion for Space Flight*, McGraw-Hill, 1964.

2. Sutton, G.P., *Rocket Propulsion Elements*, 6th ed., John Wiley & Sons, 1992.

3. Jahn, R.G., *Physics of Electric Propulsion*, McGraw-Hill, New York 1968.

4. Alexeev, Yu. A., Kazeev, M.N., Pavshuk, V.A., *The New Possibilities of Magnetoplasmadynamic Thrusters,* Russian Research Center "Kurchatov Institute," Moscow. Undated (Internet)

5. Fitzhugh, A., *Magnetoplasmadynamic Thruster: Executive Summary*, Southampton University, Undated (Internet).

6. Dolson, R.C., and Biblarz, O., "Analysis of the Voltage Drop Arising from a Collision-dominated Sheath," J. Appl. Phys., V. 47, No. 12, pp. 5280-5287, Dec., 1976.

7. Diamant, K.D,. Choueiri, E.Y. and Jahn, R.G., "The Role of Spot Mode Transition in the Anode Fall of Pulsed MPD Thrusters," undated.

8. Myers, R.M., "Applied Field MPD Thruster Geometry Effects, AIAA-91-2342, June 1991.

9. Soulas, G.C., and Myers, R.M., "Mechanisms of Anode Power Deposition in a Low Pressure Free Burning Arc," IEEE Trans. On Plasma Science, Vol. 24, No. 2, pp. 478-486, April 1996.

10. Gallimore, A.D., Myers, R.M., Kelly, A.J., and Jahn, R.G., "Anode Power Deposition in an Applied-Field Segmented Anode MPD Thruster," Journal of Propulsion and Power, Vol. 10, pp. 262-268, April, 1994.

11. Gallimore, A.D., Kelly, A.J., and Jahn, R.G., "Anode Power Deposition in Magnetoplasmadynamic Thrusters," Journal of Propulsion and Power, Vol. 9, pp. 361-368, June, 1993.

12. Gallimore, A.D., Kelly, A.J., and Jahn, R.G., "Anode Power Deposition in Quasisteady Magnetoplasmadynamic Thrusters," Journal of Propulsion and Power, Vol. 8, pp. 1224-1231, December, 1992.

13. Sleziona, P.C., Auweter-Kurtz, M. And Schrade, H.O., "Numerical codes for Cylindrical MPD Thrusters," IEPC 88-038, 20th Int'l. Elec. Prop. Conf., Garmisch-Partenkirchen, W. Germany, October 1988.

14. Sleziona, P.C., Auweter-Kurtz, M., and Schrade, H.O., "Numerical Evaluation of MPD Thrusters," AIAA 90-2602, July, 1990.

15. LaPointe, M.R., "Numerical Simulation of Self-Field MPD Thrusters," AIAA-91-2341, NASA-CR-187168, July, 1991.

16. Myers, R.M., Mantenieks, M.A., and LaPointe, M.R., "MPD Thruster Technology," NASA-TM-105242, AIAA-91-3568, September, 1968.

17. Hugel, H., "Effects of Self-Magnetic Forces on the Anode Mechanism of a High Current Discharge," IEEE Trans. On Plasma Science, Vol. PS-8, pp. 437-442, December, 1980.

18. Subramaniam, V.V. and Lawless, J.L., "Thermal Instabilities of the Anode in a Magnetoplasmadynamic Thruster," J. Propulsion & Pwr., V. 6, No. 2, pp. 221-224, March, 1990.

19. Brown, S.C., *Introduction to Electrical Discharges in Gases*, John Wiley & Sons, 1966.

20. Chung, P.M, Talbot, L, and Touryan K.J., *Electric Probes in Stationary and Flowing Plasmas: Theory and Application*, Springer-Verlag, NY, 1975.

21. Swift, J.D. and Schwar, M.J.R., *Electric Probes for Plasma Diagnostics*, American Elsevier Publishing Company, 1969.

22. Davydov, B. and Zmanovskaja, L. Zh. Tekh. Fiz., Vol. 3, p. 715, 1936.

23. Ecker, G., Masterson, K.J., Jr., and McClure, J., "Abgrenzung und Erweiterung der Langmuirschen Sondentheorie," Annalen der Physik, Vol. 15, p. 69, 1965.

24. Cohen, I.M., "Asymptotic Theory of Spherical Electrostatic Probes in a Slightly Ionized Collision-Dominated Gas," Physics of Fluids, vol. 6, pp. 1492-1499 , October 1963.

25. Kiel, R.E., "Continuum Electrostatic Probe Theory for Large Sheaths on Spheres and Cylinders," Journal of Applied Physics, v. 40, pp. 3668-373, August 1969.

26. Barad, M.S., and Cohen, I.M., "Continuum Theory of Spherical Electrostatic Probes in a Stationary, Moderately Ionized Plasma," Physics of Fluids, Vol. 17, pp. 724-734, April, 1974.

27. Su, C.H. and Lam, S.H., "Continuum Theory of Spherical Electrostatic Probes," Physics of Fluids, Vol. 6, pp. 1479-1491, October, 1963.

28. Lam, S.H., "A General Theory for the Flow of Weakly Ionized Gases," AIAA Journal, v. 2, pp. 256-262, February 1964.

29. Sutton, G.W., and Sherman, A., *Engineering Magnetohydrodynamics*, McGraw-Hill, NY, 1965.

30. McKee, H.B. and Mitchner, M., "Electrostatic Probes for Diagnostics in a Collison-Dominated Weakly Ionized Plasma," Electricity from MHD (International Atomic Energy Agency, Vienna), v. 1, p. 107, 1966.

31. Cohen, I.M., and Schweitzer, S., "First-Order Effects of Production on the Continuum Theory of Spherical Electrostatic Probes," AIAA Journal, Vol. 6, pp. 298-304, February, 1968.

32. Su, C.H., and Sonin, A.A., "Theory of the Electrostatic Probe in a Moderately Ionized Gas," Physics of Fluids, Vol. 10, pp. 124-126, January, 1967.

33. Stahl, N. And Su, C.H., "Theory of Continuum Flush Probes," Physics of Fluids, v. 14, pp. 1366-1376, July 1971.

34. Godyak, V.A., and Sternberg, N., "Smooth Plasma-Sheath Transition in a Hydrodynamic Model," IEEE Transactions on Plasma Science, Vol. 18, pp. 159-168, February, 1990.

35. Nasser, E., *Fundamentals of Gaseous Ionization and plasma Electronics.* New York: Wiley-Interscience. 1971.

36. Biblarz, O., "Approximate Sheath Solutions for a Planar Plasma Anode," IEEE Trans. Plasma Sci., V. 19, No. 6, pp. 1235-1243, December, 1991.

37. Shih, K.T. and Pfender, E., "Electrode Energy Transfer Mechanisms in a MPD Arc," AIAA Journal, Vol. 8, pp. 211-215, February, 1970.

38. Chen, F.F., *Introduction to Plasma Physics*, Plenum Press, 1976.

39. Biblarz, O., "Plasma Constriction at the Electrodes Arising from Continuity Considerations," unpublished.

40. Douglas-Hamilton, D. H., "Recombination Rate Measurements in Nitrogen," Journal of Chemical Physics, Vol. 58, No. 11, pp. 4820-4823, 1973.

41. Phelps, A.V., and Pitchford, L.C., "Anisotropic Scattering of Electrons by N2 and its Effect on Electron Transport," Physical Review A, Vol. 31, No. 5, pp. 2932-2949, 1985.

42. Cobine, J.D., *Gaseous Conductors*, Mc-Graw Hill, 1941.

43. Ingold, J.H., "Glow Discharges at DC and Low Frequencies", *Gaseous Electronics, Vol. 1: Electrical Discharges*, Hirsh, M.N., and Oskam, H.J., eds., Academic Press, 1978.

44. Miller, H.C., "A Review of Anode Phenomena in Vacuum Arcs," IEEE Transactions on Plasma Science, Vol. PS-13, No. 5, pp. 242-252, October, 1985.

45. Persson, K.B., "Inertia Controlled Ambipolar Diffusion," Physics of Fluids, Vol 5, No. 12, pp. 1625-1632, 1962.

46. Woods, L.C., Journal of Fluid Mechanics, Vol. 23 (pt. 2), pp. 315, 1965.

47. Forrest, R.J., and Franklin, R.N., Br. J. Appl. Phys., Vol. 17, pp. 1569, 1966.

48. Self, S.A., and Edwald, H.N., "Static Theory of a Discharge Column at Intermediate Pressures", Physics of Fluids, Vol. 9, pp. 2486-2492, 1966.

49. Bohm, D., in *The Characteristics of Electrical Discharges in Magnetic Fields*, Gutherie, A. and Wakerling, R.K., Eds., McGraw-Hill, 1949, Chapter 3.

50. Valentini, H.B., "Removal of singularities in the hydrodynamic description of plasmas including space-charge effects, several species of ions and non-vanishing ion temperature," Journal of Physics D: Applied Physics, Vol. 21, pp. 311-321, 1988.

51. Franklin, R.N., *Plasma Phenomena in Gas Discharges*, Clarendon, Oxford, 1976.

52. Brown, S.C., *Introduction to Electrical Discharges in Gases*, John Wiley & Sons, 1966.

53. Biblarz, O. and Riggs, J.F., "Anode Sheath Contributions in Plasma Thrusters," AIAA 93-2495, 29th Joint Propulsion Conference and Exhibit, 28-30 June 1993.

54. Strogatz, S.H., *Nonlinear Dynamics and Chaos*, Addison-Wesley Publishing, 1994.

55. Guckenheimer, J. and Holmes, P., *Nonlinear Oscillations, Dynamical Systems, and Bifurcations of Vector Fields*, Springer-Verlag, 1983.

56. Von Engel, A., *Ionized Gases*, Oxford University Press, 1965.

57. Cobine, J.D., *Gaseous Conductors*, McGraw-Hill, New York, 1941.

58. Compton, K.T., and Langmuir, I., "Electrical Discharges in Gases: Part II. Fundamental Phenomena in Electrical Discharges," Reviews of Modern Physics, Vol. 3, April, 1931, pp. 191-257.

59. Langhaar, H.L., *Dimensional Analysis and Theory of Models.* John Wiley & Sons, 1951.

60. Kline, S.J., *Similitude and Approximation Theory.* McGraw-Hill Book Company, 1965.

61. Sedov, L.I., *Dimensional & Similarity Methods in Mechanics.* (transl.), Academic Press Inc., 1960.

62. Frenzen, C.L., Class Notes: Naval Postgraduate School Courses MA 3610, MA 4321 Non-linear Dynamics and Bifurcations, 1996.

63. Haken, H. Light, *Volume II: Laser Light Dynamics*, North-Holland Publishing Company, 1985, Ch 2-4, 5-8.

INITIAL DISTRIBUTION LIST

	No. Copies
1. Defense Technical Information Center 8725 John J. Kingman Rd., STE 0944 Ft. Belvoir, VA 22060-6218	2
2. Dudley Knox Library Naval Postgraduate School 411 Dyer Rd. Monterey, CA 93943-5101	2
3. Chairman Department of Aeronautics & Astronautics, Code AA Naval Postgraduate School Monterey, California 93943-5106	1
4. Professor Oscar Biblarz Department of Aeronautics & Astronautics, Code AA/Bi Naval Postgraduate School Monterey, California 93943-5106	3
5. Associate Professor Christopher L. Frenzen Department of Mathematics, Code MA/Fr Naval Postgraduate School Monterey, California 93943-5000	3
6. Professor Karlheinz E. Woehler Department of Physics, Code PH/Wh Naval Postgraduate School Monterey, California 93943-5000	1
7. Commander, Space & Naval Warfare Systems Command Space Technology Directorate (SPAWAR-40) 2451 Crystal Drive Arlington, Virginia 22245-5200	1
8. LT Brigitte Horner 612 Thunderbird Ct, Apt A Chesterfield, Missouri 63017	2